Advanced Non-Associated Plasticity with Enhanced Isotropic and Non-Isotropic Hardening for Sheet Metals

Submitted by

Mohammed Ageel Alharbi

Bachelor of Science in Mechanical Engineering, 2011 Qassim University

Master of Science in Mechanical of Engineering, 2015 Southern Methodist University

Master of Science in Civil Engineering, 2019 Southern Methodist University

A thesis submitted in total fulfillment of the requirements for the degree of

Doctor of Philosophy

Department of Engineering

College of Science, Health and Engineering

La Trobe University

Victoria, Australia

June 2020

Table of Contents

List of Abbreviations

AB	Anti-Buckling
AHSS	Advanced High Strength Steel
ARB	Accumulative Roll Bonding
ASTM	American Standard for Testing and Materials
BCC	Bodies Concentrated Cubic
CPU	Central Processing Unit
CDM	Continuum Damage Machine
CCD	Charge-Coupled Device
CNC	Computer Numerical Control
DD	Diagonal Direction
DIC	Digital Image Correlation
EBSD	Electron Back Sparsis Design
FEA	Finite Element Analysis
FCC	Face Concentrated Cubic
GTN	Gurson Tvergaard Needleman
RD	Rolling Direction
RTM	Reduced Texture Methodology
TD	Transverse Direction
MDS	Modified Duncan Shabel
MMC	Modified Mohr Circle
NIST	National Institute of Science and Technology
VPSC	Visco-Plastic Self-Consistent
VUMAT	Method to Simulate Fracture
UTS	Ultimate Tensile Strength

List of Figures

List of Tables

List of Notations

x,y,z — The symmetry axes of orthotropic material analogous to the RD, TD, and ND directions in thin sheet metal.

$\boldsymbol{\sigma_x, \sigma_y, \tau_{xy}}$— Three in-plane cartesian components of applied Cauchy stress σ in the orthotropic coordinate system of the sheet metal.

$\boldsymbol{\Phi_{2y}, Y_1, Y_2, Y_3, Y_4}$ — Hill's 1948 quadratic anisotropic yield stress function in-plane stress and its four material constants.

$\boldsymbol{\Phi_{2p}, P_1, P_2, P_3, P_4}$ — Hill's 1948 quadratic anisotropic flow stress function.

$\boldsymbol{\Phi_g}$ **,** $\boldsymbol{A_1 ..., A_9}$ — 4th order anisotropic yield stress function of Gotoh in Cartesian stress components and remaining nine material constants.

$\boldsymbol{\sigma_1, \sigma_2, \theta}$ — In-plane principal stresses & loading angle between $\boldsymbol{\sigma_1}$ and rolling direction of sheet metal.

$\boldsymbol{\sigma_\theta, R_\theta, \sigma_b, R_b}$ — Yield stresses and plastic strain proportions under uniaxial tension at loading orientation angle θ and equivalent biaxial tension correspondingly.

$\boldsymbol{\varphi_4, \psi_{4a}, \psi_{4b}}$ — Yield stress function of Gotoh recast in intrinsic variables ($\boldsymbol{\sigma_1}$, $\boldsymbol{\sigma_2}$, **θ**) and the two sub-determinants of its Hessian matrix.

ρ, ω — Polar coordinates for the two principal stresses $\boldsymbol{\sigma_1}$ and $\boldsymbol{\sigma_2}$

$(\varepsilon'_1, \varepsilon'_2, \boldsymbol{\theta})$ —The in-plane principal plastic strain increments and the straining loading orientation angle between the major principal plastic strain increment ε'_1 and the rolling direction (RD) of the sheet metal.

$\boldsymbol{\tau}$ **and** $\boldsymbol{\dot{\gamma}}$—The yield stress in stress-controlled pure shear loading and plastic strain increment in strain/displacement-controlled pure or simple shear loading.

Declaration of Authorship

I, Mohammed Alharbi, solemnly declared that this thesis is entirely my work, original, and also that any work of others or published work added in this thesis is properly accepted as text citation, refers and compiled in the reference section. No other's person's work has been used without acknowledgment in the main text of the thesis. This thesis has not been submitted for the award of any degree in any other tertiary institution.

Signed: Mohammed Alharbi

Dated:17/06/2020

Abstract

Anisotropic mechanical properties offer valuable insight towards plastically deformed material composed of metallic properties especially rolled sheets or pressed sheets. There are multiple important applications of metal deforming and plasticity due to their framework characteristics. For instance, general anisotropic elasticity with independently specified anisotropy controlling each of the yield, kinematic hardening, and scalar hardening, and rate dependence matrices. This study presents extensive research work on the plasticity and foldable molding of anisotropic sheet metals along with the support of constitutive modeling-based numerical derivations. By using the simulation and modeling-based software design, it is demonstrated that the anisotropic plasticity of an aluminum-based material can be modeled using the polycrystalline plasticity modeling approach.

Moreover, the suggested phenomenological models employ immediate change-based orthotropic yield formation dependent on weight and probably obtain the optimum capacity of the anisotropic plastic under many frame points, highly precise and computationally capable conditions.

In this study, a comprehensive testing method was developed for the analysis of the anisotropic plasticity of sheet metals. The plasticity tests do not only include traditional single-axis tractable testing in different material directions but also equipped with specific joined-pressure and shear biaxial tests so that a practical 3d yield surface can be included. The research results indicate that the expulsion of aluminum sheet metal AA6111-T4 is very anisotropic and has R-values varying from 0.19 and 1.08. The AA6111-T4 currently shows only traverse anisotropy with an almost unintended range of R-values.

A shear constraint was very recently proposed to evaluate and calibrate the advanced non-quadratic anisotropic yield criteria and to eliminate the non-physical numerical artifacts in those criteria. This investigation points out that such a shear constraint is unnecessary for plane-stress orthotropic plasticity in general. Using the well-known Hill's 1948 quadratic and Gotoh's 1977 quartic yield functions for orthotropic sheet metals in-plane stress, it is shown problem-solving that pure shear stressing, and pure shear straining loading conditions are not equivalent except for very special cases. By conducting a series of

shearing experiments on an aluminum sheet metal, the actual test results are shown not to provide any unequivocal supporting evidence to the newly proposed shear constraint. The non-physical numerical artifacts of the non-equivalence in pure shear stressing and pure shear straining of sheet metal are the intrinsic features of an anisotropic material. The newly proposed shear constraint should thus not be accepted to be universally applicable for anisotropic plasticity modeling of sheet metals. Such a proposed constraint itself shall be regarded as a provisional simplifying assumption of reduced anisotropy only for some particular sheet metals under consideration.

Acknowledgments

I acknowledge the valuable help I got from the people I interacted with writing this thesis. I am thankful to my supervisors Professor Wei Tong, Associate Professor Ing Kong and Dr Vipul Patel; whose supervision was impactful in explaining the insightful requirement of the thesis. I appreciate the continuous help and motivation of my colleagues, and for their top-notch cooperation, you upheld me considerably and had always been keen to support me.

I solely thank my seniors, whose guidance helped me keep things on track. I want to thank you for your brilliant collaboration, and for most people of the open doors, I was given to direct my examination and further my exposition. You provided me with the support that I helped to pick out the perfect direction and efficaciously complete my thesis.

I am thankful to my sponsorship Qassim University for the funding providing to my research and degrees.

Moreover, I am thankful to my family for granting me a conducive environment to finish my thesis and the smart direction they provided me all through my studies. Finally, my gratitude goes to my fellow researchers, who had been of notable assist in wondering over our problems and discoveries, just as giving glad diversion to rest my brain outside of my exploration.

Name: Mohammed Alharbi

Date: 17/06/2020

Chapter 1

Introduction

1.1 General

The advancement of material science technology has revolutionized human being's lifestyles. The development of effective methods for the testing and characterization of materials is essential to achieve the desired material properties. Tensile and shear testing are generally employed to estimate the mechanical strength of a material. Tensile testing describes the capability of a material against the deformation force applied perpendicular to its surface. Whereas shear testing examines the strength of the material on the subject of deformation force parallel to the surface. The concept of the aforementioned properties can further be extended to describe the anisotropic plasticity of the automotive sheet metals [2].

Similarly, anisotropic plasticity can be described using the yield criteria. Although it may experience some deviations from the original values, the estimation may be suitable for the analysis. During the sheet metal forming process, when compressional stress is applied to a material, it deforms into a new structure, which can be viewed as a transitory phase. This compression ultimately imparts more strength to the material. This is because of the metallic sheets compression i.e., the distance decreases between metallic layers results in the increase in the collective strength of sheet metals. For the analysis, it is essential to specify the biaxial pressure to relate it with the variations in a material. The selection of a suitable modeling parameter (e.g., uniform strain) to describe the anisotropic plasticity is crucial [3].

Sheet metals can exhibit anisotropic properties that may affect their behavior of ductility, deformation, and strain profiles. Thereby it is important to properly analyze their properties. Based on the anisotropic behavior, suitable yield functions can be implemented to predict the behavior or properties of sheet metals. The model is called general anisotropic elasticity with independently specified anisotropy controlling each of the yield, kinematic hardening, and scalar hardening, and rate dependence matrices. The models of sheet metals can predict the plasticity behavior at the microstructure level.

Further, the models are expected to simulate the plasticity for the sheet metals exhibiting anisotropic behavior at a higher level. This can be achieved by extending the microstructure into the large sheets by layering using the models.

In modeling, generally, it is assumed that the microstructures in the sheet metals are uniform. However, practically in sheet metal, the uniform microstructure does not represent the whole sheet metal. Some of the regions consist of structures that are not uniform. Therefore, the models are accounted for the effect of non-uniform microstructures by including the number of variables and coefficients. The plasticity models may be classified as advanced plasticity and the lower scale models.

1.1.1 Advanced Plasticity Modeling

Advanced plastic modeling is based on the theory that deals with the materials or sheet metals for the yield potential over a macroscale level. The model based on this approach can predict the plasticity behavior of a small sheet metal that undergoes shear defects. The advanced plasticity modeling can further be divided into two types, namely isotropic plasticity, and anisotropic plasticity advanced models. For better modeling results, it is suggested to use the experimentally determined parameters to estimate stresses other than using von Mises distortion energy theory. For instance, using this approach the distortion energy function of a linear elasticity can be generalized using quadratic or non-quadratic polynomial functions to estimate plastic flow potential (more details in Chapter 2) [3].

1.1.2 Lower Scale Modeling

This modeling approach is based on power law and has been applied for the prediction of deformation response in the case of crystal and polycrystalline structures. Nevertheless, this approach has limitations of restricted scale and shaping difficulties. This is probably due to the unpredictable microstructures, which otherwise require an extensive number of parameters to achieve reliable accuracy. For example, in metals, the plasticity behavior can be explained based on the gem structures, crystallographic surfaces, and fracture mechanics. However, in practice, the material is composed of complex microstructure where the particles and structure distributions are not the same. This results in poor predictability at the lower scale level. The benefit of this method is the use of parameters that are based on the mechanical evaluation which explains the response generally for the whole microstructure [3].

During the plastic deformation of the polycrystalline materials, the crystallographic textures and the mechanical response can be explained using the visco-plastic self-consistent polycrystalline model (VPSC), where each grain of material behaves as an ellipsoidal interacting surface. The yielding behavior can be experimentally determined by conducting the biaxial compressional test using the laminated sample sheets. Further, the yield surfaces can be predicted by employing VPSC models using the data of crystallographic textures as input. This approach is more suitable for polycrystalline materials to describe plasticity behavior.

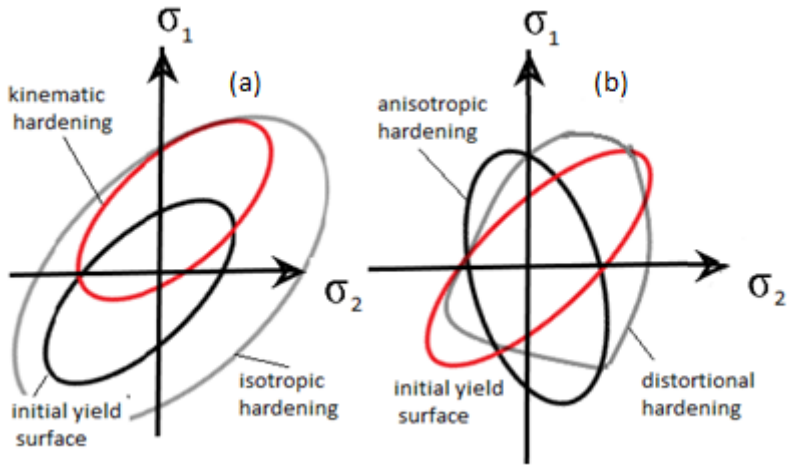

Figure. 1.1 Yield surface development along with the sheet metals (a) kinematic hardening (b) anisotropic hardening.

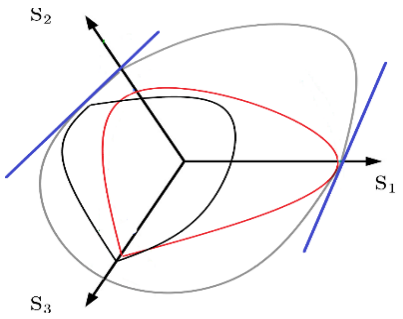

Figure 1.2: Yield surface evolution.

Varma et al. [3] carried out the VPSC modeling study. This allows the estimation of the dislocation density over the complete plastic deformation process for each slip system. Further, it can explicitly predict the impacts of back stresses and bending. Figure 1.1

depicts yield surface development along with the sheet metals, where Figure 1.1 (a) represents the kinematic hardening case and Figure 1.1 (b) shows anisotropic hardening. It is important to mention that VPSC modeling is only applicable to the configuration without any bent. Figure 1.2 shows yield surface profiles.

The forming of sheet metals involves a large plastic deformation which may cause material failure due to the occurrence of strain localization. Many theories have been reported to describe the failure phenomena by accounting for damage in the constitutive models. The most widely adopted approach can be further classified as micromechanics-based damage formulations and continuum damage theories. The examples of the aforementioned approach are damage theory and continuous damage mechanics (CDM). Micromechanics-based damage formulations describe the failure in terms of the internal variable which represents the volume fraction of the micro-cavities created during loadings. This approach is most applicable to porous materials and also for sheet metals. Nevertheless, the second approach (CDM) is based upon the internal variable that defines the surface density of microcracks which may be derived from the irreversible thermodynamic process [4].

This stress space enables the creation of an analytical backward Euler stress return to a volumetrically non-associated frictional plasticity model that includes dependency using a modified Reuleaux deviatoric section on lode angle and the intermediate principal stress as well. The single-step procedure considers a robust algorithm for all stress return regions. This method provides substantial computation speed than the conventional iterative backward Euler method [5]. It was reported that the non-associated flow frictional perfect plasticity model has been further extended by modifying the main yield surface via the introduction of an additionally modified Reuleaux cone. The developed constitutive models were implemented with the system of logarithmic strain–Kirchhoff stress/updated Lagrangian finite deformation [6].

It was considered a non-associated flow of rule model to increase accuracy without characterizing a tremendous amount of content parameters [7]. This demonstrates the diverse ability of plastic yields with less complicated information. This thesis includes non-related diffusion to contemplate anisotropy in every plastic line or yield stress.

1.2 Significance of the Study

Anisotropic plasticity material modeling for automotive sheet materials is a necessary procedure that characterizes the nature of the different materials utilized for a given purpose. Kretsis et al. [8] reported that understanding the shear and tensile quality of a sheet stays major in characterizing the heap bearing limit of the given sheet. For example, shearing tests will help to decide the pressure that a sheet can withstand. Similarly, the tensile tests are fundamental means to determine the ductile behavior of the sheets. This exploration will give information that will assure the influence of the different layers at anisotropic plasticity of the sheets that are utilized in the development. In-plane shear testing has been increasingly used to characterize the sheet metals for getting information on their anisotropic yielding and plastic flow models. Comparing to uniaxial and biaxial tension tests, an in-plane shear test has, in general, more complicated boundary conditions, and the deformation may only be approximated as either pure shear or simple shear with or without axial tension. This is somewhat different from the situation of the classical plasticity studies using tension-torsion testing of thin-walled tubes. We presented an examination of the in-plane shear testing of sheets for the anisotropic plasticity constitutive model. The in-plane shear tests are classified with a major focus on pure shear stressing, pure shear straining, and simple shear (straining) types.

1.3 Timeline

The cumulative period for this thesis is three years, including the research period. The first year will be spent in the accumulation of ideas that numerous resources are essential for this research study. The shearing and pliable lab tests will be performed throughout the second year at Southern Methodist University. Each research will be conducted on different materials and the test results will be recorded as per the occurrence. In the third year, the results of the various tests will be investigated at La Trobe University. The investigations also included every possible data and written survey that could help to improve the association of automotive sheets.

1.4 Research Question

This research focused on addressing miscellaneous issues given in the research question that “What is the impact of tensile and shearing testing on the anisotropic plasticity

constitutive model of sheet metals and its respective R-values?”

1.5 Research Objectives

This work explores advanced anisotropic plasticity modeling and its uses in the field of sheet metals. The major objectives of this research study are given as follows,

1. To compare associated, non-associated, and quadratic models of the plasticity of automotive aluminum and steel sheet metals.
2. To characterize the plastic anisotropy of automotive aluminum sheet metals by tensile and shearing tests.
3. To enhance the isotropic and anisotropic hardening with non-quadratic yield functions.

1.6 Thesis Outline

The remainder of the thesis is divided into six chapters as follows:

Chapter 1: A brief introduction of the project is addressed including a general introduction, scope of the project, and research objectives. The main objective is to compare associated, non-associated, and quadratic models of the plasticity of automotive aluminum and steel sheet metals. There are two types of modeling and focusing on advanced plasticity modeling.

Chapter 2: This chapter focuses on the literature review. There are on the literature review many advanced plasticity modelings such as Hill's and Hoffman but the focusing will be on Hill's-1948 model and how to improve it.

Chapter 3: This chapter focuses on the materials and methodology and how to use the experimental results for the tests, calculation of the R-values, and the comparison between isotropic and kinematic hardening.

Chapter 4: This chapter describes two anisotropic plasticity models with seven independent material constants with finite element methods. The use of non-associated plasticity models has been grown an increasing interest in developing to analyze finite elements of processes of sheet metal.

Chapter 5: This chapter presents the advanced non-associated plasticity with enhanced

isotropic and non-isotropic hardening in associated plasticity and the non-quadratic yield function. There are two types of pure shear loading conditions on a sheet metal shear testing and its three special cases.

Chapter 6: Lastly, this chapter brings to suggestion, future work in polycrystalline plasticity modeling with reduced texture methodology. While this postulation on anisotropic plasticity and the split of sheet metals is a significant amount of research, there are still several unknown issues of strain: minimal disfiguring of kinematics.

Chapter 2

Literature Review

2.1 Introduction

The polycrystalline plastic structure of a metal determines the compression strain used in the experimental models. The yield surface's precise dimension may have complex forms depending on the specific model used [10]. There are many plasticity models of polycrystalline plasticity.

Models based on the reduced texture method (RTM) are known as the biologically observable plasticity models of polycrystalline plasticity, which are well suited for basic research. Surface calculations are not mandatory for model alignment, although they may be useful for implementing crystal instruction evaluations. Instead, with more precise surface descriptions, the modified surface is an extremely rough approximation of the original cover. The plastic conduction is of a displaced aluminum compound such that a 2 mm thick expulsion layer was studied. The result shows a joint surface direction along with the thickness holding, given a highly anisotropic force stress-strain reaction. A test program that includes both complete and reduced thickness instances was organized. This provides a chance to perform the uniaxial strain tests with identifiable model criteria and examine various methods for the non-relative stacking model. The mechanical reaction of full-thickness cases is represented using a 12-grain model, whereas an 8-grain model is used for the decreased thickness examples.

2.1.1 A Non-Associated Plasticity Model with Anisotropic

Anisotropy in the mechanical and metallurgical characteristics of sheet metals is attributed to the crystallographic surfaces that form due to the plastic deformation phenomena. Dislocation theories can explain the deformation mechanisms based on microstructural variables, which can be modeled using numerical modeling approaches. Nevertheless, several studies have been reported to highlight the deficiencies in the numerical models. Therefore, it is required to study the available literature to develop the metals' microstructures' proper analysis over various conditions. Accurate estimation can be obtained using experimental and simulation data related to the study of microstructural variables [11]. Non-quadratic yield properties can explain the phenomena of anisotropy and its formation. The structural framework can explain whether the metal will retain or lose the properties that are attained on the subject of deformation after the strain is released.

The estimation of lateral solidification is essential for the evaluation of particular spring-back calculations. As shown in Figure 2.1, the accuracy of the back-spring calculations differs. It is because the support of testing metal needs to be removed before the performance of a test. This chapter details the literature review of the following outline:

- Evaluation of R-values for the mathematical modeling of anisotropic sheet metals plasticity.
- Study of the effect of minor dimensional and deviations in strain measurements on R-values.
- Impacts of R-values on different anisotropic characteristics of sheet metals.

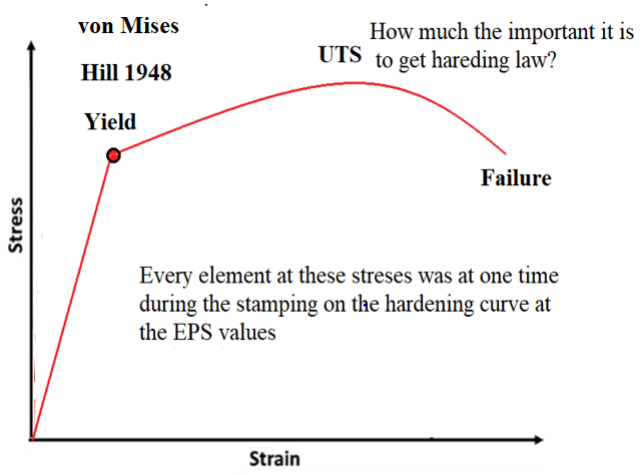

Figure 2.1: Stress and strain data at the end of testing metals.

2.1.2 Advanced Applications in Forming Sheet Metals

The automotive industry is one of the most dominant sectors of the time. The economies of several countries are highly dependent upon their automotive industry. The competition in this industry has led the manufacturers to continually improve the latest car models' designs and quality. The vehicle manufacturing industry's advancement and innovation are highly dependent upon the effective sheet metal forming process.

Conventional materials and the manufacturing processes are not reliable to meet future requirements. Therefore, further advancement and developments are required in this sector to implement innovative scientific technology to meet modern requirements. The long-term goal-oriented effort contributes to extraordinarily excellent success initiatives for productivity building and cost reduction. The use of lightweight design specifications is the most appropriate way to meet this criterion. The innovation in design also demands new materials, and otherwise, new materials also require new innovative shaping techniques and new ideas for tooling [12].

In any event, both customers and legal requirements require a higher level of well-being. The use of top-quality components will satisfy the demands. There is a trade-off between the quality of a material and its formability which implies that high-quality materials may offer low formability and vice versa. The designing of sheet metals should involve balancing both quality and formability parameters to meet the requirements.. It is thus of

extreme importance to find a decent trade between quality and formability. The use of lightweight design requirements is one of the critical inclinations in the car business, which should have been apparent from the fundamental needs. Materials from the materials science side can meet the use of this plan guideline by elements of high explicit quality (ultimate tensile stress/ρ) and high exact strength (elastic modulus/ρ). The use of high-quality steels, light metals, compounds (mainly aluminum and magnesium), as well as expands on a wide range of non-metallic materials, is an increasingly diverse pattern of growth [13].

2.1.3 The Dynamics behind Inducing Anisotropic Plastic Behavior in Materials

For plastic anisotropy in materials, the three most significant causes are:

1. Anisotropy of crystallographic characteristics individually in polycrystalline metals.
2. The directionality of the distribution of specific stages and imperfections in composites of multi phases (for example, stringy structures).
3. Propagation of strains due to distortion.

To improve the hardness or elasticity of a material, when the material undergoes tempering or other processes the impacts of the anisotropic properties may be exposed on the surface of the materials [14]. As a rule, the orientation of the sheet toward the component created is discovered as being important when a high level of anisotropy exists on the plane of the sheet.. In the case of anisotropic plastics, the material with a higher width to thickness ratio and the strain of a tensile measure (ordinary to the plane of the sheet) has a better quality. Furthermore, a substantial, standard anisotropic proportion reduces the risk of wrinkling or swelling in the component of shallower, readily moulded sections (e.g., exterior car boards).

A strategy was developed by Saito et al. [15] in 1998 for the production of ultrafine quality grain materials. The method involves the movement of the sheet metals pass through the operations, such as rolling, slicing, and piling. A systematic description of the test convention can be found by Beausir et al. [16-17], discussing the effect of the accumulative roll bonding (ARB) methodology on the anisotropic plastic output of sheet metals.

The observed connection between the metal and the subsequent anisotropic material

properties may impact the material's elastic behavior on the distortion history.. A point posed in these lines; anisotropy is not a property and, preferably, depends more strongly on processing history than materials of a kind.

2.1.4 Standards for Anisotropic Plastic Behavior in Materials

Over the past few decades, strategies have aimed at promoting the depiction of plastic anisotropy, testing, and yield calculation methods. For instance, the Lankford coefficients modify the parameters, taking into account the anisotropic concentrations, and are measured at various fronts concerning the traveling heading by uniaxial tensile measures. The related relation determines the coefficient:

$$R_{\propto} = \frac{\varepsilon_{trans}^{p}}{\varepsilon_{thick}^{p}} \quad (1)$$

Where α is the point from an anisotropy-bearing (for example the moving heading in worked sheet tests) and it defines the plastic strain the transverse way (90° from α) and the through-thickness course, separately. Notably, anisotropic materials may demonstrate a variety in both the Lankford coefficient and the yield deviation with α. The yield criteria for anisotropic materials can take one of two structures: either the segments of the pressure tensor and quadratic or non-quadratic [18].

Bassani et al. [19] suggested a definite strain yield value that is restricted to planar isotropic status or, to be more precise, to products with transverse isotropic plastic properties. It implies that the effects on the sheet's surface are not precisely the same as those on the path by the width of the layer. The foundation is suggested to be related to the performance of body-centered cubic (BCC) and face-centered cubic (FCC) metals whose surfaces give a transversal and topically plastic material such as in Figure 2.2.

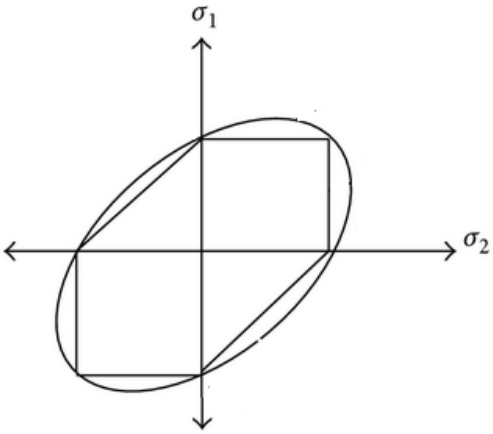

Figure 2.2: Illustrate the quadratic (nonlinear), and non-quadratic (linear) yield.

2.1.5 Anisotropic Yield Conditions for Plane Stress

The arrangement of yield criteria given for the plane stresses condition is restrictive ; (i) they are constrained in the kind of anisotropy that they can portray and (ii) they are constrained to frameworks in which the plane stresses deviation can be related. Plane stresses are the unique case where the stressed segments in one of the symmetrical headings are zero. The most extreme scenario is when z-heading problems (through-thickness) are small, $\sigma_{xx}= \sigma_{yz} = \sigma_{xz} = 0$. It decreases the friction bar. A thin plate is the first cause of such a condition, explicitly a geometry, where the transverse area is in one plane larger than others. The proposed standards intended to show orthotropic plastic actions during the stacking of low-pressure situations.. Orthotropic materials are those falling into the symmetry group with three (symmetrical) opposite planes. The typical case of the substance that displays such anisotropy is metal tubes.

Since they are typically generated in a continuous process by rolling the material, the orthotropic headings become:

$$[\boldsymbol{\sigma}] = \begin{bmatrix} \sigma_{xx} & \sigma_{xy} \\ \sigma_{yx} & \sigma_{yy} \end{bmatrix} \tag{2}$$

(i) The moving course,

(ii) The transverse bearing to the moving bearing

(iii) The opposite plate bearing.

According to Bassani et al. [19] restricted materials exhibit transverse isotropic elastic

properties, specifically, into the states of planar isotropy. This implies that the sheet plane features are independent but unique in contrast to the features on the way through the plate thickness. The norm intended to relate to FCC and BCC metal behavior, whose surfaces provide a transversal insulated plastic property and take into account the framework illustrated in Eq. 3, where ϕ describes the non-dimensional yield work, σ_1 and σ_2 are the significant limitations in sheet, "biaxial yield pressure" and fundamental shear yield limitations in the plate's plan, separately, and "m" and "n" are two, dimensionless parameters which can be regressed to improve the suitability with the yield surface

$$\emptyset = \left|\frac{\sigma_1 + \sigma_2}{2\sigma_b}\right|^n + \left|\frac{\sigma_1 - \sigma_2}{2\sigma_0}\right|^m = 1 \tag{3}$$

2.1.6 Hill's Yield

Hill's yield basis involving anisotropy throughout a substance with general strain develops requirements for materials subjected to plane stresses conditions. Design behavior of an-iso-sensitive, a situation in which changes the response of the material, was suggested to be the most prohibitive in use. The model is provided by the corresponding relation when the indications for all pressure segments are invalidated Hill [20] [21].

$$\emptyset = \frac{\sigma_1^2}{\sigma_0^2} - \frac{c\sigma_1\sigma_2}{\sigma_0\sigma_{90}} + \frac{\sigma_2^2}{\sigma_{90}^2} + \left\{(p+q) - \frac{p\sigma_2 + q\sigma_2}{\sigma_b}\right\}\frac{\sigma_1\sigma_2}{\sigma_0\sigma_{90}} = 1 \tag{4}$$

Where, c, p and q are the dimensionless parameters and σ_0 and σ_{90} are the performance constraints of the substance in different rolls and crossheads are involved. As the Logan and Hosford et al. [22] rule proposes, Hill's shape also demands that the central ropes be parallel to the orthotropic rubrics. Hill offered a new yield foundation to expel the containment forced by this yield paradigm for use under general plane stresses conditions. With the ultimate goal of experimentation, he submitted the shear pressure element. He suggested a model that again reliant on the guideline stress terms.

$$\emptyset = \left|\sigma_x + \sigma_y\right|^m + \left(\frac{\sigma_b}{\tau_0}\right)^m \left|\left(\sigma_x + \sigma_y\right)^2 + 4\sigma_{xy}^2\right|^{\frac{m}{2}} + \left|\sigma_x^2 + \sigma_y^2 + 2\sigma_{xy}^2\right|^{\frac{m}{2}-1}\left\{-2\alpha\left(\sigma_x^2 - \sigma_y^2\right) + b\left(\sigma_x - \sigma_y\right)^2\right\} = 2\sigma_b^m \text{ [23]} \tag{5}$$

Where m, a, b are dimensional parameters that can be modified to shift the convexity of the yield surface. In this case, because of that yield norms, variations in parameter m do not sufficiently describe the surface of yield, which is tentatively resolved for polycrystalline metals or materials.

2.1.7 Anisotropic Yield Criteria for General Stress

The requirements of yield for the analysis of the anisotropic creation of products under generic stresses are competitive. Their application has lesser restrictions than the ones that the plane stresses condition supported. Hoffman et al. [24] compared the characteristics based on positive and negative strain, including elective content symmetries, multi-dimensional space, and multi-axial tension conditions. The general yield standard is quadratic and is shown as indicative in Eqs (6-7), where *Fi* and *Fij* are the parameters that are decided based on the material quality.

$$\phi = F\iota\,\sigma\iota + F\iota j\sigma\iota\sigma j = 1 \tag{6}$$

$$\begin{bmatrix}\sigma_1\\ \sigma_2\\ \sigma_3\\ \sigma_4\\ \sigma_5\\ \sigma_6\end{bmatrix} = \begin{bmatrix}\sigma_{xx}\\ \sigma_{yy}\\ \sigma_{zz}\\ \sigma_{yz}\\ \sigma_{zx}\\ \sigma_{xy}\end{bmatrix} \tag{7}$$

This model is beneficial in applications of composite anisotropic with specific yield characteristics in strain. Despite the similarity of right terms in the base to the alteration between “positive” and “negative yield stresses”. In practical applications, this method is not exceptionally reasonable as it needs tests to determine the criteria of material quality on all physical premises. In any scenario, in ever more favorable situations, the best understood and the more commonly employed parameters are extracted from the general case.

Hoffman et al. [24] suggested a yield base that could be significant under general conditions of concern for orthotropic materials that indicate the structural an-iso-sensitive

$$\phi = C_1(\sigma_y - \sigma_x)^2 + C_2(\sigma_z - \sigma_x)^2 + C_3(\sigma_x - \sigma_y)^2 + C_4\sigma_x + C_5\sigma_y + C_6\sigma_z + C_7\tau_{yz}^2 + C_8\tau_{zx}^2 + C_9\tau_{xy}^2 = \sigma_u^2 \quad (8)$$

Hoffman et al. [25]. establishes the relationships between the materials' parameters and testing data to get C_1, C_4, and C_7, and the six remaining constants are decided by the points x, y, and z. The key advantage to this method is the way it contrasts the quality of tensile and compressive yields. Further, it can predict the characteristics for other cases in which the situation is not the same.

2.1.8 Hill-1948 Model

The 1948 yield foundation of Hill is a von Mises speculation standard which contains anisotropy on materials with three symmetrical planes [18]. It is related using the quadratic model as:

$$\rho = F(\sigma_y - \sigma_z)^2 + G(\sigma_z - \sigma_x)^2 + H(\sigma_x - \sigma_y)^2 + 2L\tau_{yz}^2 + 2M\tau_{zx}^2 + 2N\tau_{xy}^2 = \sigma_u^2 \quad (9)$$

The tensile and compressive yield properties are considered identical. Both systems are close to the basic Hoffman of the straight deformation model. The yield surface is curved and represents the von Mises yield model for isotropic materials. The constants F, G, H, M and N that are explicit to materials anisotropy and x, y, and z. is usually parallel to the moving path because of the sheet metals, and y and z are separately symmetrical. The constants can be described through the corresponding relationships to maintain a uniaxial tension (x, y, z) [18].

$$\frac{1}{X^2} = G + H; \frac{1}{Y^2} = H + F; \frac{1}{Z^2} = F + G \quad (10)$$

Furthermore, the above expressions can be rearranged to acquire precise articulations for the constants regarding the uniaxial yield stresses:

$$2F = \frac{1}{Y^2} + \frac{1}{Z^2} - \frac{1}{X^2}; 2G = \frac{1}{Z^2} + \frac{1}{X^2} - \frac{1}{Y^2}; 2H = \frac{1}{X^2} + \frac{1}{Y^2} - \frac{1}{Z^2} \quad (11)$$

The constants L, M, and N are related to the shear yield qualities. At the point when the geometry of the issue requires a circumstance of plane stresses, the yield foundation is reduced to Eq. 12.

$$\frac{1}{x^2}\sigma_x^2 - \left(\frac{1}{x^2} + \frac{1}{y^2} - \frac{1}{z^2}\right)\sigma_x\sigma_y + \frac{1}{y^2}\sigma_y^2 + \frac{1}{\tau^2}\tau_{by}^2 = 1 \qquad (12)$$

When recreating sheet metal forming forms, it is maybe increasingly advantageous to revise the plane stresses yield basis regarding the anisotropy proportions r_0, r_{90}, and r_{45} Barlat et al. [25].

$$\sigma_x^2 - \frac{2r_0}{1+r_0}\sigma_x\sigma_y + \frac{r_0+r_{90}}{r_{90}(1+r_0)}\sigma_y^2 + \frac{r_0+r_{90}}{r_{90}(1+r_0)}(2r_{45}+1)\tau_{xy}^2 = \sigma_0^2 \qquad (13)$$

On account of material shows ordinary anisotropy ($r_0 = r_{90} = r$), it is considered that $\sigma_0 = \sigma_{90}$ and the yield model takes the separated structure where is σ_u the uniaxial yield stress.

$$\sigma_1^2 - \frac{2r}{1+r}\sigma_1\sigma_2 + \sigma_2^2 = \sigma_u^2 \qquad (14)$$

Generally, the Hill norm is the most commonly employed model due to its relatively simple definition and wide-ranging materiality. The central positive aspect is that the standard tensile tests can easily be used to determine the model parameters. Nevertheless, Hill's yield's drawback is that it usually cannot accurately represent the quadratic form.. Thereby several yield problems can be overestimated as an aspect of the path of average anisotropy using the Lankford coefficients. For example, polycrystals subjected to normal stress, suggested by Barlat et al. [26] for a completely defined solution to this model are known to produce better results.

The numerical formulae available to represent plastic properties/production of materials are not limited to those cases described. However, the analysts also have suggested additional suitable parameters to consider the impact of the anisotropic constants on the yield surface [27]. In all cases, off-plane stress and general control, the parameters under review here are most comprehensive and commonly revised. The accurate check linked to every open law is the guarantee of the anisotropic (consistent) parameters necessary to exactly 20 yield

estimates. The following area discusses the methods now used to guarantee certain conditions for the fulfillment of the specific products anisotropic yield criterion.

2.2 Testing of Sheet Metals

The plastic behavior of compressed sheets has been significantly decreased by the plastic strain proportions attributable to tensile strain evaluation on various edges of the planes of the surface. The relevant stress-strain relationship is depicted in Figure 2.3. The last parameter for the entire image is the Lankford coefficient (R estimate), known as the proportion of plastic stress in the direction of width (ninety degrees from the tensile hub) to plastic force via the sheet thickness [28].

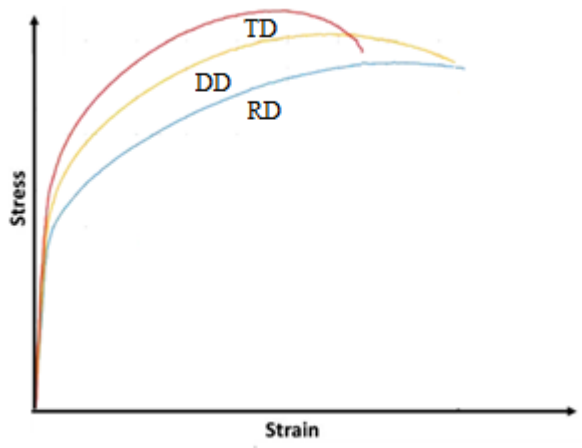

Figure 2.3: Relationship between stress and strain under uniaxial load in 3 directions.

The R-value is commonly calculated in this method after the illustration has failed. Benchmarks for the R-values assurance at specific strains, such as the "ASTM E517" standard proposes a 20% strain estimate. Because R-values are generally dependent on the size of the load [29]. Averaging strategies of the R-values at 0°, 45°, and 90° were used to explain in the example of resistance to an impression of decreasing and anisotropy plane.

$$\Delta R = \frac{R_0 + R_{90} - 2R_{45}}{2}, \bar{R} = \frac{R_0 + R_{90} + 2R_{45}}{4} \quad (15)$$

2.2.1 Sheet Metals' Biaxial Testing

Sheet metals testing in multi-directional phases is gradually becoming progressively crucial. Biaxial tests with cross-cutting samples are considered one of the most effective

techniques. Moreover, it is essential to note that uniaxial strain tests can only provide precise test information for the isotropic materials and that the consequences of standard uniaxial tests may not appropriate due to anisotropic materials.

Makinde et al. [31] developed a biaxial testing machine that took synchronous tensile stacking cross-sectorial. The device had changed the displacement cycle (strain control), and the resulting stress is measured using two load units, with one symmetrical leading and the other opposite. Various types of cross-examples between the grasps can be placed, and both large and small strains can be identified. The device determines the uniformity of the tension within the calculated duration. The inherent anisotropy is known in both the functional reaction and the rigid reaction of the substance.

Kuwabara et al. [32] further improved the machine to reduce the costs and its precision. The structure contained two sets of water chambers, each of which is designed to connect a similar weight via the restricted chambers. This extension was used to limit cross-example horizontal understanding due to small variations of opposing related influences. Similarly, the load cells were performed to determine the relevant problems, and the equivalent strains measured using stress measurement in the example's focal point. In low carbon steel tests, the concern can be described using the approaches of Hill paradigm of quadric yield and the Hosford yield level [33].

Besides the modification required for the structure and improvement of reasonable biaxial testing, a standout amongst the most testing parts of such a testing framework lies in the plan of the test sample. Albeit cross-molded geometries are commonly used to perform biaxial tests on sheet metals, the structure of the sample is the primary concern that limits the uses of the test [33].

The modeling techniques such as finite element modeling, and the other techniques have utilized the structure level information to effectively describe the anisotropic plastic products. Although many changes in the research arrangements have been made in recent years, a need for more frequent and reliable testing methods persists. Also, the principle of using space methods for depicting anti-anisotropic yields has been researched by Lin et al. [33] in that it includes plans for investigating small multi-hub stress areas, universal

usability of testing equipment, marginal example preparation, and adequacy over a variety of material structures.

2.2.2 Geometrical Constraints

The design of a set-up will affect the predicted results during a study. Potential impacts include touch domains where rubbing takes on a role or structure delicate for a particular manipulation process. Such supposed geometric specifications can be illustrated by touch or grating with the device used locally, by the asymmetry of the equipment collection, by non-isotropic behavior or by a geometry that contributes to the pressure fixing phase. An unusual example is sheet metal anisotropy, which refers to the requirement of checking the moving bearing of the surface in more than one way. At the point of biaxial deformation, the anisotropy is more unstable and is bound to fall short [37].

2.2.3 Measuring Stresses, Strains or Forces

Stresses are usually determined either by a pressure or force field or by the region in which they are released. A computerized panel connection set-up that can quantify strains on top or base surface should be possible for sheet metal to estimate strain fields. Stresses can be calculated by using an FE-algorithm, but ideally, the substance model is accurate. The other arrangement is to determine the power and the chip zone, just as uniaxial stress tests are performed. It is conceivable only when it is possible to decide on both the authority on land and the region. It fits for a simple pressure test, but this is often inefficient with increasingly complicated situations.

2.2.4 Modeling of Hardening

According to the viscoplasticity theories , all of the features of the inelastic behavior can be described using the same variable. In this scenario, the model of hardening can describe the strain rate dependent on plastic flow, creep and stress relaxation. The model consists of tensorial relations, a scalar function, and evolution equations [26].

2.2.5 Testing Dedicated to Sheet Metals

Generally, the testing methods are organized here into four fundamental classifications, including, (i) uniaxial testing, (ii) multi-pivotal testing, (iii) cyclic testing, and

(iv) tests to determine sheet metallic formability limits. The four classifications can be inspected in this region concentrating on the conventional testing strategies.

2.3 Uniaxial Tensile Test

The uniaxial test is one of the most common tests that can be employed to determine the properties of the material such as, yield strength, ultimate strength, Lanford coefficient and elongation at break. The test can be performed according to the standard of ASTM D1708. It is typically performed monotonically to fail the specimen at the single strain rate. However, it can also be performed using the multiple load cycles to determine the characteristics of a material's complex behavior. Moreover, in spite of this standard testing strategy, the more sophisticated technology such as digital image correlation (DIC) can also be utilized for more precise and accurate results [45].

2.3.1 Layer Compression Test

The layer compression test is usually employed to characterize sheet metals to determine the onset of yielding and the hardening behavior within uniaxial compression loading. To test the anisotropic materials, the relevant experimental setup needs to be adjusted. Perhaps that can be achieved by by installing a second optical strain measurement system to extract data from both of the symmetrical axes. Examinations found that reproducibility is better than possible in uniaxial tensile tests through chronicle flux curves at pressure estimations to zero. However, by using two 3D optical pressure calculation systems, it is possible to study the period subordinate anisotropic cloth behavior regionally. Therefore, it is essential to maintain a non-frictional connection between the example and the apparatus at a strategic distance to a 3D stress country. The single plates must be fully aligned around their moving bearings and focused [47].

2.4 Biaxial Tensile Tests

The flat biaxial tensile test is an inventive set-up for evaluating the conformity of sheet metal precisely because the yielding locus is within the central pressure quadrant. It is, in fact, beneficial to assess the share of traces opposite and against the moving heading of the

biaxial anisotropic coefficient. The equation of biaxial anisotropy indicates the the yield locus's orientation in the tensioning equipment and is used for adjusting the various yield requirements. Biaxial tensile measurements are currently under development. The planar biaxial tensile can typically be seen in extension utilizing cross-molded instances. Various experts developed biaxial devices to check the judgments and drawbacks of all the endorsed opinions, tested in a detailed analysis [48].

The biaxial check devices can replace forced biaxial machines , for instance, only in biaxial body operated machines. The above utilizes symmetrical arm or cam systems to add biaxial loads for a cross-instance in an aircraft. The stroke is always applied to the actuator, but due to the close, peripheral, non-geometric geographical settings, it isn't easy to indicate that it may not be entirely accurate. Although massive distortions are correlated with the case, the disposal-pushed devices will suffer the harmful effects of cinematic adverse features, forcing the instance to bow facially [49]. Conversely, four unfixed actuators are the most reliable technique in the illustration focal section, also owing to the secure anisotropic material behavior to be the admirably typical biaxial conditions. The actuators can be hydraulic, water-driven or entirely electro-powered and near-circular controls are done with specific load cells per hub to regulate.

In general, the vast majority of the movement is at the target region and is kept away in different areas of the instance from pressure fixations. As models, an example of geometry [50] has been designed and enhanced to prevent uniform strain dispersion in the context of the standard.

A recreational illustration of stacking numbers can also be useful in the measuring zone for determining the pressure field based on the related loads, exchanging of exterior loads for the inside anxieties being a significant concern in “planar biaxial” testing for the measurement of plastic yield.

The possibility of accurate strain dimension, prioritized by non-contact approaches, is another serious issue. Whether or not the resulting strain is measured correctly, the realistic estimate of strains is generally lower in planar biaxial experiments than those used in the lumps above. In 2013, an integrated biaxial cruciform design system for the development

and processing of four loosely operated, multi-hub mechanical powered actuators with continuous strain critique were designed and established at the “National Institute of Standards and Technology” (NIST) Automotive Lighting Center in Gaithersburg. A research configuration design and a sample sheet metal case have been eliminated [50].

2.5 Shear Test

The primary purpose of the shear test is to determine the shear strength of a material. The simple testing techniques were proposed by T. C. Lämmer H [51] and D. Banabic et al. [52]. This is an important characteristic of a material to test in a practical situation. For instance, if a bolt is used to protect two sheet metals together it will face shear forces if the sheet metals obtain any forces in the direction parallel to their planes that will attempt to tear them apart.

Any other means of testing the fabric under shear situations is to analyze the in-plane torque first proposed by Marciniak et al. [53]. The example of this review, fixed in the test set up, is a simple roundabout block, stainless steel braced along the edges, and the inside pivot. The sheer tension state is supplied by turning the inner hinge, enabling the shear molding inside the instance's free territory. Considering the shear stress's linearity to the rectangular wave, the most crucial advantage in the internal grip is that of shearing. The intense stress declines with expanded outspread separations. A technique is developed to evaluate the stream bend from the torque bent over the pivot point.

As a consequence of “sheet thickness” and “inner surface cover,” the functioning window of the in-aircraft torsion control has been provided as long as it is possible to grip. Apart from performing a real “shear test” with two shear spans and the “in-plane torque,” each other's basic shear test technique, in compliance with the well-known ASTM B831, used to break down material conduct with shaving disfiguration, is suggested: as a consequence of this method, a single, practical shear test is proposed.

A reform in ASTM shear test to discover the constituent actions of AA5754 anywhere strains are implemented by adding two ratings on the two dimensions of a shear part. Since the strain dispersion in shear tests remains strongly reliant on the condition of the shear

field, the use of the frameworks for “optical strain” estimation is slowly contributing to actual results. To identify the fixture bends using the visual stress measurement method, a scanning technique based on the aircraft torsion test was introduced, which contributed to comfort pressure measurements of up to one joint use of computational and analytical methods to improve the research effort.

2.5.1 Advanced Modeling of Sheet Metal Forming

The treated steels are widely used in the automotive industry and local appliances due to their astounding quality, high formability, and erosion protection. In comparison, the use of tempered steel surges the mechanical assets of a shaped part. It is noted that the expected springbuck effect can occur which is related to the flexible reversible strain recovery after instruments have been expelled. During the formation process in hardened steels, the little thickness of the sheet is usually required to decrease the weight of the section supplied. The shaping of mild steel has been considered an important issue to handle for the advancement of the business.

From a hardware configuration perspective, there is no doubt that this problem can be solved by a stable springbuck forecast that relies on the comparison of the numerical re-enactment of forming. In this regard, a great deal of work has been undertaken that is associated with the required empirical models. More significantly, due to unknown causes, the precise understanding of the behavior of the substance and evaluation in a comparable basic model of its revealed physical relationships are most motivating. Models are seen most recently tackle the exact anisotropy simulation, the effect, and damage of batching. As a result, the integration of a robust modulus decaying into the system modeling for consistent spring back expectations; the impact of combining the Mori–Tanaka model with isotropic plasticity was taken into account. Sheet metals typically show critical anisotropy of plastics, whatever it is. The goal to construct a mechanically stable model, ready to analyze the consequent degradation of solidity in the process of material deformation and plastic anisotropy [54].

2.5.2 Constitutive Modeling and Numerical Implementation

As the harm mechanics imply, the resulting gaps remain the fundamental conductor for decreasing the solidity of malleable materials, which means that this proof has to be taken into considerations in part modeling to attract material behavior more technically. That is particularly important concerning recreation research at spring back. The "Gurson-Tvergaard–Needleman" (GTN) model which establishes the specific laws to create folding harm in porous materials, considers vacuum nucleation and nullification (two critical components of non-vacuum harm development).

Thus, take visually observable solidity manipulation into account, it mixed the "Gurson–Tvergaard–Needleman" (GTN) with the Mori-Tanaka model, which takes into account firmness deteriorating due thus circular voids. Furthermore, the Anisotropic Hill48 Model was reliably aggravated to the model as the sheet metal has also been anisotropic due to its rolling effect. In this context, we suggest the Gurson–Tvergaard–Needleman (GTN), Hill, and Mori–Tanaka System that is consistently reinforced—considering the initials of every one of the three models.

2.5.3 Hardening and Plastic Anisotropy

In the case of the Tira-2300 tractable testing machine, the overall solidification and plastic anisotropy of the observed stain were estimated using Standard Trial Test. Dimensions of folding sheets were 0.67 and 20.2 mm, each of the equivalent thickness and width respectively. The study determined the tractable intensity F and the length after extension = L of control duration original length based on the traceable testing machine. Figure 2.4 shows graphically the established links F–L for the three coils, which include the moveable headers (0°), transversal trajectories (90°) and a sidelined bearing (45°). The cold moving sheet metals demonstrate an extraordinary degree of plastic anisotropy, that is obviously cannot be ignored without question in empirical retro-elements, from the solidification curve shown in Figure 2.4.

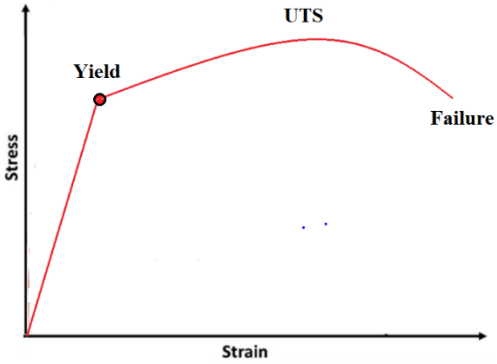

Figure 2.4: Tensile test.

2.5.4 Assimilating Plastic Anisotropy into Metal Materializing Simulations

The creation of today's well-personalized and optimized technologies offers consumers of molded products a vast and endless range of applications. The high-quality multi-stage steels and aluminum composites for the car business are separated precedents. Such metal forming materials slowly need ample quantitative representational calculation to expand their appeal as far as mechanical properties and surface appearance is concerned. Current solutions to the management of reproductions of plastic molding are usually based on the use of non-strictly narrow portion strategies to deal with substantial differential conditions linked to a very highly posed shaping issue. The main objectives of such reconstruction are to predict the material forms after forming, in particular, the spread of thickness, to minimize disappointments related to material streamlining during forming, and to estimate the ultimate mechanical characteristics of the example framed.

The areas of project plans streamline, forecast pressing power, and recreating the final surface appearance of the component are other linked fundamental applications. The last point of view comprises both visible (e.g., wrinkling) and microstructural structures (e.g., ridging, or orange strip), which adjust the surface's consistency—the regeneration of continuum-type metal forms logically solid, micro construction-conscious re-enactments in conjunction with the study. While financially satisfying entail the proper determination of the included substances as far as their constitutive behavior is concerned. Therefore, minimal re-enactments of today typically utilize three material knowledge structures covering solidification, the production of break points, and anisotropy.

This explores precise and practical ideas for the combination of flexible plastic anisotropy into the metal shaping of specific re-enactments of parts. Instead of specifying angles associated with topological or morphological microstructure anisotropy, unique elocution is provided to crystallographic anisotropy of polycrystalline content.

Accurate surface approximations, surface yield description focused on the theory of crystallographic homogenization, mixed product and homogenization strategies, the crystal plasticity limited product strategy, and the late proposed surface section diamond limited component development are all the ideas that will be discussed next time. The current state of anisotropy development between mechanical systems and basic science is usually exceptional. In automated practice, the use of experimental or semi-exact polynomials for the approximation of yield surfaces is a standard strategy although the various crystallization techniques.

The value of observational methods in modern practice is attributed to their fast measurement periods, taking necessary mechanical information into account and being adaptable for new suit focuses obtained by surface details. Despite the surface modification, there is a significant lack of analytical methodologies. According to its physical basis and the aggregation of surface shifts, prevalent in metallic stone plasticity, minimal part methodology in fundamental research is. The real drawback of the useful plasticity approaches is the lengthy calculation periods that, by using the yield surface, a factor of 50 ± 100 exceeds them. The continuous presentation of surface part gem plasticity limited component strategy, which surpasses the calculation time of yield surface figures by a factor of only 15 ± 25, achieves development in the speed of metallic stone plasticity strategies [55].

2.5.5 Plastic Anisotropy

The crystalline plastic anisotropy also leaves the orientation of the electronic link and the subsequent structure of the metallic stone grid. All views define which slip aircraft and which vectors (Burgers vectors) operate to transfer grid disengagement or to trigger a thermal shift of plastic value.

$$\sigma_{xp} = \frac{\sigma_{xU}}{K_i}; d\varepsilon_{zp}^{p} = K_i d\varepsilon_{zU}^{p} \tag{16}$$

Where

$$K_i = \left\{ \frac{\gamma_{90,0} + \gamma_{0,90}\alpha^M + \gamma\gamma(1)\alpha^M}{\gamma_{90,0}(1) + \gamma} \right\}^{\frac{1}{M}} \tag{17}$$

And α inferred to as the stress ratio, σ_y/σ_x, given by

$$\alpha^{-1} = 1 + (\gamma_{90}{}^{-1})^{(M-1)} \tag{18}$$

The main result of this "anisotropy" in the prevailing environment is that metals are disfigured differently from the intrinsic anisotropy of minerals in a continuum design. If the uniform vectors b_j^s and regular slip plane b_j^s accessible in a particular stone cross-section of the different slip frames are developed, it quickly identified the directions component s dyadic artifacts which are compatible with the following formula.

$$m_y^x = n_i^s b_j^s \tag{19}$$

With symmetric portion being

$$m_{ij}^{sym,s} = \frac{1}{2}(n_i^s b_i^s) \text{ (crystal coordinates)} \tag{20}$$

$$m_{kl}^{sym,s} = \frac{1}{2}(a_{ki} n_l^s a_{lj} b_j^s + a_{lj} n_j^s a_{ki} b_l^s \text{ (sample coordinates)} \tag{21}$$

This is offered in metallic directions of stone. It should be remembered that all slip vectors are uniform under the conditions. Transforming the latter into an organizational process in coordinates. Where a_{ki} and alj are the shifting gates between the framework of the metallic stone and the structure of the case. The use of these different path factors "m_{ij}^{sym}" is a simple kinematical description on a single metallic stone's yield surface using the distinctive open slip structures for converting an external load into slip geometry [56].

2.5.6 Out-of-Plane Shear

In both the L-T and W-T programs, simulated training is carried out for out-of-plane shear

piling. The associated bending of the building shear pressure is almost the same (for the L-course tension is about 3% higher). At about 15 MPa, the underlying yield point was found. The strain continues to grow monotonically. The careful evaluation of the molded forms shows a molding of the vault structure by an off-plan shear. Notice the apparent hop near the target of the vertical cell unit limits in the removal area—that influence three aspects.. For example, the UW-uprooting field is constant and meets regularity conditions along with the limits for shear along the W-bearing, but it shifts along with the L heading, which provides an impression of a hop when you take a gander in the W-T plane project. At the braze joints, as the "net cross-section" is the littlest, are the most potent strains [57].

2.6 Uniaxial in-Plane Tension

From the literature survey, it was noted that the uniaxial in-plane pressure was generating a strain curve. The strong stress curves are monotonous, and their forms are like standard metal. The underlying yield stress for the whole sandwich material for the strength in the L-course is around 130 MPa and an estimate of about 160 MPa for a design strain of 0.15 is achieved [57].

Chapter 3

Materials and Methodology

3.1 Introduction

Rolled sheet metals are in general textured polycrystalline solids and their plastic flow behavior depends on the sheet metal orientations [20, 21]. The plastic anisotropy of sheet metal can be in part characterized by its plastic flow pattern when the sheet metal is subjected to a simple stress state. The research results indicate that the expulsion of aluminum sheet metal AA6111-T4 is very anisotropic and has R-values. The AA6111-T4 currently shows only traverse anisotropy with an almost unintended range of R-values.

3.2 Materials

The research results based on the lab experiments indicate that the expulsion of aluminum sheet metal AA6111-T4 is very anisotropic and has R-values. In Chapter 4 we used the materials such as steel, zinc, brass zirconium, and titanium. In Chapter 5 we focus on the lab experiments of aluminum AA6111-T4.

3.3 Methodology

The research methodology was designed based on the simulation of experimental conditions and parameters of the defined model through simulation software. This examination depended on the basic strategies for investigating the connection between the components chosen in plasticity (during the tensile test) and it is one of the essential components for surveying future investigation results. The ductile checks and shearing measures are among the tests to determine the plastic values of the various materials. Many methods can be used to obtain accurate results for the plastic region. The goal was to govern the nature of the various dissimilar materials tested during the study, depending on the results of the experiments [9]. This dissertation utilizes the plastic flow sheet metals and their anisotropic properties to compare non-related and non-related quadratic models. Finite element analysis was conducted on the hole expansion using the dual-phase steel sheet. The software used for analysis is ABAQUS using the material subroutine based on

Fortran's UMAT and VUMAT substitutes. Here, the uniaxial and biaxial yield strengths and plastic strain ratio were used as the parameters to measure the convex fourth-order and sixth-order homogenous polynomial yield functions.

3.3.1 Shear Testing of Thin Flat Sheet Metals and Their Presentations Constitutive Modeling

A variety of researchers have recently considered an in-plane shear test for plastic anisotropy of moving light plate [42] as an alternative for uniaxial pressure and biaxial stress test. Pressurized analyses of slight wall-mounted cylinders are the old-style approach used to examine metal performance with sophisticated strain under biaxial pressures. Not at all as with a single uniaxial pressure test when the proportion of anisotropy of the plastic current, of the hub torsion, is used. This does not relate to the plastic tension check and the plastic strain proportion.

3.3.2 Shear Testing and Its Three Special Cases

As the terms shear, pure shear, and simple shear are used in the literature for the shear testing; a concise definition will be given at first. We adopted the loading orientation angle (θ) and principal stresses (σ_1, σ_2) or the intrinsic variables as called by Hill to characterize the mechanical loading of a flat sheet metal element in-plane stress. So $\sigma_1 > \sigma_2 \geq 0$ defines biaxial tension (uniaxial tension when $\sigma_2 = 0$) while $\sigma_1 > 0$ and $\sigma_2 < 0$ is the stress state of a material element in an in-plane shear test. If the in-plane shear test is done under displacement boundary conditions, then the principal strain increments (θ_0) and the straining orientation angle $(\varepsilon'_{p1}, \varepsilon'_{p2})$ should be used instead. As it is usually understood for an orthotropic sheet, the mechanical loading is on-axis or coaxial if $\theta_0 = \theta$ and is off-axis or non-coaxial when $\theta_0 \neq \theta$.

For finite deformation including cases of only small strain but restricted rotation, the in-plane material spin ω˙ should also be specified as part of either stress or strain-controlled loading conditions on the sheet metal test piece. The following three cases are most relevant to our discussion here: pure shear stressing, pure shear straining, and simple shear (straining). As a plane-stress yield function in anisotropic plasticity is most often formulated using the applied Cauchy stress, the ideal shear test condition would be under

pure shear stress, that is, $\sigma_1 = -\sigma_2 > 0$, see Figure 3.1(a). This may be accomplished in principle using a biaxial test machine with no material spin. A free-end torsion test of the thin-walled tube can be regarded as a pure shear stress test with a finite material rotation.

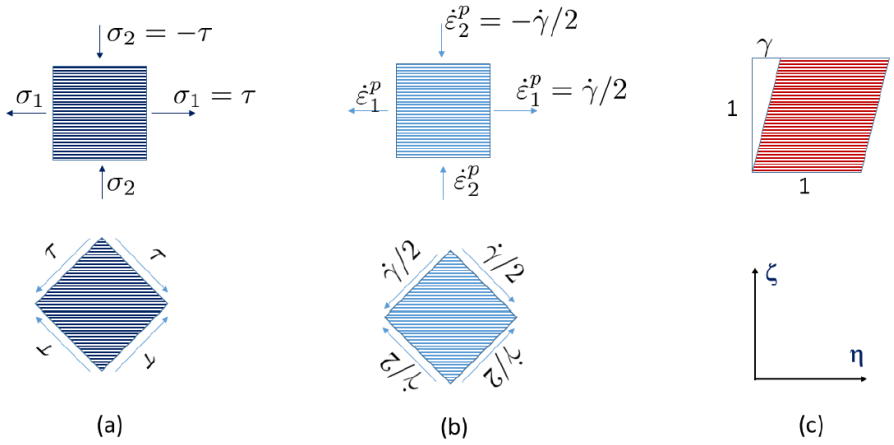

Figure 3.1: (a) Pure shear stressing; (b) pure shear straining; (c) simple shear (straining) of a unit sheet metal element with the fixed laboratory coordinate axes (the in-plane material symmetry axes xy is not specified as they are in general at a certain angle from the laboratory coordinate axes).

Figure 3.1 shows the shear test for the sheet metal forming. Not at all, like the in-plane shear test of sheet metal in two-shear or single shear designs, for a fixed end torsional analysis of slim walled tubes, do not entirely recommend the relocation limit conditions on each side of a rectangular shear area as determined by the fundamental shear failure. Instead, the narrow rectangular measuring area of a test piece is torn on its two long borders, while the two short edges are calm. The free edge effect and the short distance are both non-uniform and dynamic in the measurement section of this test item.

3.4 Finite Deformation Kinematics of Metallic Sheets

The noticeable consequences of 2D's limited defect of fundamental shear are summarized before presenting the anisotropic plastic modeling of sheet metal with structural shear. As illustrated in Figure 3.1(c), the two in-plane axes of fixed cartesian coordinate system with respect to load and displacement measurements in the laboratory testing are designed by η and ζ respectively (noting by convention, x and y axes are designated as the in-plane material symmetry axes of sheet metal). The simple shear misconfiguration of sheet metal

in-plane strain is characterized with a 2D displacement field (*u, v*) *as u* (*η, ζ*) = ηζ *and v* (*η, ζ*) = *0*, where ζ is the amount of shear. The corresponding deformation gradient and its polar decay are given.

$$F = RU = \begin{pmatrix} 1 & \gamma \\ 0 & 1 \end{pmatrix}, U = \frac{1}{\sqrt{4+\gamma^2}} \begin{pmatrix} 2 & \gamma \\ \gamma & 2+\gamma^2 \end{pmatrix}, R = \frac{1}{\sqrt{4+\gamma^2}} \begin{pmatrix} 2 & \gamma \\ -\gamma & 2 \end{pmatrix} \quad (22)$$

The edge of the in-plane material revolution R because of straightforward shear is: ψ = −arcsine (Rηζ) = −arcsine (γ/p 4 + γ 2). For $\gamma = 1$, ψ = −26.57° (clockwise). Dismissing any versatile distortion (unbending plastic estimation), one has the Eulerian rate of plastic disfigurement and material turn of straightforward shear additionally as

$$D^p = \frac{\dot{F}F^{-1} + F^{-T}\dot{F}^T}{2} = \frac{1}{2}\begin{pmatrix} 0 & \dot{\gamma} \\ \dot{\gamma} & 0 \end{pmatrix}, W = \frac{\dot{F}F^{-1} - F^{-T}\dot{F}^T}{2} = \frac{1}{2}\begin{pmatrix} 0 & \dot{\gamma} \\ \dot{\gamma} & 0 \end{pmatrix} \quad (23)$$

3.4.1 Anisotropic Plasticity Modeling of a Thin Sheet

The quadratic yield potential and its consequent evolution to discuss anisotropic plasticity modeling of the small sheet which is experiencing shear defects on the plane to make the image in this sector increasingly concrete and articulate. Hill's yield function is given in three Cauchy stress pieces for a moved board with its underlying orthotropic plane by XY

$$\phi_2(\sigma_x, \sigma_y, \tau_{xy}) = \bar{\sigma}^2 = A_1\sigma_x^2 + A_2\sigma_x\sigma_y + A_3\sigma_y^2 + A_4\tau_{xy}^2 \quad (24)$$

where A_1, A_2, A_3 and A_4 are four non-dimensional content constants, the yield pressure, and plastic strain proportion figures are routinely chosen based on two single pivoting and inconsistent hub stress tests. If the sheet metal is plenary isotropic or is initially in-plane isotropic (i.e., $A_1 = A_3 = 1$, $A_2 = -2R/(1+R)$, $A_4 = (2 + 4R), (1+R)$), the stacking direction of the plastic edge will remain so during the resulting straight shear distortion (it will be possible to set it to zero always). Hill's performance potential would, therefore, become the following polynomial quadratic form.

$$P_2 = A_{1\sigma_x^2} + A_2\sigma_x\sigma_y + A_3\sigma_y^2 + A_4\tau_{xy}^2 + A_5\sigma_x\tau_{xy} + A_6\sigma_y\tau_{xy} + B_1\sigma_f\sigma_x + B_2\sigma_f\sigma_x + B_3\sigma_f\tau_{xy} \quad (25)$$

In the cases where A_5, A_6, B_1, B_2, and B_3 are additional, non-dimensional material constants that record loss of orthotropic symmetry (permitting the odd-request shear pressure conditions) and the likely impact of the plastically disfigured sheet metal (allowing asymmetry in σ_1 and σ_2). Every continuously non-dimensional element in Eq. (25) may also change due to anisotropic solidifying strain with the resulting fundamental shear distortion. The simple shear test, like uniaxial pressure testing, is handled with a clear (starting) path edge of stacking by a standard technique for modeling or decoding results from an easy shear test on the level of sheet metal. The results of this test are described as the symmetry of orthotics and stay set for the lab facilitate system [43]. This could only be suggested if the substance revolution is immaterial for the isotropic sheets on a surface or the shear straining, say $\psi \leq 5^{\circ}$ so $\gamma = 2\tan\psi \leq 0.175$.

The actual hub strain amount would be up to 0.10 or 10 % for the proportionate hinge strain as per the von Mises. The standard technique often requires the orthotropic symmetry of the sheet metal to continue with its hatchet stake pivot reliably in simple shear [44] and to find the further production approach how it is conceivable for the orthotropic sheet metal hatchet stake to transform freely out of the content revolution. That is, if everything is said to be done, the alleged plastic turn could not be zero in off hub stacking conditions. These techniques are content for significant simple shear disfiguration situations. Regarding model precise shear test results without anisotropic reinforcement, a separate stream law regarding plastic turns can be used (i.e., allowing content constants in a yield capability staying autonomous for the proportional plastic stress ε'_p). Until now, for sheet metal formation experiments, this option seems to be very seldom examined [44].

3.4.2 Measurement of Plastic Flow Anisotropy of Sheet Metal

Plastic thin sheet metal anisotropic flow typically described in a plastic strain ratio as measured in a set of uniaxial tensile tests having angles from 0° to 90° tensile loading axis to rolled sheet metal. Recent testing approaches are defined, and a new approach methodology is being implemented utilizing full-field digital imaging strain visualization,

used for the calculation of plastic stress ratios. Potential error causes are described in detail in both (new and old) approaches with the focus upon the highest precision and accuracy in the plastic strain ratio. To make this precise, absolute statistical results apply to the anisotropic plasticity models to the plastic strain ratios.

The study aims to provide a good starting point for experimental analysis of anisotropic fluid flow in thin sheet metals on the transfer to strain paths, other than uniaxial compression in large plastic strains under specific stress conditions. Wheel sheets are usually polycrystalline textured solids, and their flow behavior depends on the orientation of sheet metals. Whenever plastic anisotropy of sheet metals is exposed to specific stress conditions, this can be defined by its fluid flow pattern. This ratio of synthetic strain rate that is set as actual width ratio increases the plastic strain with the real improvement of the thickness of the plastic deformation, which is probably one of the most straightforward measures of the plastic flow pattern used in sheets loaded with uniaxial straining.

$$R = \frac{d\varepsilon_w^p}{d\varepsilon_t^p} = -\frac{d\varepsilon_w^p}{d\varepsilon_t^p + d\varepsilon_w^p} \tag{26}$$

In action, the average of total real diameter plastic strain (P_{X1}) over the cumulative correct thickness plastic strain is often used (also called the Lankford equation in some literature).

$$R = \frac{\varepsilon_w^p}{\varepsilon_t^p} = -\frac{\varepsilon_w^p}{\varepsilon_\sigma^p + \varepsilon_w^p} \tag{27}$$

If the shift in the ratio of axial elongation is believed to be trivial, therefore two meanings must be identical. When anisotropic flux potential constants are evaluated, this constancy of R is essential. The term "plastic strain ratio" shall be utilized in the latter two descriptions, but the relative Eq. (27) and composite Eq. (26) strain forms of their measurement shall be referred to, respectively.

$$B = \sqrt{\frac{(1 + R_0)(R_0 + 4R_0R_{90} + R_{90})}{4R_0(1 + R_0 + R_{90})}} \tag{28}$$

As a quality control tool for different manufacturing processes, plastic strain values, and

their adjustments during spinning, grinding, and deformation can further be used. In comparison, anisotropic flow potential constants are calculated using R values, see the below Section 3.4.3. It is, therefore, appropriate to accurately determine the plastic stress ratios. The testing methods have been addressed and possible sources of error in the R-values of the plastic strain ratio. The goal is to implement a full-field digital image correlation methodology for the plastic strain ratios and the applications for anisotropic sheet metal material flow analysis on improvements in strain paths, large plastic strains, and under specific stress conditions, other than uniaxial pressure.

3.4.3 Numerical Analysis of Error in R

R-value errors are first numerically tested using multiple data sets simulated. The R-values of enhanced actual axial strain are considered to be stable (from 0.5 to 25%). The exact width strain (as needed in some of the calculations used for the measurement of relative R-values errors) is calculated for a given pure axial strain and R-value.

$$\varepsilon_w^p = -\frac{R\varepsilon_\alpha^p}{1+R} \tag{29}$$

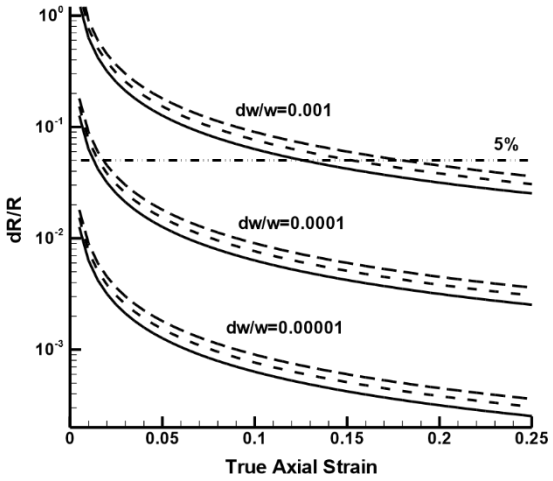

Figure 3.2: Errors in R-values in terms of the errors in length measurements.

Figure 3.2 shows the length measurement errors provided by the equation's errors in R-values, the three found instances correlate with errors in width measurements of 0.127 um, 1.27 um, and 12.7 um, respectively, in the implementation of the regular 12.7um (0.5 inches) ASMT sheet metal tensile specimens. The horizontal dashed and dotted line shows

a decrease in R values of 5% loss. The results show that the calculated width error should be 1.27 um or lower to ensure that R-values errors are within 5%.

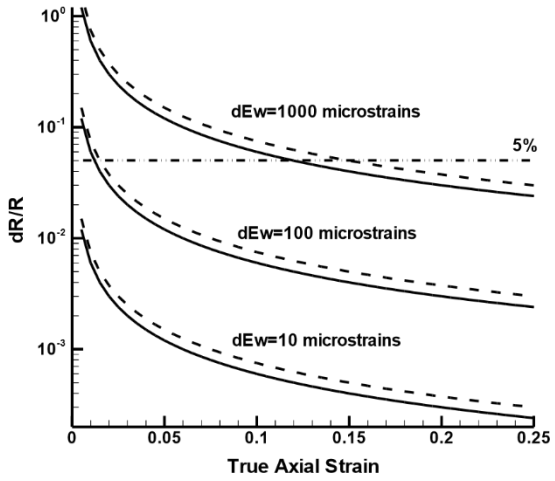

Figure 3.3: Errors in R-values in terms of the errors in strain measurements (solid line: R=1; dashed line: R=0.25 or 2).

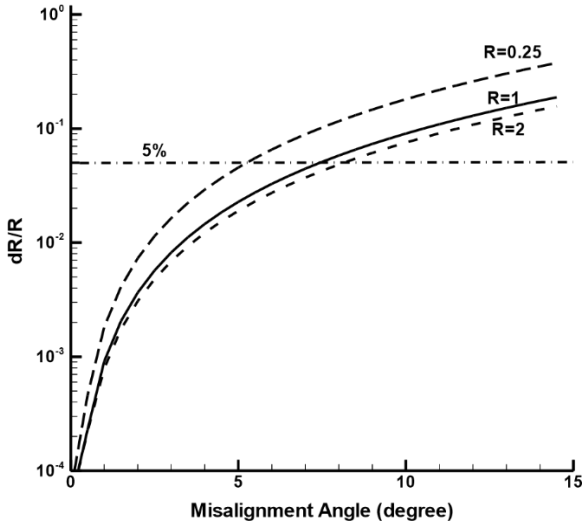

Figure 3.4: Errors in R-values due to the misalignment between the digital image coordinates and the tensile specimen axes.

Figure 3.4 indicates R-value errors. Again, it shows the cut-off of a 5% error in R values on the horizontal dashed and dotted line. Since strains can be calculated in 100 or less, even at low strain rates, R values can be estimated at 5%. As per equations Eq. (29) Minimum R-value relative errors shall be 5.828 times relative to R=0.707 strain errors. If strain defects are of the order of 1,000 micro strains, even axial stress more significant than 15%

can be accurate with R-values.

When stresses are calculated based on digital images [3.2-3.4], a few misalignments can occur between the picture coordinates and the axes of the tensile specimen. Figure 3.4 shows the effect of this misalignment on R-value errors (see Eq. 26). When the angle for misalignment is 5 pounds or less, for R=0.25 to 2, the error is approximately 5% or less.

3.4.4 Material Behavior Models and Forming Sheet Metal Limits

The reintroduction of the numerical form technique in sheet necessitates includes (i) modes that define the movement behavior of sheet metal and (ii) models that anticipate sheet metal forming, under certain constrained circumstances. The primary class includes a robust model and yield standard. The second class contains the phenomenological modes of sheet metal forming limits, which show a developmental pattern ranging from experimental fit to theoretical methods. In this Section, these two classes are analyzed with a quick analysis of the creation state, their obvious growth highlights, importance, and breaking impacts. The area also includes a segment that devotes itself to modeling the exchange of degrees and developing microstructural stresses.

3.5 Discussion and Concluding Remarks

3.5.1 Possible Measurement Errors and Their Effects on Measured R-values

1. Plastic strain (loaded vs. unloaded)
2. Noisy (std) in strains: frame averaged vs. non-averaged images
3. Ut-of-plane motion: additional tensile tests with special imaging arrangements

3.5.2 Calculation Methods and the Variations of Measured R-values

1. Incremental and total strains.
2. Three ROIs.
3. Full-field versus end-to-end (1D or 2D videos).

3.5.3 Concluding Remarks

It has been observed that research is being done to develop the non-associated plasticity models and applying them in finite element analyses of sheet metal forming processes. The advanced class of non-associated plasticity models has mainly been developed to improve the accuracy and capability to describe the anisotropy in both the cases of pressure-insensitive yielding and incompressible plastic flow of sheet metal under uniaxial and biaxial tension conditions. The accuracy of models is found to be dependent upon the types and number of experimental inputs for their parameter calibration.

Chapter 4

Two Anisotropic Plasticity Models Non-Associated with Seven Independent Material Constants

Author's Original Contribution

In this research study, the author's original contribution is the modeling results on anisotropic yielding and plastic flow under uniaxial tension, biaxial tension, and pure shear given in Section 4.4 and 4.5. An official statement endorsing this contribution in the present research study has been attached in Appendix D.

4.1 Introduction

In recent years, the use of non-associated plasticity models has been grown an increasing interest in developing to analyze finite elements of processes of sheet metal [5]. In contrast with previous non-associated model elasticity designed explicitly for the dependency of pressure in the yield of frictional materials like metals, rocks, and soils that are artifacts with unsensual plastic flows [10], this form of non-associated plasticity models is primarily designed to increase anisotropy precision in pressure-insensitive yield and tint parameters.

Hill [10] only suggests a typical related anisotropic plasticity theory which in quadratic stress yield features have only 4 members of constant during the stress time has just 4 material constants which are in their function of quadratic yield stress in-plane stress. The recognized shortcoming of the related quadratic plasticity principle of Hill [58] in 1948 has been overcome through the application of different non-quadratic output stress functions differently. These non-quadratic orthotropic impact functions usually come in the same shape as the complete homogeneous polynomial (fractional, μx, etc.) and the non-quadratic load angle, like the fourth polynomial suggested by Gotoh et al. [59] in 1977. non-quadratic function in terms of two principal stresses σ_1; $\sigma_2$and cosine functions of the loading orientation angle [20]. The orthotropic impact functions are normally described under one of three types. The positive effects and convexity of the YLD 2000-

2D [59] whose exponents were set at eight and six for metals of BCC and FCC correspondingly are especially common with non-quadratic stress output functions. Besides, ratios of yield stresses and plastic strain under biaxial friction and same uniaxial friction, nine and fewer. Experiencing inputs are often used to calibrate contents in these non-quadratic yield strain functions. For comparison, when a configuration that is not connected to a certain form is associated with an analog model, the situation is less clear.

If the parameters are measured in the same number as the test data of both forms, real experimental results of the anisotropic metal plasticity surface must be defined similarly. The performance differences can only be obtained through their particular interpolation and their statistic 75 characteristics that are essential in determining boundary value issues.

In this analysis, we propose to further judge the dissimilarities and similarities between the associated variant of the Pearce et al. [60] quartic plasticity model and the non-associated quadratic plasticity model and. As indicated earlier, in the particular quartic output function of the stress of the corresponding plasticity model was suggested and tuned with the similar 7 experimental inputs to identify the flow stress and yield in an unassociated quadratic model, just 7 independent material constants are available. The positive and convex range of yielding and flow stress functions are determined in this Section 4.3 for the case of the specialty of planar isotropy if every model accepts the three inputs of the experiment exactly similar result way. A variety of selected sheet metals are then used for both anisotropic plasticity models which include four yield stresses and three load ratio steps.

In Chapter 4, the modeling results in uniaxial and biaxial stress are compared side-by-side in the anisotropic yield and plastic flow. We reflect briefly and ultimately on the relative value of using quadratic plasticity models that are not correlated with them for the functional study of metals.

4.2 The Non-Associated Hill's 1948 Quadratic Plasticity Model

The model is the further elaboration of the quadratic model associated with Hill in 1948 quadratic stress yielding function $\phi_{2y}(\sigma)$ and an additional quadratic flow potential $\phi_{2p}(\sigma)$. The output of stress function is as similar as the function of quadratic stress-output of Hill during plane tension in 1948.

$$\phi_{2y}(\sigma_x, \sigma_y, \tau_{xy}) = f^2\sigma = Y_1\sigma_x^2 + Y_2\sigma_x\sigma_y + Y_3\sigma_y^2 + Y_4\tau_{xy}^2 \quad (35)$$

If the four constants are Y_1, Y_2, Y_3, and Y_4 which are to be matched with 4 production stresses, $f(\sigma)$ indicate the independent yield stress rate denoted by $f(\sigma) - \sigma_f = 0$, while σ_f denotes the yield strength of sheet metal. While σ_f is an increasing function of a scalar isotropic hardening monotonically like similar plastic strain and plastic work. The square potential of flow has a similar polynomial structure but has a dissimilar material collection

$$\phi_{2p}(\sigma_x, \sigma_y, \tau_{xy}) = g^2(\sigma) = P_1\sigma_x^2 + P_2\sigma_x\sigma_y + P_3\sigma_y^2 + P_4\tau_{xy}^2 \quad (36)$$

While these three ratios of plastic strain were determined during uniaxial stresses that can be used to calculate P_1, P_2, P_3, and P_4. When the yield requirement is achieved, increments to plastic strain may be determined using the flow rule which may be measured from 3 estimated plastic strain ratios under uniaxial tension.

$$\dot{\varepsilon}_p = \lambda \partial g / \partial \sigma \; with \; \lambda \geq 0 \quad (37)$$

It implies that in their yield and flow tension features, the unassociated quadratic model has up to 7 content parameters. The measured performance and flow stress functions of the device is in Eq. (36) can be obtained with the most typical experimental pressure measures (σ_0, σ_{45}, σ_{90}, σ_b, R_0, R_{45}, R_{90}) of the sheet metal as inputs

$$\phi_{2y} = \frac{\sigma_f^2}{\sigma_0^2}\sigma_x^2 + \left(-\frac{\sigma_f^2}{\sigma_0^2} - \frac{\sigma_f^2}{\sigma_{90}^2} + \frac{\sigma_f^2}{\sigma_b^2}\right)\sigma_x\sigma_y + \frac{\sigma_f^2}{\sigma_{90}^2}\sigma_y^2 + \left(4\frac{\sigma_f^2}{\sigma_{45}^2} - \frac{\sigma_f^2}{\sigma_b^2}\right)\tau_{xy}^2 \quad (38)$$

$$\phi_{2p} = \sigma_x^2 - \frac{2R_0}{R_0+1}\sigma_x\sigma_y + \frac{R_0R_{90}+R_0}{R_0R_{90}+R_{90}}\sigma_y^2 + \frac{(2R_{45}+1)(R_0+R_{90})}{(R_0+1)R_{90}}\tau_{xy}^2 \quad (39)$$

In which yield strength of sheet metal shown about yield $f(\sigma) - \sigma_f = 0$ is often taken as σ_0.

$$\frac{\sigma_0^2}{\sigma_0^2} = \frac{1}{4}\left(1 + 2\frac{\sigma_0^2}{\sigma_{45}^2} + \frac{\sigma_0^2}{\sigma_{90}^2}\right) + \frac{1}{2}\left(1 - \frac{\sigma_0^2}{\sigma_{90}^2}\right)cos2\theta + \frac{1}{4}\left(1 - 2\frac{\sigma_0^2}{\sigma_{45}^2} + \frac{\sigma_0^2}{\sigma_{90}^2}\right)cos4\theta \quad (40)$$

$$R_0 = \frac{R_{45}R_{90} + R_0R_{45} + 2R_0R_{90} - (R_0R_{45} - 2R_0R_{90} + R_{45}R_{90})cos4\theta}{2R_0 + 2R_{90} + 2(-R_0 + R_{90})cos2\theta} \quad (41)$$

$$R_b = \frac{R_0}{R_{90}} \quad (42)$$

4.2.1 The Associated Gotoh's 1977 4th Order Plasticity Model of Reduced Anisotropy

Gotoh et al [60] in 1977 suggested using the symmetry of orthotropic along with plane stress 4th order homogeneous polynomial yield function of stress.

$$\phi(\sigma_x, \sigma_y, \tau_{xy}) = A_1\sigma_x^4 + A_2\sigma_x^3\sigma_y + A_3\sigma_x^2\sigma_y^2 + A_4\sigma_x\sigma_y^2 + A_5\sigma_y^4 + A_6\sigma_x^2\tau_{xy}^2 + A_7\sigma_x\sigma_y\tau_{xy}^2 + A_8\sigma_y^2\tau_{xy}^2 + A_9\tau_{xy}^4 = 1 \quad (43)$$

Throughout his original work, Gotoh et al [60] has proposed a series of 9 linear equations by utilizing the same yield stress test while A_1, A_2, and A_9 were their 9 material constants. It is introduced in the unique work of Gotoh et al. [60], a lot of 9 linear conditions utilizing one yield stress estimation σ_b out of an equivalent biaxial tension test and estimations of 4 yield stresses and 4 plastic strain proportions (σ_0, σ_{45}, σ_{90}, σ_θ, R_0, R_{45}, R_{90}, R_θ, where θ = 22.5° or 67.5°) from four uniaxial strain tests to exceptionally decide those 9 material

constants. For straightforward correlation with the non-associated quadratic model, a rendition of Gotoh's yield stress work [60] which demand just the 7 test inputs (σ_0, σ_{45}, σ_{90}, σ_b, R_0, R_{45}, R_{90}).

Even though there are a few different means to decrease the experimental input requests for factor recognizable proof of yield stress work of Gotoh et al. [60] as recommended before, we utilized here the adaptation of yield stress work of Gotoh et al. [60] having explicitly lessened the planar anisotropy.

To replace the Cartesian stress segments (σ_x, σ_y, τ_{xy}) in Φ_4 (σ_x, σ_y, τ_{xy}) with the chief stresses and stacking point (σ_1, σ_2, θ), the changed yield stress work of Gotoh [60] Φ_4 (σ_1, σ_2, θ) comprises of 5 similar stress terms with 3 one-of-a-kind Fourier cosine arrangement works in 2θ as their coefficients. I If the higher request sinusoids, for example, cos6θ and cos8θ in Gotoh's yield stress work [60] Φ_4 will have to be barred, nine material constants of Gotoh [60] need to meet the accompanying two situations.

$$2A_1 - A_2 + A_4 - 2A_5\sigma_x - A_6 + A_8 = 0 \tag{44}$$

$$A_1 - A_2 + A_3 - A_4 + A_5 - A_6 + A_7 - A_8 + A_9 = 0 \tag{45}$$

Subsequently, the entirety of nine material constants Gotoh et al. [60] can be gotten dependent on just 7 test contributions in addition to these two imperatives of diminished anisotropy (assuming $\sigma_f = \sigma_0$ as usual).

To replace the cartesian stress segments (σ_x, σ_y, τ_{xy}) in Φ_4 (σ_x, σ_y, τ_{xy}) with the chief stresses and stacking point (σ_1, σ_2, θ), the changed yield stress work of Gotoh [60] Φ_4 (σ_1, σ_2, θ) comprises of 5 similar stress terms with 3 one-of-a-kind Fourier cosine arrangement works in 2θ as their coefficients. I If the higher request sinusoids, for example, cos6θ and cos8θ in Gotoh's yield stress work [60].

$$
\begin{aligned}
A_1 = 1, A_2 = -\frac{R_0}{1+R_0}, A_3 \\
= \frac{3R_0 - 1}{1+R_0} + \frac{3R_{90} - 1}{1+R_{90}}\left(\frac{\sigma_0}{\sigma_{90}}\right)^4 + \left(\frac{\sigma_0}{\sigma_b}\right)^4, A_4 \\
= -\frac{4R_{90}}{1+R_{90}}\left(\frac{\sigma_0}{\sigma_{90}}\right)^4, A_5 = \left(\frac{\sigma_0}{\sigma_{90}}\right)^4, A_6 \\
= \frac{1+5R_0}{1+R_0} + 4\left(\frac{\sigma_0}{\sigma_{90}}\right)^4 - 2\left(\frac{\sigma_0}{\sigma_{90}}\right)^4, A_7 \\
= \frac{4R_0}{1+R_0} + \frac{8-8R_{45}}{1+R_{45}}\left(\frac{\sigma_0}{\sigma_{90}}\right)^4 - \frac{4R_{90}}{1+R_{90}}\left(\frac{\sigma_0}{\sigma_{90}}\right)^4 \\
- 2\left(\frac{\sigma_0}{\sigma_b}\right)^4, A_8 \\
= -1 + 4\left(\frac{\sigma_0}{\sigma_{45}}\right)^4 + \frac{1+5R_{90}}{1+R_{90}}\left(\frac{\sigma_0}{\sigma_{90}}\right)^4, A_9 \\
= \frac{16R_{45}}{1+R_{45}}\left(\frac{\sigma_0}{\sigma_{45}}\right)^4 + \left(\frac{\sigma_0}{\sigma_b}\right)^4
\end{aligned}
\tag{46}
$$

Only for the three constants A_6, A_7, and A_8. In like manner, the uniaxial tensile yield stress σ_θ and plastic strain proportion R_θ and equivalent biaxial plastic strain proportion R_b will be given as needs be from the yield condition $\Phi_4 - \sigma f_4 = 0$ and the related stream rule as.

$$
\begin{aligned}
\frac{\sigma_0^4}{\sigma_\theta^4} = \frac{1}{4}\left(1 + 2\frac{\sigma_0^4}{\sigma_{45}^4} + \frac{\sigma_0^4}{\sigma_{90}^4}\right) + \frac{1}{2}\left(1 - \frac{\sigma_0^4}{\sigma_{90}^4}\right)cos2\theta \\
+ \frac{1}{4}\left(1 - 2\frac{\sigma_0^4}{\sigma_{45}^4} + \frac{\sigma_0^4}{\sigma_{45}^4}\right)cos4\theta
\end{aligned}
\tag{47}
$$

$$
R_0 = \frac{C_0 + C_1 cos2\theta + C_2 cos4\theta}{D_0 + D_1 cos2\theta + D_2 cos4\theta} \tag{48}
$$

$$
R_b = \frac{(1+R_0)(1+R_{90})\sigma_0^4 + 2(R_0 - R_{90})\sigma_b^4}{1+R_0)(1+R_{90})\sigma_0^4 - 2(R_0 - R_{90})\sigma_b^4} \tag{49}
$$

While the duration of algebraic expressions is taken as 3 yield stresses and 3 proportions

of plastic strain in uniaxial voltage, for C_0, C_1, C_2, D_0, D_1, and D_2. The first three definitions for the Fourier cosine sequence are in two pounds, however, tension proportions are 2nd and 4th orders, respectively, Eq. (43), and Eq. (49), correspondingly. In the non-associated quadratic model

1. R-values are completely different from yield stress.
2. Additional cos2θ and cos4θ words are contained in the R-values calculation even with a reduction in anisotropy. The representations of the plastic strain ratio R- and R_b are very distinct.

4.3 Positivity, Convexity, and other Restricting Conditions

To confirm that the plastic distortion of strain hardening surface isn't inherently or unstable and dissolves beneficial plastic job decreases, all output and flow tension features are constructive and convection-friendly for non-zero applications. The functions ϕ_{2y} (σ) and ϕ_{2p} (σ) given in Eqs. (42 and 43) are used for quadratic output and flow pressure in Eq. (50) If the needed and satisfactory conditions are met Eq. (51), their positivity and convexity are 175 certain if it meets the following necessary conditions

$$Y_1 > 0, Y_3 > 0, Y_4 > 0, 4Y_1Y_3 > Y_2^2 \tag{50}$$

$$P_1 > 0, P_3 > 0, P_4 > 0, 4P_1P_3 > P_2^2 \tag{51}$$

A double differentiable function such as Yield function of Gotoh et al. [60] Φ_4 (σ), on the other hand, its Hessian matrix is given as

$$\nabla^2\phi_4(\sigma_x, \sigma_y, \tau_{xy}) = \begin{pmatrix} \frac{\partial^2\phi_4}{\partial\sigma_x^2} & \frac{\partial^2\phi_4}{\partial\sigma_x\partial\sigma_y} & \frac{\partial^2\phi_4}{\partial\sigma_x\partial\tau_{xy}} \\ \frac{\partial^2\phi_4}{\partial\sigma_y\partial\sigma_x} & \frac{\partial^2\phi_4}{\partial\sigma_y^2} & \frac{\partial^2\phi_4}{\partial\sigma_y\partial\tau_{xy}} \\ \frac{\partial^2\phi_4}{\partial\tau_{xy}\partial\sigma_x} & \frac{\partial^2\phi_4}{\partial\tau_{xy}\partial\sigma_y} & \frac{\partial^2\phi_4}{\partial\tau_{xy}^2} \end{pmatrix} \tag{52}$$

The yield stress function of Gotoh et al. [60] is firmly curving only if their Hessian

matrix. $\nabla^2\Phi_4$ is positive on the yield surface for any functional Cauchy stress σ. $\Phi_4(\sigma) - \sigma_f^4(\bar{\varepsilon}^p) = 0$. No simple algebraic expressions for such a convexity condition are known to exist for nine material constants of Gotoh et al. [60] in the 4th order function of yield stress $\Phi_4(\sigma)$. Instead, a numerical minimization approach will have to be used to establish the positive definiteness of both Φ_4 and its Hessian matrix.

4.3.1 Planarly Isotropic Yield and Flow Stress Functions

For sheet metals, it might be simpler to contrast the planar isotropy (at times likewise called transverse isotropy) and the realms of constant values of allowable material which guarantee the positive and convexity of the yield and flow stress functions in these two structures. In other terms, the plastic strain and yield stresses ratios in this situation are self-governing of the load-orientation angle of the uniaxial friction in the rolling direction or are the same:

$\sigma_\theta = \sigma_0$ and $R_\theta = R_0$. The quadratic yield stress work $\phi_{2y}(\sigma)$ and flow stress work $\phi_{2p}(\sigma)$ of planarly isotropic sheet metal has the accompanying structure as indicated by Eqs. (51 and52) with $\sigma_f = \sigma_{45} = \sigma_{90} = \sigma_0$ and $R_{45} = R_{90} = R_0$

$$\phi_{2y}(\sigma_x, \sigma_y, \tau_{xy}) = \sigma_x^2 + \left(\frac{\sigma_0^2}{\sigma_b^2} - 2\right)\sigma_x\sigma_y + \sigma_y^2 + \left(4 - \frac{\sigma_0^2}{\sigma_b^2}\right)\tau_{xy}^2 \qquad (53)$$

$$\phi_{2p}(\sigma_x.\sigma_y, \tau_{xy}) = \sigma_x^2 - \frac{2R_0}{1+R_0}\sigma_x\sigma_y + \sigma_y^2 + 2\frac{1+2R_0}{1+R_0}\tau_{xy}^2 \qquad (54)$$

Essentially, the 4th request yield stress work $\Phi_4(\sigma)$ has the accompanying structure for the planarly isotropic sheet metal as per Eq. (54)

$$\Phi_4(\sigma_x, \sigma_y, \tau_{xy})$$
$$= \sigma_x^4 - \frac{4R_0}{1+R_0}\sigma_x^3\sigma_y + \left(\frac{\sigma_0^4}{\sigma_b^4} + 2\frac{3R_0-1}{1+R_0}\right)\sigma_x^2\sigma_y^2$$
$$- \frac{4R_0}{1+R_0}\sigma_x\sigma_y^3 + \sigma_y^4 + 4\frac{1+2R_0}{1+R_0}\sigma_x^2\tau_{xy}^2 \quad (55)$$
$$- \left(2\frac{\sigma_0^4}{\sigma_b^4} + 8\frac{2R_0-1}{1+R_0}\right)\sigma_x\sigma_y\tau_{xy}^2 + 4\frac{1+2R_0}{1+R_0}\sigma_y^2\tau_{xy}^2$$
$$+ \left(\frac{\sigma_0^4}{\sigma_b^4} + \frac{16R_0}{1+R_0}\right)\tau_{xy}^4$$

At the point where the above-mentioned flow stress capacities and yield capacities for a planarly isotropic sheet metal are reevaluated regarding the in-plane chief stresses (σ_1, σ_2), their structures become significantly less difficult

$$\phi_{2y}(\sigma_1, \sigma_2) = \int^2(\sigma_1, \sigma_2) = \sigma_1^2 + \left(\frac{\sigma_0^2}{\sigma_b^2} - 2\right)\sigma_1\sigma_2 + \sigma_2^2 \quad (56)$$

$$\phi_{2p}(\sigma_1, \sigma_2) = g^2(\sigma_1, \sigma_2) = \sigma_1^2 - \frac{2R_0}{1+R_0}\sigma_1\sigma_2 + \sigma_2^2 \quad (57)$$

$$\phi_4(\sigma_1, \sigma_2) = \sigma_1^4 - \frac{4R_0}{1+R_0}\sigma_1^3\sigma_2 + \left(\frac{\sigma_0^4}{\sigma_b^4} + \frac{6R_0-2}{1+R_0}\right)\sigma_1^2\sigma_2^2$$
$$- \frac{4R_0}{1+R_0}\sigma_1\sigma_2^3 + \sigma_2^4 \quad (58)$$

It is expressed here that in the non-associated quadratic and the associated 4th order anisotropic pliancy models, just 2 non-dimensional factors are available. By and by, these two factors are straightforwardly identified with the conventional Hill [58] quadratic model.

$$\left(\frac{\sigma_0}{\sigma_b}\right)^2 = \frac{2}{1+R_0} \; or \frac{\sigma_0}{\sigma_b} = \sqrt{\frac{2}{1+R_0}} \quad (59)$$

4.3.2 Positivity and Convexity Domains of Admissible Yield Stress and Plastic Strain Ratios

For the quadratic yield and flow stress functions $\varphi_{2y}(\sigma_1, \sigma_2)$ and $\varphi_{2p}(\sigma_1, \sigma_2)$ given in Eq. (56), Eq. (57) Eq. (58), the positivity and convexity conditions of Eq. (50) and Eq. (51) apply as well. The permissible values for the yield stress proportion σ_0/σ_b and plastic strain ratio in uniaxial tension R_0 are confined by positivity and convexity conditions as

$$2 > \frac{\sigma_0}{\sigma_b} > 0, R_0 > -0.5 \tag{60}$$

Distinct case of planar isotropy, the Hessian matrix of $\varphi_4(\sigma_1, \sigma_2)$ of Eq. (58) may be transcribed in relations of two principal stresses as

$$\nabla^2\phi(\sigma_1, \sigma_2) = \begin{matrix} \frac{\partial^2\phi_4}{\partial\sigma_1^2} & \frac{\partial^2\phi_4}{\partial\sigma_1\partial\sigma_2} \\ \frac{\partial^2\phi_4}{\partial\sigma_2\partial\sigma_1} & \frac{\partial^2\phi_4}{\partial\sigma_2^2} \end{matrix} \tag{61}$$

According to linear algebra, $\nabla^2\varphi_4$ is positive definite only if it's all sub-factors are positive. If one defines

$$\varphi_{4a} = \frac{\partial^2\phi_4}{\partial\sigma_1^2, \varphi_{4b}} = \begin{vmatrix} \frac{\partial^2\phi_4}{\partial\sigma_1^2} & \frac{\partial^2\phi_4}{\partial\sigma_1\partial\sigma_2} \\ \frac{\partial^2\phi_4}{\partial\sigma_2\partial\sigma_1} & \frac{\partial^2\phi_4}{\partial\sigma_2^2} \end{vmatrix} \tag{62}$$

So, the firm positivity and convexity conditions for planarly isotropic Gotoh's yield stress function $\varphi_4(\sigma_1, \sigma_2)$ are

$$\varphi_4(\sigma_1, \sigma_2) > 0, \varphi_{4a}(\sigma_1, \sigma_2) > 0, \varphi_{4b}(\sigma_1, \sigma_2) > 0 \tag{63}$$

It is noted that $\psi_{4a}(\sigma_1, \sigma_2)$ is a quadratic polynomial of the following form.

$$\varphi_{4a}(\sigma_1,\sigma_2) = 12\sigma_1^2 - \frac{24R_0}{1+R_0}\sigma_1\sigma_2 + 2\left(\frac{\sigma_0^4}{\sigma_b^4} + \frac{8R_0}{1+R_0} - 2\right)\sigma_2^2 \quad (64)$$

whose positivity and convexity per Eq. (63) and Eq. (64) are ensured if

$$\frac{\sigma_0^4}{\sigma_b^4} + \frac{8R_0}{1+R_0} - 2 > 6\left(\frac{R_0}{1+R_0}\right)^2 \quad (65)$$

By replacing the principal stresses (σ_1, σ_2) with their polar coordinate demonstration

$$\sigma_1 = \rho cos\omega, \sigma_2 = \rho sin\omega, \rho = \sqrt{\sigma_1^2 + \sigma_2^2} > 0 \quad (66)$$

we obtain more essentially practical positivity and convexity conditions for φ_4

$$\varphi 4(cos\omega, sin\omega) > 0, \psi 4b(cos\omega, sin\omega) > 0, \quad (67)$$

for $-45^o \leq \omega \leq 45^o$ due to planar isotropy. In a real numerical assessment of the above mentioned two conditions, one rather will just need to locate the base estimations of those two capacities as far as ω and ensure both are sure for a given pair of σ_0/σ_b and R_0.

4.3.3 Other Constraints on Quadratic Yield and Flow Stress Functions

In the non-associated anisotropic plasticity principle, specific additional limitations or situations are often compulsory in the output and flow stress functions to confirm the plastic flow analysis for a sheet metals material is non-singular and stable.

$$\lambda = \frac{vE}{(1+v)(1-2v)} > 0, \mu = \frac{E}{2(1+v)} > 0 \quad (68)$$

In a situation of transversely isotropic sheet metal under two principal stresses σ_1 & σ_2, Eq. (68) becomes

$$\left(\frac{\partial f}{\partial \sigma_1} \quad \frac{\partial f}{\partial \sigma_2}\right)\begin{pmatrix}\lambda+2\mu & \lambda \\ \lambda & \lambda+2\mu\end{pmatrix}\begin{pmatrix}\frac{\partial g}{\partial \sigma_1} \\ \frac{\partial g}{\partial \sigma_2}\end{pmatrix} > 0 \tag{69}$$

Complex relationships in plastic flow non-singularity Eq. The condensed scenario of in Appendix A and B. The findings for the disease Eq are described. It is identical to the derivatives produced by the test but in a different manner.

An additional criterion of plastic stability is dependent upon a non-negative rate for each rate of stress and the resulting overall stress rate is positive (the situation is sufficient to make sure the unique nature of the boundary value issue in the elastic-plastic solid [67,72]. For function $f(\sigma) = \sigma_f\ (\bar{\varepsilon}^p)$

$$2\sigma_f'(\bar{\varepsilon}^p) \geq \sqrt{\nabla f : C\nabla f(\nabla g : C\nabla g)} - \nabla f : C\nabla g \geq 0 \tag{70}$$

While $\sigma_f^0 = \partial\sigma_f/\partial\bar{\varepsilon}^p$ and C is the linear elastic stiffness matrix of the material.

$$E_p = \frac{1}{2} max\ [\sqrt{(\nabla f : C\nabla f)(\nabla g : C\nabla g)} - \nabla f : C\nabla g] \tag{71}$$

The prerequisite of correspondent plastic SS curve of material develops into

$$\sigma_f'(\bar{\varepsilon}^p) \geq E_p \tag{72}$$

One can discover Equation numerically from Equation in Appendix A and B by utilizing the polar directions given by Equation. And the yield condition $f(\sigma) = \sigma_f\ (\bar{\varepsilon}^p)$.

4.4 Applications to Selected Sheet Metals

A whole of twenty-one sheet metals was used for analyzing and assessing their simulation capacities and mathematical properties in a comprehensive manner. Their mechanical characteristics are described in Table 4.1, which has together with the average yield stress and the two hundred and seventy average plastic strain proportions under uniaxial stress.

$$\sigma_{ave} = \frac{\sigma_0 + 2\sigma_{45} + \sigma_{90}}{4}, R_{ave} = \frac{R_0 + 2R_{45} + R_{90}}{4} \quad (73)$$

Of convenience, these nine materials were considered to be linear isotropy elasticity and their manual meaning for the modulus E and Poisson ratio of Young modules are also involved in Table 4.1. The lasting 12 sheet metals are generic FCC and BCC papers, with 7 previously reported mechanical characteristics.

The yield stresses in the plastic equivalent work of the 7 sheet metals with a power-law plastic pressure-strain connection recorded were evaluated by the rolling axial plastic stress to save energy, E_p values determined by Eq. (71) for all 21 sheet metals and R_b values calculated through both Eq. (50) and Eq. (51).

These three tables often include twelve sheet metals with planar anisotropy. The following two tables give details of these computed effects.

4.4.1 Verification of Positivity, Convexity, and Other Conditions

First, with the approximation of all twenty-one sheet metals to be flat isotropic, the values for yield stress and the plastic strain were tested by positive and convex realms of the non-associated quadratic model by Eq. (63) and associated quadratic model by Eq. (64) and Eq. (65). (R_{ave}) and the quadratic model was approximated by R_{ave}.

Motivated by the convexity condition of Eq. (60). In addition to μ_0/5-σ_b, we implemented here an alternate plastic thinning ratio of μ_0 to create the convex domain graphically under uniaxial tension.

Table 4.1: Yield stress and plastic strain ratios of nine sheet metals reported by Pearce [59].

No.	Materials	$\frac{\sigma_{ave}}{\sigma_b}$	R_{ave}	E (GPa)	ν	E_p (GPa)
1	Zinc	0.9924	0.18	96.5	0.3	4.42
2	Rim Steel	0.8627	0.38	200	0.3	10.80
3	Aluminum-hard	0.7837	0.43	70	0.3	5.13
4	Aluminum-soft	0.8642	0.68	68	0.3	1.63
5	Brass	0.8997	0.77	117	0.34	1.58
6	Ti containing steel	0.8732	1.32	205	0.3	0.29
7	Cu containing steel	0.7836	1.62	209	0.33	0.86
8	Titanium	0.6158	3.8	110	0.34	0.055
9	Zirconium	0.5482	3.8	94.5	0.34	0.52

$$\eta_0 = -\frac{\dot{\varepsilon}_3^p}{\dot{\varepsilon}_1^p} = \frac{1}{1+R_0} \tag{74}$$

The utilization of the new pair of non-dimensional factors σ_0/σ_b versus $\eta_0 = 1/(1 + R_0)$ is equal in building the arched area yet it has a pleasant property of being a encased square from (0,0) to (2,2). The outcomes on the positivity and convexity spaces of the two models utilizing the two arrangements of factors separately. The alleged "irregular" conduct of a few sheet metals is likewise demonstrated in the two Figures in 4.10.

Table 4.2: Six non-ferrous sheet metals with their seven experimental inputs [110,111]

No.	**10**	**11**	**12**	**13**	**14**	**15**
Materials	**Brass**	**Copper**	**Aluminum**	**A5052-O**	**A5182-O**	**A6016-T4**
$\frac{\sigma_f}{\sigma_0}$	1	1	1	1	1	1
$\frac{\sigma_{45}}{\sigma_0}$	0.9633	0.9526	0.9618	0.9896	0.9931	0.9514
$\frac{\sigma_{90}}{\sigma_0}$	0.9689	0.9508	1.0024	1	0.9931	0.9375
$\frac{\sigma_b}{\sigma_0}$	0.9826	0.9898	0.9510	1.0521	1.1042	1.0069
R_0	0.873	0.767	0.505	0.72	0.71	0.76
R_{45}	1.000	1.161	0.396	0.51	0.94	0.26
R_{90}	0.898	0.677	0.893	0.59	0.93	0.61
$\frac{\sigma_{ave}}{\sigma_b}$	0.9911	0.9739	1.0321	0.9455	0.9010	0.9534
R_{ave}	0.9428	0.9415	0.5475	0.5825	0.8800	0.4725
E_p (GPa)	0.12	0.60	1.54	1.23	0.77	3.0
R_b	0.972	1.133	0.566	1.220	0.763	1.246
R_b	0.974	1.124	0.636	1.264	0.669	1.244

When $\sigma_0/\sigma_b > 1$ but $R_0 < 1$ [62].

The permissible limits of $2 > \sigma_0/\sigma_b > 0$ and $R_0 > -0.5$ per to guarantee positive and convex quadratic yield and flow stress elements of the non-associated model incorporate every one of the twenty-one sheet metals. Aside from sheet metals No.1–No.3, the yield stress and plastic strain proportions of the left eighteen sheet metals are likewise well inside the realms (the concealed district) of a positive and convex quartic yield stress function 2 of those 3 sheet metals, No.1 and No.2, have their yield stress and plastic strain proportions to marginally fall outside the lower limit of the permissible space.

Table 4.3: Six steel sheet metals with their seven experimental inputs [110,112]

No.	**16**	**17**	**18**	**19**	**20**	**21**
Materials	**AISI 430**	**AISI 406**	**DD Steel**	**AISI 304**	**IF Steel**	**440W HSS**
$\frac{\sigma_f}{\sigma_0}$	1	1	1	1	1	1
$\frac{\sigma_{45}}{\sigma_0}$	1	1	1.0179	0.9568	0.9881	1
$\frac{\sigma_{90}}{\sigma_0}$	1	1	0.9915	0.9454	0.992	0.988
$\frac{\sigma_b}{\sigma_0}$	1.0651	1.1605	1.0686	0.9521	1.240	1.023
R_0	0.77	1.24	1.28	0.92	2.12	0.69
R_{45}	1.11	1.35	0.92	1.07	2.15	1.02
R_{90}	1.20	1.28	1.86	0.86	2.89	0.94
$\frac{\sigma_{ave}}{\sigma_b}$	0.9389	0.8617	0.9422	1.0133	0.8000	0.9746
R_{ave}	1.0475	1.3050	1.2450	0.9800	2.3275	0.9175
E_p (GPa)	1.54	0.57	1.59	0.20	0.53	1.35
R_b	0.642	0.969	0.688	1.070	0.734	0.734
R_b	0.557	0.945	0.623	1.057	0.538	0.714

In short, if you want to model these 3 sheet metals with roughly planar isotropy using positive and convex quartic stress yield functions, your σ_{ave}/σ_b yield stress ratios of 2.1%, 2.2%, and 9.2% correspondingly above experimental stress yields. Only by coincidence, Hill's analogous associated quadratic model agrees with the planarly isotropic form of two sheets of metal No.18-19.

The material constant in yield and flow stress functions for the two plasticity models for the 12 sheet metals described here in Table 4.2 and Table 4.3 were readily obtained using the algebraic ratios provided in Eq. (53) and Eq. (54). Table 4.4 and Table 4.5 respectively provide these measured substance constants. The positive and convexity characteristics of quadratic output and stress flow functions ϕ_{2y} and ϕ_{2p} were tested in Eq. (56) and Eq.

(57) carrying 6 non-ferrous and 6 sheet metals of steel for each of them. The positivity of the quartic stress function Φ_4 and its concentration through the positive clarity of the Hessian Eq. matrix (52) has also been checked using the numeric minimization approach to support each of the 12 as well.

In contrast to the corresponding model for quartic plasticity, the restraining condition per Eq was defined, although the positivity and convexity of the output and flow stress functions of the unexpected model. The check-in the Eq. (68) is still required for each of 9 sheet metals with planar isotropy, the basic equation form is used for Young's Modulus (E) and Poisson ratio − listed in Table 4.3 and Eq. (69). Each of the 12 sheet metals having flat anisotropy has also been shown to satisfy this restrictive condition.

The E_p was also calculated for illustrative purposes. For every sheet of metal despite the condition of Eq. (72) sometimes is not essential or adequate only. That is what Eq is all about. The Eq. (44) can hang on to sheet metals No.6 and No.8 if limited strains only for most of the nine sheets and can grasp a diffuse onset strain. The E_p values were calculated between 0.12 GPa and 3.0 GPa for the 6 non-ferrous and 6 steel plate metals with planar anisotropy. The condition of Eq. (72) will remain for the bulk of these twelve sheet metals only at minor strains and may hold up for sheets No.10 and No. 19 to the onset strain of diffuse necking.

Table 4.4: Material constants of the six selected non-ferrous sheet metals.

No.	10	11	12	13	14	15
Y_1	1	1	1	1	1	1
Y_2	-1.0295	-1.0855	-0.8895	-1.0966	-1.1938	-1.1514
Y_3	1.0652	1.1062	0.9952	1.0000	1.0139	1.1378
Y_4	3.2749	3.3873	3.2183	3.1811	3.2356	3.4328
P_1	1	1	1	1	1	1
P_2	-0.9322	-0.8681	-0.6711	-0.8372	-0.8304	-0.8636
P_3	0.9851	1.0752	0.7113	1.1281	0.8617	1.1397
P_4	3.1588	4.0100	1.8640	2.6076	2.9700	1.9396
A_1	1	1	1	1	1	1
A_2	-1.8644	-1.7363	-1.3422	-1,6744	-1.6608	-1.7273
A_3	2.9499	2.5304	2.4433	1.9748	2.2870	2.3675
A_4	-2.1475	-1.9759	-1.8689	-1.4843	-1.9816	-1.9619
A_5	1.1347	1.2236	0.9905	1.0000	1.0281	1.2945
A_6	6.3750	6.3702	6.0261	5.8452	5.7451	6.3148
A_7	-6.1573	-6.5197	-1.6115	-2.0841	-4.7334	0.0996
A_8	6.9275	7.0570	6.5337	5.6551	6.1220	7.1386
A_9	10.3633	11.4808	6.5264	6.4509	8.6430	5.0025

4.4.2 Comparison of Modeling Capabilities on Anisotropic Yielding and Plastic Flow

Form Table 4.3 has 6 steel sheet metals No. 10-21 and 6 non-ferrous and, differentiates directional reliance of uniaxial tension yield stress σ_θ and plastic strain proportion R_θ on the load angle θ by the two variants. Each diagram frequently the contributions with three load angles (0°, 45°, 90°). The outcomes between the non-associated model and the associated model show no cover. That is, Hill's [58] quadratic function and flux are under uniaxial strain with Gotoh's low degree stress [60] fitting admirably with that of Hill's quadratic yield and stream works under uniaxial tension.

All models compare yield and stream surface under biaxial stress. For comfort, here you can just present the instance of zero-shear tension (τ_{xy} = 0). Each plot additionally incorporates three trial information purposes of performance tension from two uniaxial voltage estimations and one equal biaxial test. For a solitary presentation/strength (for strong lines) the related setup has a non-associated yield surfacing, both in a crushing line and a stream sheet. While the yield surfaces of the two models are fundamentally the same in size and structure as the two of them have to travel through these three experimentally data points, there are clear contrasts among uniaxial and equal biaxial stresses under the middle of the biaxial stress condition.

With the end goal of the stream surface, the connection between the fluid super face of these models was additionally rendered regarding plastic-flow headings of the pivotal fluid strain increases after > axis on-axis tensile loading for proportional biaxial loading (i.e, $\sigma_x \geq 0, \sigma_y = \xi\sigma_x, \xi \geq 0, \tau_{xy} = 0$). With the end goal of the flow surface, the associated plastic strain changes were portrayed by methods for a stream rule. The pivotal stress vector way (σ_y,σ_x) as appeared in each plot is depicted with point $\alpha = \tan{-1}(\sigma_y/\sigma_x) = \tan{-1}(\xi)$, just as the plastic flow direction of axial plastic strain vector (ii) increase (iii), as $\beta = \tan{-1}(\varepsilon'_{py}, \varepsilon'_{px})$and the plastic flow direction of axial plastic strain increase vector (ii). shows the plastic stream bearing β in the capacity of the α-stress point as anticipated for the twelve sheet metal motion surfaces of the two variants. Likewise included as filled circles in each complot $\alpha=0^{\circ}$ and $\alpha= 90^{\circ}$ are two trial information focused of plastic strain proportions (in RD (Rolling Direction) 45° and TD (Transverse Direction)) in two uniaxial stress tests. Fundamentally the same results for sheets No.10 and No.19 are anticipated, with marginally various outcomes for three sheets of aluminum No.13-15. The quadratic equation interjects with a compliment S-molded bend (ran lines) between the two end focuses as a rule. While no third exploratory information point happens at $\alpha= 45^{\circ}$ (i.e., R_b was not part of the seven trial contributions for similar plastic stress proportions), the two models anticipated comparable qualities in R_b for the rest of the twelve sheets of metal, see Table 4.4. Assessed R_b esteems are at the most 0.1 - 0.2 between the two forms concerning sheet metals No.12, No.14, No.16, and No.20. Much the same as with the biaxial presentation surfaces, there are more prominent and more

extensive varieties among uniaxial and likewise biaxial strain inside the normal plastic stream headings under transitional stress control.

4.5 Numerical Algorithm

The local constitutive stress incorporation and systemic iterative elements are an implied finite element method. Fortran's UMAT and VUMAT substitutes for the finite element Technology ABAQUS have been evolving throughout our research. The tacit protocol carried out in UMAT changes local stress and state variables and transfers to the key programs the Jacobian matrix, while the VUMAT method only combines stress and situation variables. The general 3D method as performed [61] should obey our computational integration algorithm.

4.5.1 Local Stress Update by Predictor and Corrector

In a track-based problem such as plastic deformation, solutions including plastic pressure and tension should be coupled with the context of time. The under the routine of the customer in ABAQUS is increased overall. The new key variables are modified for the next phase k+1 in the user content sub-routine. Each segment includes an iterative method for upgrading. In the tacit finite element method, variables are modified in an iteration process. The following phase is the total modified sheet and plastic strain.

$$\epsilon_{k+1} = \epsilon_k + \Delta\epsilon^p_{k+1} = \epsilon^p_k + \Delta\epsilon^p \tag{75}$$

The increased plastic strain is derived from the constancy state if the plastic delivery situation Eq. (75) is fulfilled. The flow rule Δp = Δλpk+1, 1 may be utilized where p is a flow direction tensor that may be provided by derived flow potential p = ∂f ∂σ. The flow potential is similar to the return feature in the flow law. The following equation represents the stress increment

$$\sigma_{k+1} = \sigma_k + \Delta\sigma = \sigma_k + C:(\Delta E - \Delta E^p) = \sigma_{trial} - C:\Delta E^p \tag{76}$$

4.5.2 Structural Iteration

The normal Newton protocol (path dependency), which can contribute to faulty loading-unload, isn't ideal for plasticity issues. Instead, the structural iteration part should be used using a secant Newton method. The Jacobian matrix or algorithmic rigidity must be given (no such method is needed for the specific procedure) [62].

$$C^{alg} = \frac{d\Delta\sigma}{d\Delta\epsilon} \tag{77}$$

While Δ implies the addition b/w time steps k and k+1, and the algorithmic solidness implies proportion b/w the varieties of the all-out incrimination of stress and strain during the time increase [61].

4.6 Finite Element Calculation

4.6.1 Verification Examples

Simple test problems were first investigated for testing defined user content subroutines. If the outcomes of the numerical finite element are similar to the outcomes of the study of the simple question, the coding may be correctly applied. In the first example issue, a uniaxial tensile loading beside several load angles to the rollover direction was examined to analyze the anisotropy coefficient or the R-value plastic pressure. In other terms, the longitudinal orientation of the experiment varies from the x-axis. The analytical expression for R values is centered on the 6^{th} order yield function, and the findings were contrasted with the analytical results for 5 loading angles = θ = 0, π 8, π 4, 3π 8, π 2. In the final element analysis, one 3D continuum element was used for the materials model using the calibrated 6th order polynomial yield function referenced to POLY6a in Table 4.4. In the second example, the output state was evaluated with the same output function. Figure 4.1 indicates for specific shear stress τ_{xy} at $\bar{\epsilon}^p$ = 0.03 with the locus for the different amounts in the yield function. The yielding Eq. (77) used with the flow strength of a steel sheet,

$$\sigma_f(\bar{\epsilon}^p) = 1138(\bar{\epsilon}^p + 0.0002)^{0.099}\ MPa \tag{78}$$

Table 4.4 of the finite element model is POLY6a, and the single element model was imposed on the biaxial and shear stresses. The tests of the finite element show nearly the same effects as in Figure 4.2. Client resources are tested to be accurately configured from these findings.

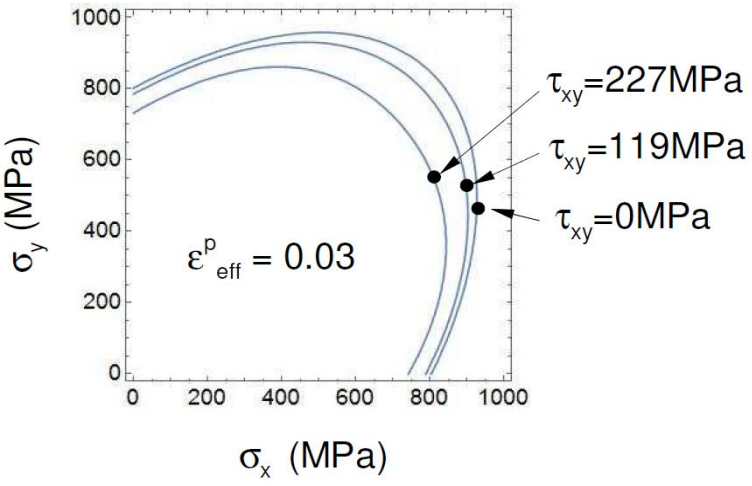

Figure 4.1: Yield locus for three different shear stresses.

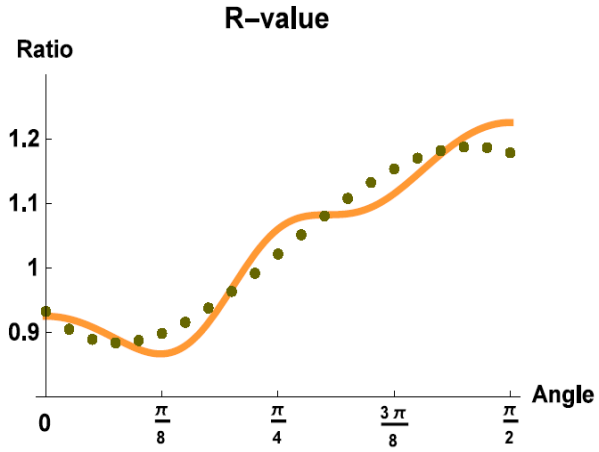

Figure 4.2: R-value of the experiment (points)and POLY6b fitting curve (yellow lone). Experimental data were extrapolated from 5 measurement data Stresses.

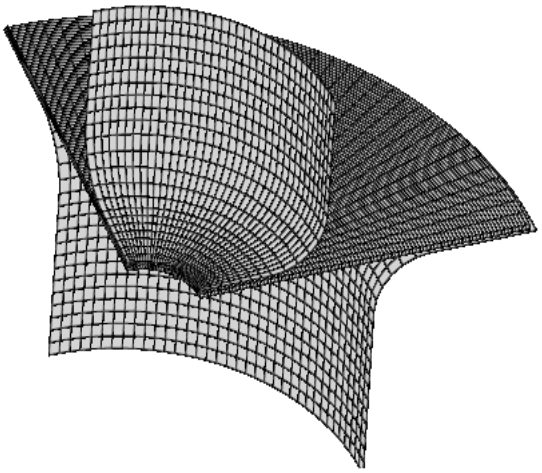

Figure 4.3: A finite element model of the hole expansion problem.

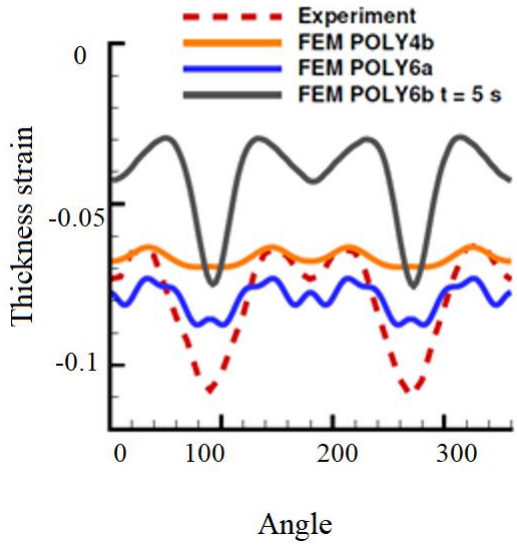

Figure 4.4: Comparison of thickness strain along the inner edge of the hole.

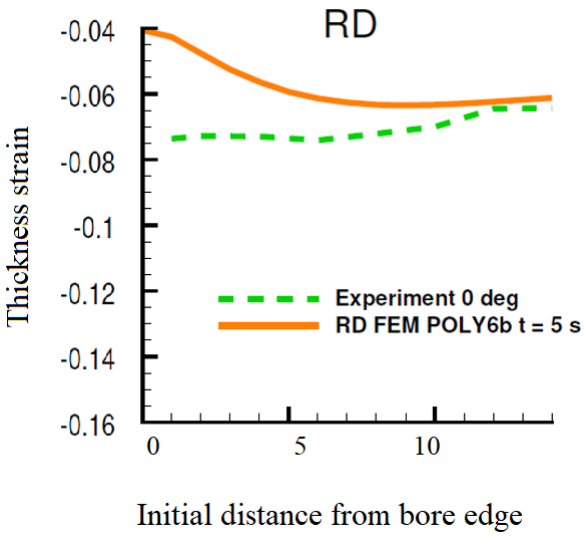

Figure 4.5: Thickness strain along the rolling direction.

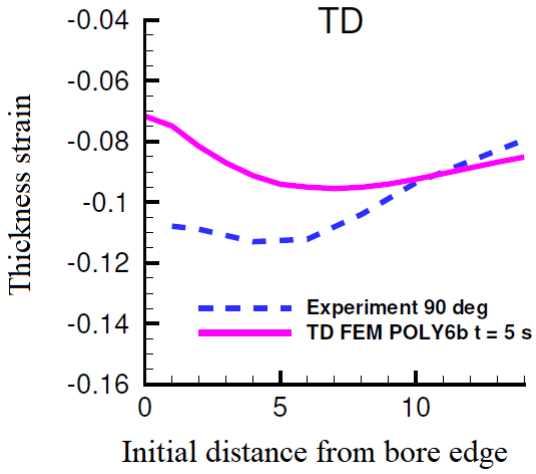

Figure 4.6: Thickness strain along the transverse direction.

4.7 Hole Expansion Simulation

Kuwabara et al. [62] hole expansion studies also documented surface deformation behavior of 780MPa. The experiment has been replicated throughout our study using polynomial yield functions of the fourth and sixth order. The experimental test substance results were released by Kuwabara et al. [62] the factors listed in Table 4.5 were based partly on the approach to direct calibration and partly on a lesser square method for the functions in 4th

and 6th order. Table 4.5 shows that all four instances of non-quadratic yield functions are purely convex using a computational minimization algorithm. The finite element layout is shown in Figure 4. 3: the punch and holding device were constructed from 8518-node solids (C3D8) used to construct sheet metal, as well as rigid shell components. The test conditions were calculated with the same weight.

There was an insignificant low friction coefficient effect and thus zero as described in this analysis. Figure 4.7 illustrates the thickness pressure at 1 mm of the bore edge. POLY6b was the closest product of checked versions. Figure 4.8 and Figure 4.9 show the thickness strain in rolling and cross directions. Finite element computing was made from a single Intel Core i7-3770 CPU, 3.7GHz, and 12 GB of RAM. The measurement time was approximately 85 minutes. On the Intel Xeon double CPU E5-2667 3.2 GHz Dell working platform, VUMAT tackled the same problem. 30 rational processors have been in place. ABAQUS The simple software is recognized to be vectorized and wall clock length to 13 minutes.

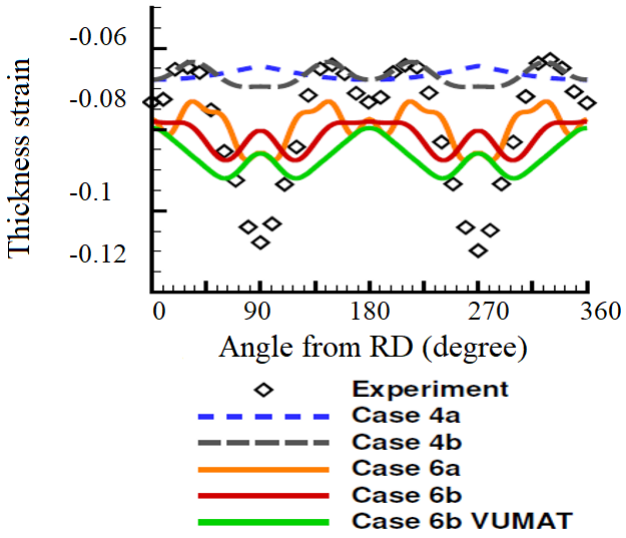

Figure 4.7: Domain comparison of thickness strain along the inner edge of the hole.

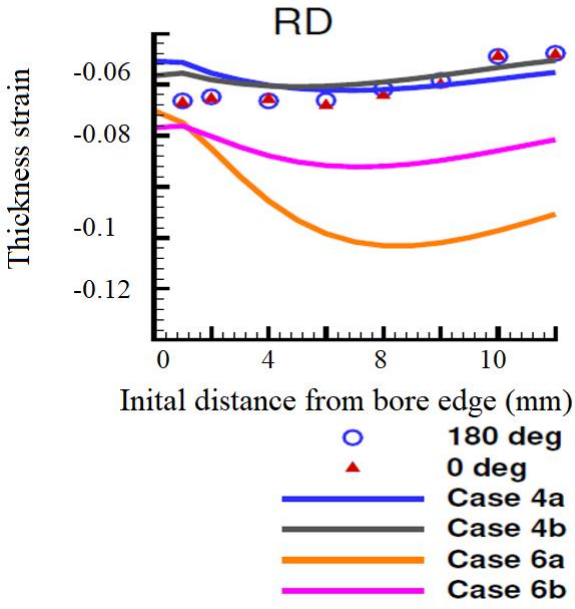

Figure 4.8: Thickness strain along the rolling direction.

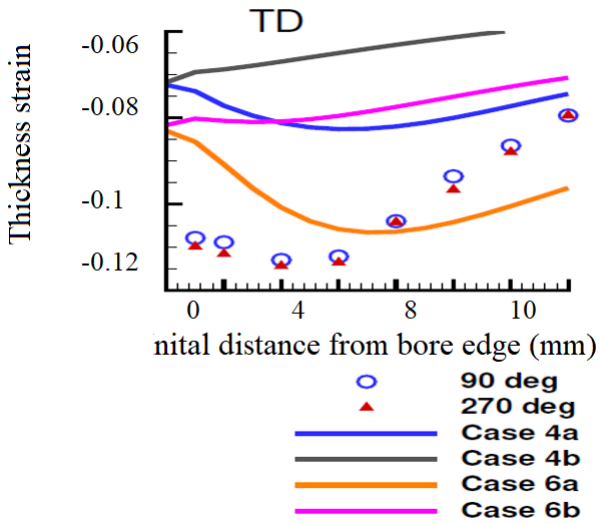

Figure 4.9: Thickness strain along the transverse direction.

Table 4.5: Coefficient values for the polynomial yield functions

Model Name	**HILL1984**	**POLY4a**	**POLY4b**	**POLY6a**	**POLY6b**
A_1	1	1	1	1	1
A_2	-0.9637	-1.94	-1.94	-2.89	-2.9
A_3	1.055	2.99	3.00	5.99	6.5
A_4	2.7507	-2.02	-2.08	-7.46	-8.2
A_5	-	0.93	0.96	6.49	8.9
A_6	-	4.34	5.86	-3.26	-3.1
A_7	-	-5.65	-5.87	1	0.95
A_8	-	4.92	5.27	3.28	5.87
A_9	-	6.54	8.07	-7.80	-14.8
A_{10}	-	-	-	19.44	31.2
A_{11}	-	-	-	-8.17	-21.6
A_{12}	-	-	-	3.46	7.36
A_{13}	-	-	-	21.87	15.77
A_{14}	-	-	-	-36.67	-34.27
A_{15}	-	-	-	24.98	21.33
A_{16}	-	-	-	21.92	24.78

4.8 Concluding Remarks

In comparison to any other strain hardening model which would always contribute to a distinctive result of a particular limit value question if its stress output feature and related flow capacity were shown to be purely positive and convex, additional plasticity stability or non-singularity of output and flow stress functions must be obtained. Most scholars, without specifying that such a study was done in their published work, have also often believed to satisfy this requirement in action. After those verifications, a non-associated model can still display a negative plastic working pattern for second-order through definite short, elastic-plastic loading-unloading cycles and cause unstable and having not

even single solution in some wedge stress regions, but in many sheet metal formations study, these troublesome loading paths or background can be rarely met. Of caution, the study of finite sheet metal formation by the non-associated model should thus test in principle either the solid necessary form of Eq. (78) is satisfied, or no stress increments join the wedge stress zone $\sigma^{\cdot}: \nabla g < 0$ if a negative, second-order plastic work rate $\sigma^{\cdot}: \varepsilon^{\cdot p} < 0$ can occur.

Also, a model for anisotropic sheets of sheets with reactive yielding pressure and in compressive plastic flow activity may be selected for non-associated or related plasticity. As shown in the analysis, if the related model is more comprehensive and accepts the same number of experimental inputs as Gotoh's quartic [58] anisotropic polynomial, almost the same modeling results are produced in uniaxial tension and equivalent biaxial tension with close modeling results in contrast to non-referred quadratic m in other biaxial tension stress conditions

The unrelated quadratic model can be used for a considerably broader field of allowable experimental inputs and easier tests of the positive characteristics and convexity of its stress functions. Besides this, the related quartic model will guarantee a special and reliable approach for sheet metal in a question of boundary interest with its verified positive and convex yield stress function without any external ambiguities and concerns. A tentative guide for determining whether such a configuration is appropriate for a specific sheet metal may be used as the framework for admissible yield stresses and plastic stress proportions of the corresponding quartic model with planar isotropy as shown in Figure 4.13.

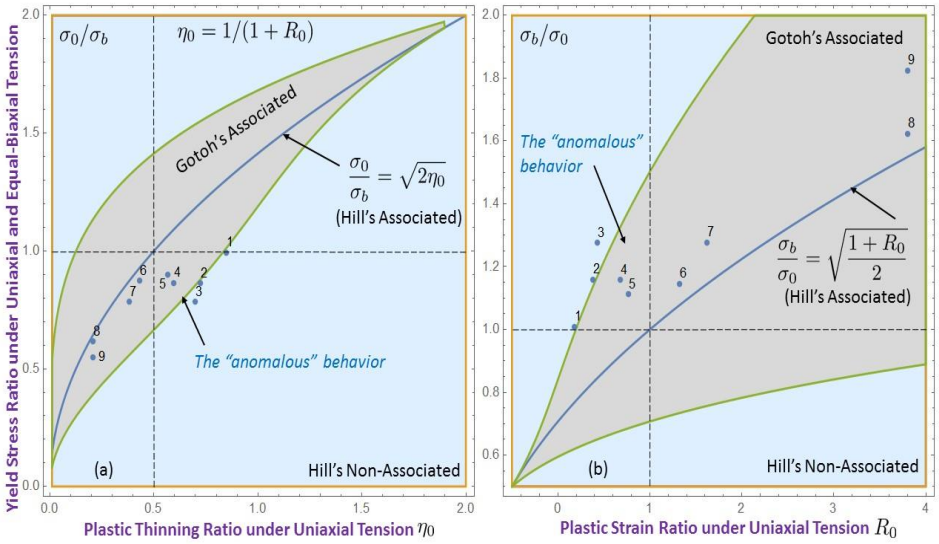

Figure 4.10: Domains of admissible yield stress and plastic strain ratios for planarly isotropic non-associated quadratic and associated quartic models versus the nine sheet metals listed in Table 4.1: (a) in terms of σ_0/σ_b vs. $\eta_0 = 1/(1 + R_0)$; b) in terms of σ_b/σ_0 vs. R_0.

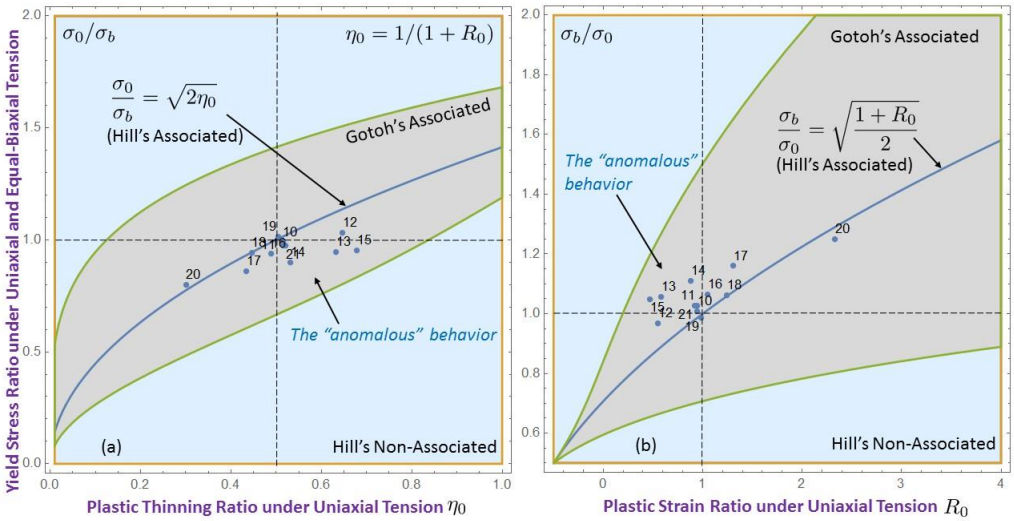

Figure 4.11: Domains of admissible yield stress and plastic strain ratios for planarly isotropic non-associated quadratic and associated quartic models versus the six non-ferrous and six steel sheet metals listed in Table 4.2 and Table 4.3 respectively: a) in terms of σ_0/σ_b vs. $\eta_0 = 1/(1 + R_0)$; (b) in terms of σ_b/σ_0 vs. R_0.

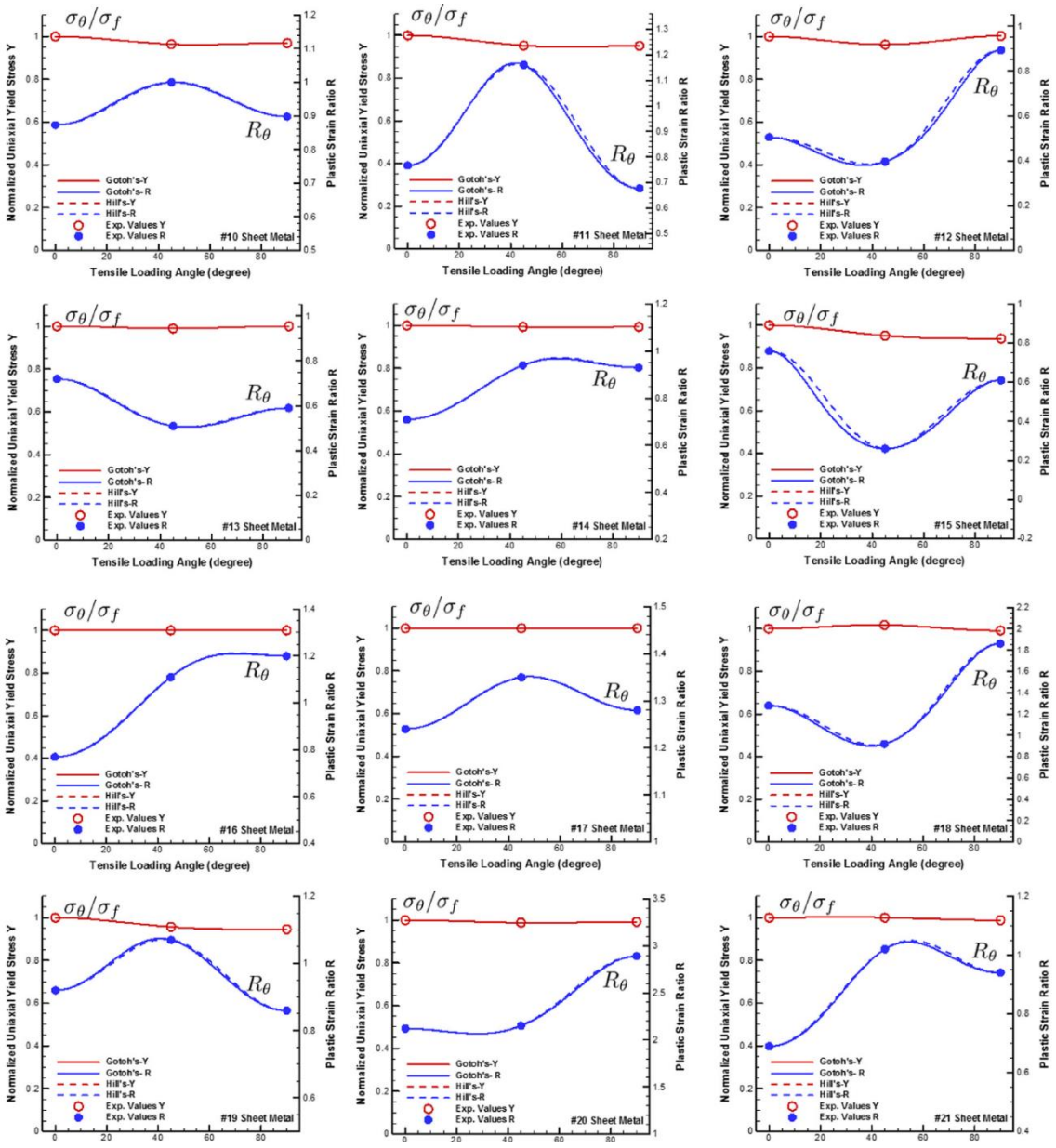

Figure 4.12: Comparison of the directional dependence of uniaxial tensile yield stress and plastic strain ratio as predicted by two models for the twelve selected sheet metals No.10-21.

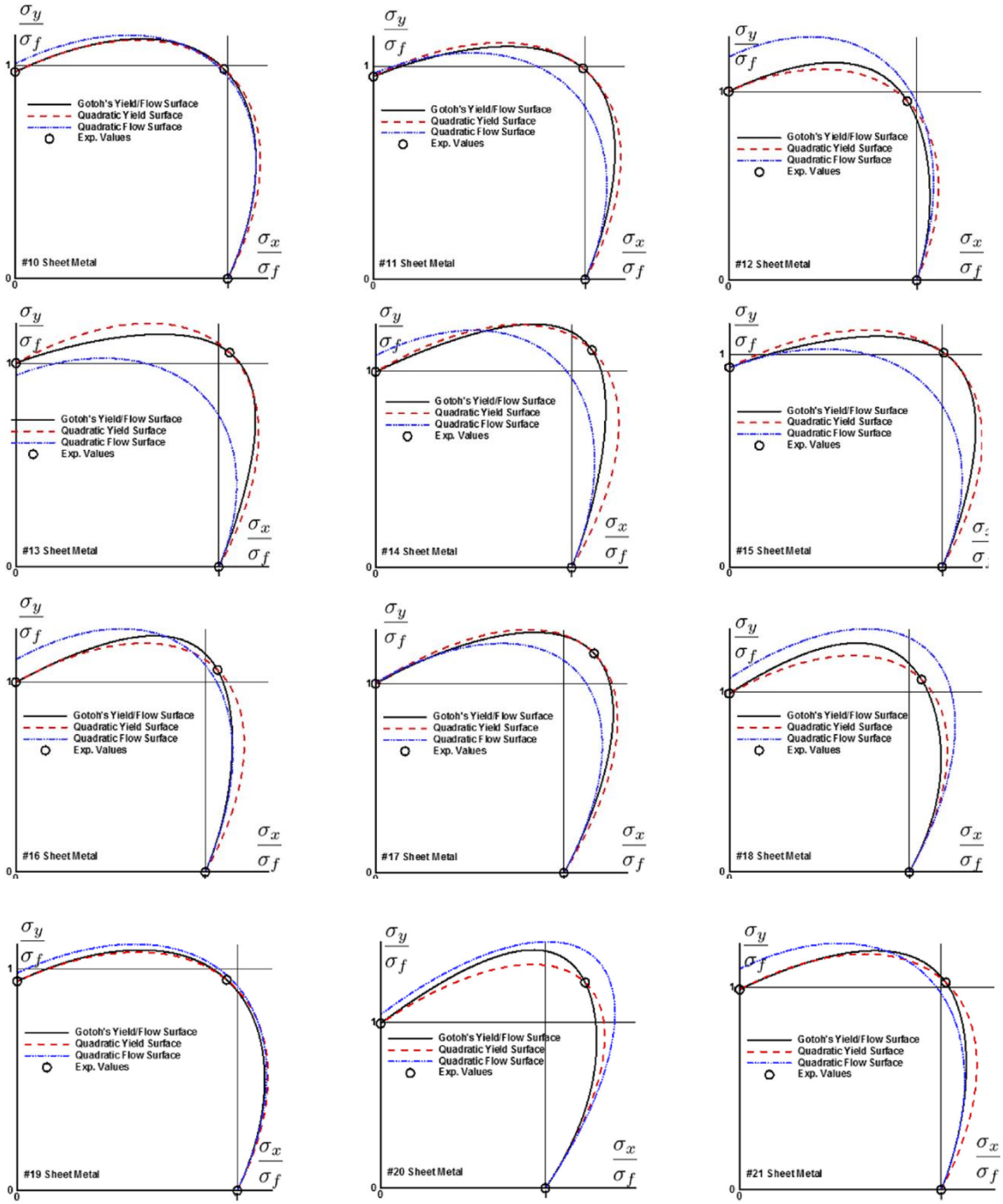

Figure 4.13: Comparison on yield and flow surfaces as predicted by two models for the twelve selected sheet metals No.10-21 under biaxial tension with $\tau_{xy} = 0$.

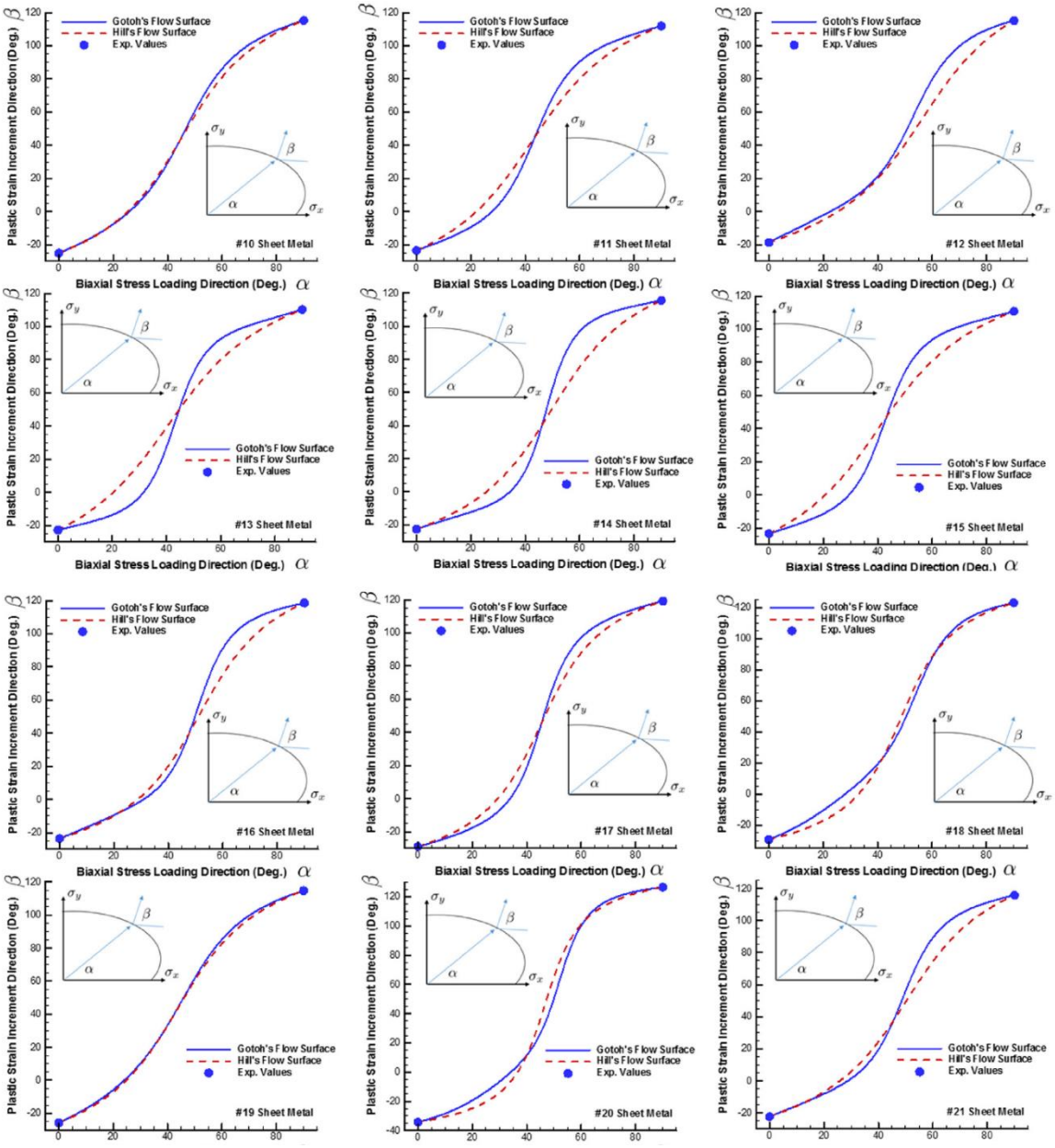

Figure 4.14: Comparison of plastic flow directions as predicted by two models for the twelve selected sheet metals No.10-21 under biaxial tension with $\tau_{xy} = 0$.

Chapter 5

Quadratic Yield Function with Enhanced Isotropic and Non-Isotropic Hardening in Associated

Author's Original Contribution

In this research study, the author has contributed to the following sections,

- Section 5.1.2: Figures 5.1-5.3
- Section 5.1.6: Shearing experiments and results on an AA6111-T4 sheet in Figures 5.5-5.10

The modeling results in Figures 5.10-5.11 are shown as maps obtained from digital image correlation analysis of different image frame numbers for various shearing test samples. An official statement endorsing this contribution in the present research study has been attached in Appendix D.

5.1 Introduction

A macroscopic anisotropic plasticity model that can adequately capture the directional and multi-axial dependence of the yielding, plastic flow, and strain hardening behavior of sheet metal is often required in analyzing and simulating an industrial forming operation of the sheet metal. The phenomenological approach treats the sheet metal as a continuum and often formulates a general mathematical framework of macroscopic anisotropic plasticity in terms of a stress-based yield function [60]. At present, a yield function that is calibrated via experimental inputs from mechanical tests is still most widely used in industrial sheet metal applications as it is both more accurate and computationally more efficient [70].

In principle, any scalar-valued function of the Cartesian stress components of the plane stress tensor $\sigma = (\sigma_x, \sigma_y, \tau_{xy})$ can be used as the plane stress yield function $f(\sigma_x, \sigma_y, \tau_{xy})$ for sheet metal as long as it is both physically consistent and mathematically concise and well-posed. In practice, three types of constraints are imposed on a yield function of sheet metal in terms of their degrees of generality. The most fundamental constraint is to require

a yield function to be positive and convex [60]. The second level of constraints is often imposed in metal plasticity, including pressure insensitive yielding, plastic incompressibility [60], and an associated (or occasionally a non-associated) flow rule [60]. The third level of constraints may often be regarded as simplifying constitutive assumptions of a reduced degree of anisotropy about strain hardening and material symmetry of a particular metal under consideration due to lack of relevant experimental inputs. Depending on the need to balance the model complexity and capabilities, various strain hardening features (isotropic, kinematic, differential, and anisotropic) and various degrees of material anisotropy (isotropic, planarly isotropic, orthotropic, and monoclinic) have been considered for sheet metal modeling in the past. A constitutive assumption about the so-called central asymmetry (that is, tension-compression asymmetry or strength differential effect) also belongs to the third type of provisional constitutive modeling constraints in metal plasticity.

Abedini et al. [60] has recently proposed a new shear constraint in their evaluation and calibration of the non-quadratic anisotropic yield stress function YLD2000-2D for two aluminum sheet metals AA2090-T3 and AA7075-T6 in-plane stress [60]. Specifically, they insist in Section 5.2 experimental results of their paper that the principal stress ratio σ_2/σ_1 and the principal plastic strain increment ratio $\varepsilon'_p/2, \varepsilon'_p/1$ should in general be the same as -1 for any orthotropic sheet metal under either pure shear stressing or pure shear straining loading conditions regardless of the loading orientation and the actual degree of plastic anisotropy in the sheet metal. In this study, we clarified in Section two types of pure shear loading conditions on a sheet metal first the difference between these two types of pure shear loading conditions often used in shear testing of sheet metal and then the difference between the on-axis/off-axis and coaxial/non-coaxial loading conditions on an orthotropic material. We next showed in Section 5.1.1 by Hill's quadratic and Gotoh's quartic anisotropic plastic models the general equivalency of these two types of 45° off-axis pure shear loading conditions but the general non-equivalence of these two types of on-axis pure shear loading conditions as given by the well-established Hill's 1948 quadratic and Gotoh's 1977 quartic anisotropic yield functions [60] In Section 5.1.6 on an AA6111-T4 sheet, we described the shearing experiments on an AA6111-T4 sheet based on two shear test coupon geometries commonly used for sheet metals. We presented in Section 5.3 some relevant

experimental results of these shearing tests which do not support the proposed shear constraint. We further pointed out that the very approximate nature of any shearing test of sheet metals in practice would not strictly and unequivocally lend itself as the physical basis at all for the universal shear constraint newly proposed by Abedini et al. [60]. In other words, such a constraint is one of the provisional third type constraints that overly restricts the well-established Hill's and Gotoh's orthotropic yield functions by reducing their total numbers of independent material constants by at least 1 and 2 respectively.

5.1.1 Two Types of Pure Shear Loading Conditions on a Sheet Metal Shear Testing and Its Three Special Cases

As the terms shear, pure shear, and simple shear are all used in the literature to the so-called shear testing [60], a concise definition will be given at first for rolled sheet metals. We adopt the principal stresses and the loading orientation angle $(\sigma_1, \sigma_2, \theta)$ or the intrinsic variables as called by Hill [60] to characterize the mechanical loading of a flat sheet metal element in-plane stress.

So $\sigma_1 > \sigma_2 \geq 0$ defines biaxial tension (uniaxial tension when $\sigma_2 = 0$) while $\sigma_1 > 0$ and $\sigma_2 < 0$ is the stress state of a material element in an in-plane shear test. If the in-plane shear test is done under displacement boundary conditions, then the principal plastic strain increments and the straining orientation angle $(\varepsilon'_p/2, \varepsilon'_p/1, \theta)$ should be used instead. As it is usually understood for an orthotropic sheet, the mechanical loading is on-axis if $\theta = 0^\circ$ or $\theta = 90^\circ$ and it is off-axis when otherwise. Furthermore, the mechanical loading is coaxial in stress and strain if $\theta = \theta$ and it is non-coaxial in stress and strain when $\theta \neq \theta$. For orthotropic sheet metals, on-axis loading is always coaxial, but off-axis loading may or may not be coaxial. For finite deformation including cases of only small strain but finite rotation, the in-plane material spin ω˙ should also be specified as part of either stress or strain-controlled loading conditions on the sheet metal test piece.

The following three cases are most relevant to our discussion here: pure shear stressing, pure shear straining, and simple shear (straining). Pure shear stressing refers to pure shear in stress inmost standard textbooks on mechanics of materials (see, e.g., page 33 of [60]) and in the anisotropic plasticity literature [60]. As a plane-stress yield function in

anisotropic plasticity is most often formulated using the applied Cauchy stress σ, the ideal shear test condition would be under pure shear in stress, that is, $\sigma_1 = -\sigma_2 > 0$, see Figure 5.1 (a). This may be accomplished in principle using a biaxial test machine with no material spin [60]. A free-end torsion test of the thin-walled tube may be approximated as a pure shear stress test with a finite material rotation if the hoop stress is zero [60].

In classical studies of elasticity and fracture mechanics of flat rubber samples, the pure shear strain test consisting of a thin rectangular rubber strip held by rigid clamps along its two long edges is often used [60]. Such a test should be more precisely called the out-of-plane pure shear strain test or the in-plane plane strain stretching for a flat test piece without material rotation. The equivalence of pure shear straining and plane-strain stretching (on two different planes of the same test piece) is due to the material incompressibility in rubber elasticity. Similarly, as shown in Figure 5.1(b), in-plane pure shear plastic straining $\varepsilon'_p/2, \varepsilon'_p/1 > 0$ or $\varepsilon'_p/2, \varepsilon'_p/1 = - \varepsilon'_p/3 = 0$ would automatically require no thickness change in sheet metal due to plastic incompressibility. It is thus equivalent to the out-of-plane plane strain stretching ($\varepsilon'_p/1 > 0$, $\varepsilon'_p/3 = 0$).

In-plane shear tests reported in the literature for sheet metals [60]. are however more commonly referred to as simple shear (straining) in-plane stress, see Figure 5.1(c). Unlike in a fixed end torsion test of thin-walled tubes, those in-plane shear tests of sheet metal in either double-shear [60] or single-shear [60] configurations do not fully and accurately prescribe the displacement boundary conditions on all four sides of a narrow rectangular gauge section as dictated by the simple shear deformation [60]. Instead, the narrow rectangular gauge section of a sheet metal test piece is sheared along its two long edges while its two short edges are stress-free. Both the free edge effect and short (narrow) gauge length make the actual stress and strain states in the gauge section of such a test piece rather non-uniform and complex [60]. Even though the center gauge region of the sheet metal shear test piece may undergo the plastic deformation very close (but not completely identical) to simple shear at finite strain levels [94], the overall quality and fidelity of the stress and strain measurement data in an in-plane simple shear test is thus rather inferior to those obtained from a standard uniaxial tensile test. Another significant difference between the simple shear and uniaxial tension tests is the large material rotation infinite simple shear.

As the initial yielding is the focus in our current investigation, pure shear straining and simple shear straining may be treated equivalently in this context (i.e., the material rotation is small at the initial stage of plastic yielding in simple shear).

5.1.2 Selected On-axis and Off-axis Pure Shear Loading Conditions

It is very important to clearly distinguish three coordinate systems commonly used in modeling and testing sheet metals in-plane stress, namely, (1) the sheet metal material symmetry axes XY (corresponding to the rolling and transverse directions of sheet metal), (2) the principal stress axes $\sigma_1\sigma_2$, and (3) the laboratory test coordinates ηζ. We give first in this subsection a somewhat detailed description of four coaxial pure shear loading cases applied to sheet metal in terms of these three coordinate systems, see Figures 5.1, 5.2, 5.3, and 5.4. The first three pure shear cases considered here correspond to the stress state points (1), (2), and (3) depicted in Figure 5.1 [76]. For simplicity, we treat the elastic deformation to be negligible in the following analysis and exclude any rigid body motion. There are two types of shearing loading conditions commonly applied to a unit square material element: pure shear stressing and simple shear straining. The term "stressing" is used here to emphasize the point that this particular pure shear is a stress-controlled loading condition. Similarly, the term "straining" is used along with simple shear to highlight that such a loading condition is strain-increment (displacement) controlled. To be specific, we define the laboratory test coordinates ηζ to be along the directions of the shearing stresses $t > 0$ or plastic shear strain increments $\gamma/2 > 0$. One peculiar feature of 45° off-axis pure shear loading conditions is the coincidence of the principal stress axes $\sigma_1\sigma_2$ in stress-controlled loading and principal plastic strain increment axes $\varepsilon'_1\varepsilon'_2$ in strain-controlled loading (see Figures 5.1 and 5.3). Following the usual practice [76], the shear test samples are also designated as RD, DD, and TD in terms of the shearing loading direction and the rolling direction of sheet metal. In an ideal pure shear stress test, the actual loading angle in terms of θ or θ differs however from the RD, DD, and TD uniaxial tensile test samples by 45°.

45-degree diagonal shearing $\xi = 45^\circ$ (on-axis loading $\theta = \theta' = 0^\circ$)

As shown in Figure 5.2(a), either a pure shear stressing, or straining condition is applied to a square unit material element aligned at a 45-degree angle from the rolling direction (x-

axis) of the sheet metal (the DD shear test sample). The same stressing and straining conditions of 45-degree diagonal shearing may be described in terms of the unit material element aligned along the principal stress axes (and the sheet metal material symmetry axes too in this case) shown in Figure 5.2(b). Using the Cartesian components in the sheet metal material symmetry coordinate system, the pure shear yield stress and plastic strain increment tensors are shown in Figure 5.2(a) are given respectively as

$$(\sigma_x, \sigma_y, \tau_{xy})ps1 = (\tau, -\tau, 0), (\varepsilon'_x, \varepsilon'_y, \varepsilon'_{xy}) = (\frac{\dot{\gamma}}{2}, -\frac{\dot{\gamma}}{2}, 0) \quad (79)$$

The same pure shear yield stress and plastic strain increment tensors in terms of the principal stress axes shown in Figure 5.2(b) are given respectively as

$$(\sigma_2, \sigma_2, \theta)ps1 = (\tau, -\tau, 0), (\varepsilon'_x, \varepsilon'_y, \varepsilon'_{xy}) = (\frac{\dot{\gamma}}{2}, -\frac{\dot{\gamma}}{2}, 0) \quad (80)$$

where the stress loading orientation angle θ is defined as the angle between σ_1 and the rolling direction of the sheet metal with $\sigma_1 \geq \sigma_2$ [95] The plastic strain increment loading orientation angle θ is defined as the angle between ε'_1 and the rolling direction of the sheet metal with $\varepsilon'_1 \geq \varepsilon'_2$.

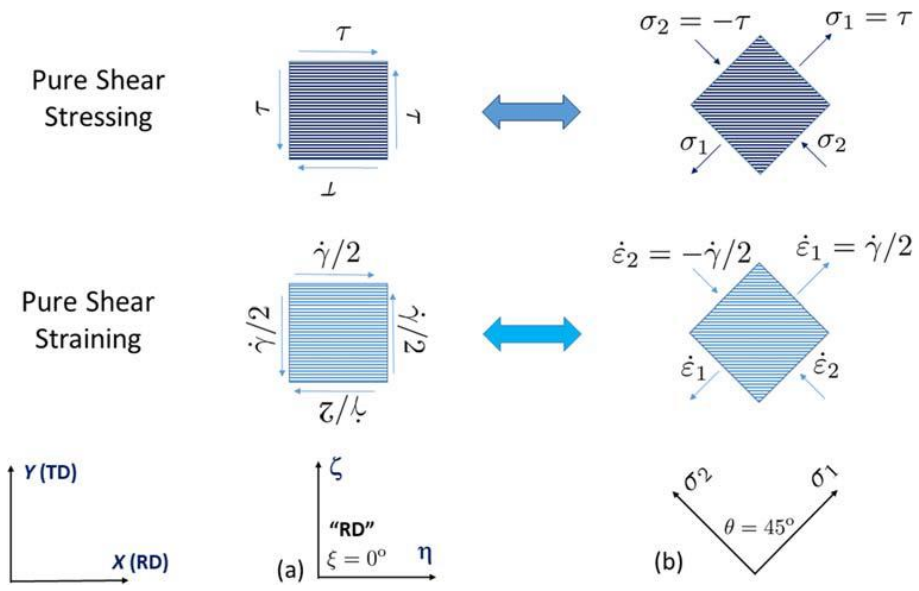

Figure 5.1: Pure shear stressing and straining of sheet metal with 0-degree parallel to its material coordinates xy: (a) the RD material element edges aligned with the laboratory (shearing) coordinates ηζ; (b) the material element edges aligned with principal stress axes $\sigma_1\sigma_2$.

In general, $\theta' \neq \theta$ but here $\theta' = \theta = 0$ is always held for the on-axis pure shear (but $\xi = 45^\circ$!).

The subscripts "ps1" and "ss1" are used to designate the first case of the pure shear stressing and straining conditions, respectively.

0-degree parallel shearing $\xi = 0^{\circ}$ (special off-axis loading = $\theta^{\cdot} = 45^{\circ}$)

As shown in Figure 5.1(a), either pure shear stressing, or straining may be applied to a square unit material element aligned with the rolling direction (*x*-axis) of the sheet metal (the RD shear test sample). They shall be called 0-degree parallel shearing loading conditions and may be described in terms of the unit material element aligned with the principal stress axes shown in Figure 5.1(b) as well. Using the Cartesian components in the sheet metal material symmetry coordinate system (at a 45-degree angle clockwise from the principal stress axes), the pure shear yield stress and plastic strain increment tensors are shown in Figure 5.1(a) are given respectively as

$$(\sigma_x, \sigma_y, \tau_{xy})ps2 = (\tau, -\tau, 0), (\varepsilon'_x, \varepsilon'_y, \varepsilon'_{xy})ss2 = (0,0\frac{\dot{\gamma}}{2}) \tag{81}$$

The corresponding representation of the same pure shear stressing and straining conditions in terms of the principal stresses and plastic strain increments shown in Figure 5.1(b) are given respectively as

$$(\sigma_1, \sigma_2, \theta)ps2 = (\tau, -\tau, 45°), (\varepsilon'_1, \varepsilon'_2, \theta)ss2 = (\frac{\dot{\gamma}}{2}, -\frac{\dot{\gamma}}{2}, 45°) \tag{82}$$

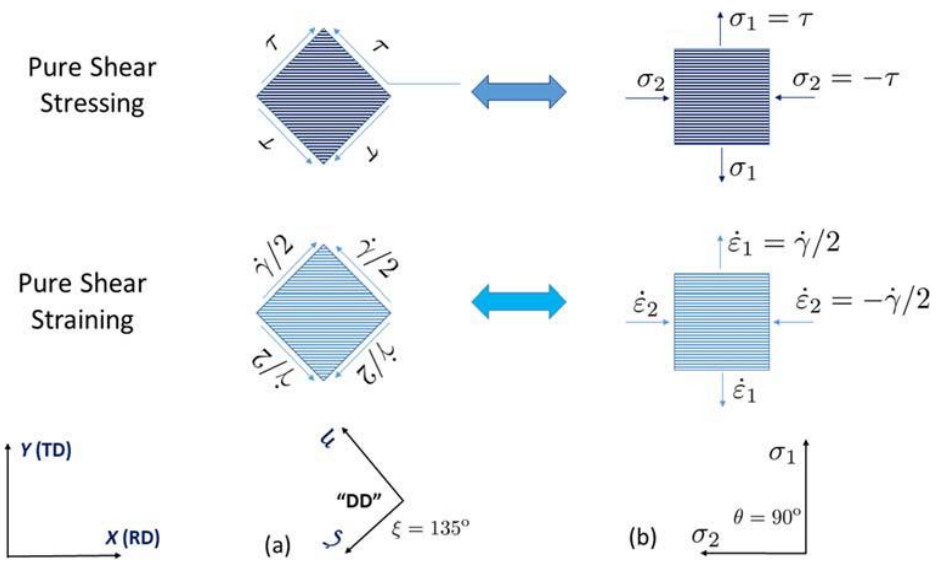

Figure 5.2: Pure shear stressing and straining of sheet metal at 135-degree diagonal to its material coordinates xy: (a) the material element edges aligned with the laboratory (shearing)

coordinates ηζ; (b) the material element edges aligned with principal stress axes $\sigma_1\sigma_2$.

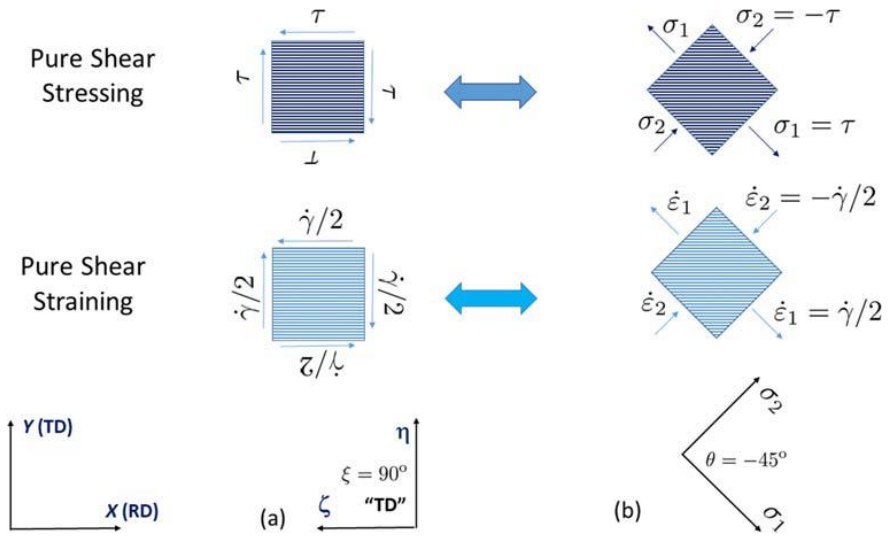

Figure 5.3: Pure shear stressing and straining of sheet metal with 90-deg or perpendicular to its material coordinates xy: (a) the TD material element edges aligned with the laboratory (shearing) coordinates ηζ ;(b) the material element edges aligned with principal stress axes $\sigma_1\sigma_2$.

135-degree diagonal shearing $\xi = 135^\circ$ (on-axis loading $\theta = \theta^{'} = 90^\circ$)

When the shear stress or plastic shear strain increments are applied in the opposite directions to a square unit material element shown in Figure 5.2(a), the pure shear loading condition will be called 135-degree diagonal shearing, see Figure 5.3(a). The corresponding stressing and straining conditions in terms of the unit material element aligned along the principal stress axes are shown in Figure 5.2(b) which are the ones shown in Figure 5.3(b) rotated counterclockwise by 90-degree. The pure shear stress and strain increment tensors are shown in Figure 5.2(a) are given respectively in terms of the cartesian components in the sheet metal material symmetry coordinate system as

$$(\sigma_x, \sigma_y, \tau_{xy})ps3 = (-\tau, \tau, 0), (\varepsilon'_1, \varepsilon'_2, \theta)ss3 = (-\frac{\dot{\gamma}}{2}, \frac{\dot{\gamma}}{2}, 0) \tag{83}$$

The same pure shear stress and plastic strain increment tensors in terms of the principal stresses and strain increments shown in Figure 5.3(b) are given respectively as

$$(\sigma_1, \sigma_2, \theta)ps3 = (\tau, -\tau, 90°), (\varepsilon'_1, \varepsilon'_2, \theta)ss3 = (\frac{\dot{\gamma}}{2}, -\frac{\dot{\gamma}}{2}, 90°) \tag{84}$$

90-degree perpendicular shearing $\xi = 90^\circ$ (special off-axis loading $\theta = \theta^{'} = -45^\circ$)

For completeness, we also consider the case of 90-degree parallel shearing shown in Figure

5.3(a), that is, the square unit material element under shearing is aligned with the transverse direction (y-axis) of the sheet metal (the TD shear test sample). The pure shear stress and plastic strain increment tensors are shown in Figure 5.3(a) are given respectively in terms of the cartesian components in the sheet metal material symmetry coordinate system (at a 45-degree angle clockwise from the principal stress axes) as

$$(\sigma_x, \sigma_y, \tau_{xy})ps4 = (0,0-\tau), (\acute{\varepsilon}_x, \acute{\varepsilon}_y, \acute{\varepsilon}_{xy})ss4 = (0,0,-\frac{\dot{\gamma}}{2}) \quad (85)$$

The corresponding representation of the same pure shear loading conditions in terms of the principal stresses and plastic strain increments shown in Figure 5.3(b) are given respectively as

$$(\sigma_1, \sigma_2, \theta)ps4 = (\tau, -\tau, -45°), (\varepsilon'_1, \varepsilon'_2, \theta)ss4 = (\frac{\dot{\gamma}}{2}, -\frac{\dot{\gamma}}{2}, -45°) \quad (86)$$

5.1.3 Modeling Pure Shear by Hill's Quadratic and Gotoh's Quartic Anisotropic Plastic Models

We are now ready to compute the plastic strain increments from an applied pure shear yield stress and to evaluate the yield stress components from an applied simple shear plastic strain increment for four shearing loading cases detailed in the previous section. More specifically, we seek after the ratio of principal strain increments $\varepsilon'_2/\varepsilon'_1$ per pure shear in stress and the ratio of principal stresses σ_2/σ_1 per simple shear or pure shear in the strain as predicted by Hill's quadratic yield/flow functions and Gotoh's quartic yield function given in Appendix.

5.1.4 Principle Plastic Strain Increment Ratio in Pure Shear

Per the yield functions and flow rule $\acute{\varepsilon}^p = \lambda \partial g/\partial \sigma$ given in Appendix, the plastic strain increments are readily computed in terms of the three stress components in the sheet metal material symmetry coordinate system as

$$\varepsilon'_x = \lambda \partial g/\partial \sigma_x, \varepsilon'_y = \lambda \partial g/\partial \sigma_y, \dot{\gamma}_{xy} = 2\varepsilon' xy = \lambda \partial g/\partial \tau_{xy} \quad (87)$$

For an associated Hill's quadratic model ($g^2 = \Phi_{2y}$), *the* plastic strain increments for the four pure shear plane stress states given by Eqs. $(78)_1$, $(80)_1$, $(5)_1$ and $(87)_1$ is (the common

factor $\lambda\tau/(2g)$ is dropped for simplicity)

$$\begin{gathered}
\left(\varepsilon'_x, \varepsilon'_y, \varepsilon'_{xy}\right)\frac{h}{ps1} \propto (2Y_1 - Y_2, Y_2 - 2Y_3, 0), \\
\left(\acute{\varepsilon}_x, \acute{\varepsilon}_y, \acute{\varepsilon}_{xy}\right)\frac{h}{ps2} \propto (0,0, Y_4), \\
\left(\varepsilon'_x, \varepsilon'_y, \varepsilon'_{xy}\right)\frac{h}{ps3} \propto (-2Y_1 + Y_2, -Y_2 + 2Y_3, 0), \\
\left(\varepsilon'_x, \varepsilon'_y, \varepsilon'_{xy}\right)\frac{h}{ps4} \propto (0,0, -Y_4)
\end{gathered} \tag{88}$$

The corresponding principal plastic strain increments and straining orientation angle are

$$\begin{gathered}
(\varepsilon'_1, \varepsilon'_2, \theta)\frac{h}{ps1} \propto (2Y_1 - Y_2, Y_2 - 2Y_3, 0), \\
(\varepsilon'_1, \varepsilon'_2, \theta)\frac{h}{ps2} \propto (Y_4, -Y_4, 45°), \\
(\varepsilon'_1, \varepsilon'_2, \theta)\frac{h}{ps3} \propto (-Y_2 + 2Y_3, -2Y_1 + Y_2, 90°), \\
(\varepsilon'_1, \varepsilon'_2, \theta)\frac{h}{ps4} \propto (Y_4, -Y_4, -45°)
\end{gathered} \tag{89}$$

In the case of using a non-associated Hill's model ($g^2 = \Phi_{2p}$), the above results are still applied with material constants (Y_1, Y_2, Y_3, Y_4) being replaced by material constants (P_1, P_2, P_3, P_4). For an associated Gotoh's quartic model ($g^4 = \Phi_4$), the plastic strain increments for the same four pure shear loading cases are computed straightforwardly as (the common factor $\lambda\tau^3/(4g^3)$ is dropped for simplicity)

$$\begin{gathered}
\left(\varepsilon'_x, \varepsilon'_y, \varepsilon'_{xy}\right)\frac{h}{ps1} \propto (4A_1 - 3A_2 + 2A_3 - A_4, A_2 - 2A_3 + 3A_4 - 4A_5, 0), \\
\left(\varepsilon'_x, \varepsilon'_y, \varepsilon'_{xy}\right)\frac{h}{ps2} \propto (0,0,2A_9), \\
\left(\varepsilon'_x, \varepsilon'_y, \varepsilon'_{xy}\right)\frac{h}{ps3} \propto (-4A_1 + 3A_2 - 2A_3 + A_4, -A_2 + 2A_3 - 3A_4 + 4A_5, 0) \\
\left(\varepsilon'_x, \varepsilon'_y, \varepsilon'_{xy}\right)\frac{h}{ps4} \propto (0,0, -2A_9),
\end{gathered} \tag{90}$$

The corresponding principal plastic strain increments and straining orientation angle are

$$(\varepsilon'_1, \varepsilon'_2, \theta)\frac{h}{ps1} \propto (4A_1 - 3A_2 + 2A_3 - A_4, A_2 - 2A_3 + 3A_4 - 4A_5, 0),$$

$$(\varepsilon'_1, \varepsilon'_2, \theta)\frac{h}{ps2} \propto (2A_9, -2A_9, 45°), \tag{91}$$

$$(\varepsilon'_1, \varepsilon'_2, \theta)\frac{h}{ps3} \propto (-A_1 + 2A_3 - 3A_4 + 4A_5, -4A_1 + 3A_2 - 2A_{43} + A_4, 90°)$$

$$(\varepsilon'_1, \varepsilon'_2, \theta)\frac{h}{ps4} \propto (2A_9, -2A_9, -45°),$$

5.1.5 Principle Stress Ratio in Pure Shear Straining

When the plastic loading condition is imposed by prescribing all plastic strain increment components (consistent with the plastic incompressibility), the corresponding yield stress components may be computed from both the flow rule and yield condition. As we are mostly interested in the principal stress ratio in simple shear straining, only the relative values among the stress components $(\sigma_x, \sigma_y, \tau_{xy})$ are first sought from the given plastic strain increments $(\varepsilon'_x, \varepsilon'_y, \varepsilon'_{xy})$ One can show that the associated Hill's quadratic model gives the following cartesian components of strain increments in terms of stresses for the four simple shear straining conditions defined by Eqs. $(78)_2$, $(80)_2$, $(83)_2$ and $(87)_2$ (again any common factor is dropped for simplicity)

$$\begin{aligned}\left(2Y_1\sigma_x + Y_2\sigma_y, Y_2\sigma_x + 2Y_3\sigma_y, Y_4\tau_{xy}\right)\frac{h}{ss1} \\ \propto \left(\frac{\dot{\gamma}}{2}, -\frac{\dot{\gamma}}{2}, 0\right), \left(2Y_1\sigma_x + Y_2\sigma_y, Y_2\sigma_x \right. \\ \left. + 2Y_3\sigma_y, Y_4\tau_{xy}\right)\frac{h}{ss2} \propto (0,0,\dot{\gamma})\end{aligned} \tag{92}$$

One can thus obtain the corresponding principal stress ratio for each case as

$$(\sigma_1, \sigma_2, \theta)\frac{h}{ss1} = (\sigma_x, \sigma_y, 0): \left(\frac{\sigma_2}{\sigma_1}\right)\frac{h}{ss1} = -\frac{2Y_1 + Y_2}{Y_2 + 2Y_3};$$

$$(\sigma_1, \sigma_2, \theta)\frac{h}{ss2} = (\tau_{xy}, -\tau_{xy}, 45°): \left(\frac{\sigma_2}{\sigma_1}\right)\frac{h}{ss2} = -1;$$

$$(\sigma_1,\sigma_2,\theta)\frac{h}{ss2}=(\tau_{xy},-\tau_{xy},45°):\left(\frac{\sigma_2}{\sigma_1}\right)\frac{h}{ss2}\ =\ -1;$$
$$(\sigma_1,\sigma_2,\theta)\frac{h}{ss3}=(\ \sigma_x,\sigma_y,90°):\left(\frac{\sigma_2}{\sigma_1}\right)\frac{h}{ss3}\ =\ -\frac{Y_2\ +\ 2Y_3}{2Y_1\ +\ Y_2};$$
$$(\sigma_1,\sigma_2,\theta)\frac{h}{ss4}=(\tau_{xy},-\tau_{xy},45°):\left(\frac{\sigma_2}{\sigma_1}\right)\frac{h}{ss4}\ =\ -1;\qquad(93)$$

Again, the above results are applied to a non-associated. Hill's model too with material constants (Y_1, Y_2, Y_3, Y_4) being replaced by (P_1, P_2, P_3, P_4). Recall from the associated flow rule, the Gotoh's quartic model gives the plastic strain increments in plane-stress as (without any common factor for simplicity)

$$\varepsilon'_x\propto 4A_1\sigma_x^2\ -\ 3A_2\sigma_x^2\sigma_y+2\sigma_y^2\sigma_xA_3-A_4\sigma_y^3,A_6\sigma_x\tau_{xy}^2+2A_7\sigma_y\tau_{xy}^2;$$
$$\varepsilon'_y\propto A_2\sigma_x^3+2A_3\sigma_x^2\sigma_y+3\sigma_y^2\sigma_xA_4+4A_5\sigma_y^3,A_7\sigma_x\tau_{xy}^2+2A_8\sigma_y\tau_{xy}^2;$$
$$\varepsilon'_y\propto A_2\sigma_x^3+2A_3\sigma_x^2\sigma_y+3\sigma_y^2\sigma_xA_4+4A_5\sigma_y^3,A_7\sigma_x\tau_{xy}^2+2A_8\sigma_y\tau_{xy}^2;\qquad(94)$$
$$2\varepsilon'_{xy}=\gamma_{xy}\propto A_6\sigma_x^2\tau_{xy}+A_7\sigma_x\sigma_y\tau_{xy}+A_8\sigma_y^2\tau_{xy}+2A_9\tau_{xy}^3$$

For the same four simple shear straining conditions defined by Eqs. $(78)_2$, $(80)_2$, $(85)_2$ and $(87)_2$, one has the following plane-stress results

$$\begin{aligned}(\sigma_1,\sigma_2,\theta)\frac{g}{ss1}&=(\ \sigma_x,\sigma_y\ ,0):(4A_1+(3k_1+1)A_2+2(k_1^2+k_1)A_3\\&\quad+(k_1^3+3k_1^2)A_4+4k_1^3A_5=0\ );(\sigma_1,\sigma_2,\theta)\frac{g}{ss2}\\&=(\tau_{xy},-\tau_{xy},45°):\left(\frac{\sigma_2}{\sigma_1}\right)\frac{g}{ss2}\ =\ -1;\\(\sigma_1,\sigma_2,\theta)\frac{g}{ss3}&=(\ \sigma_x,\sigma_y\ ,0):(4(k_2^3A_1+(3k_2^2+k_2^3)A_2\\&\quad+2(k_2^2+k_2)A_3+(1+3k_2)A_4+4A_5\\&\quad=0);(\sigma_1,\sigma_2,\theta)\frac{g}{ss4}=(\tau_{xy},-\tau_{xy},45°):\left(\frac{\sigma_2}{\sigma_1}\right)\frac{g}{ss4}\\&\quad=\ -1;\end{aligned}\qquad(95)$$

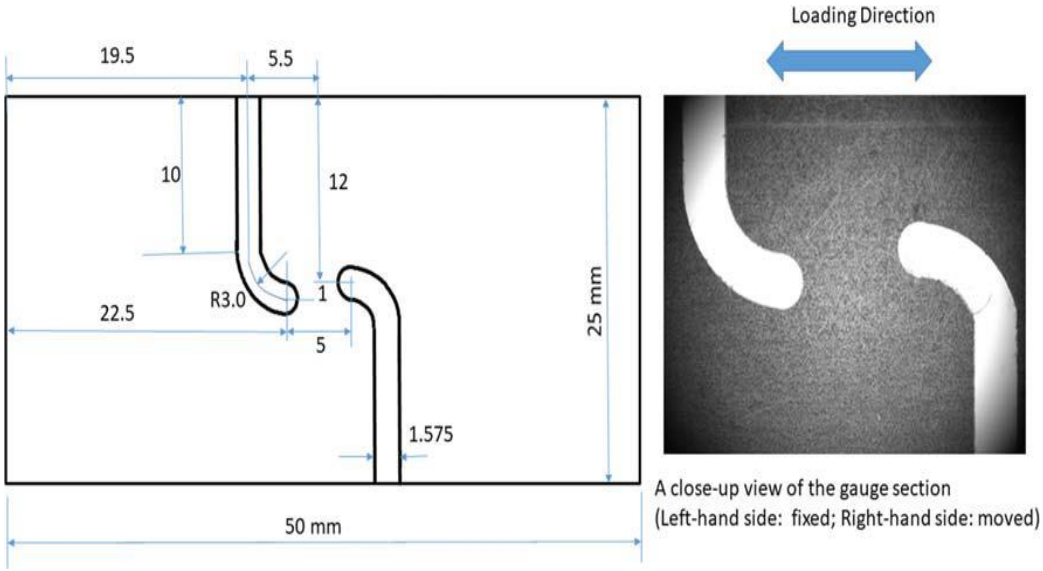

Figure 5.4: Dimensions of Type-A shearing test coupon and a close-up view image of an as-machined AA6111-T4 sheet sample with a thickness of 1.2mm.

where $\kappa_1 = (\frac{\sigma 2}{\sigma 1})\ \frac{g}{ss1}$ and $\kappa_2 = (\frac{\sigma 2}{\sigma 1})\ \frac{g}{ss3}$ are principal stress ratios given by Gotoh's yield function in simple shear loading cases #1 and #3 and they may be solved per a cubic algebraic equation for the known material constants (A_1, A_2, A_3, A_4, A_5) of given sheet metal.

5.1.6 Shearing Experiments and Results on An AA6111-T4 Sheet

It is important to note that the origin of the newly proposed shear constraint by Abedini et al. [76] was motivated in part in their effort to incorporate shearing test results into the calibration of an anisotropic yield function. Here we present some shearing experiments of our own on an AA6111-T4 sheet with two different test coupon designs. Shearing test results from our experiments were shown to highlight the difference between the idealized pure shear loading conditions and deformation states described in section modeling pure shear by Hill's quadratic and Gotoh's quartic anisotropic plastic models and the actual loading conditions and deformation states obtained in practice in a shearing test used for sheet metals.

5.1.7 Two Sheet Metal Shearing Test Using a Universal Materials Testing

Due to their comparative simplicity, shearing tests of sheet metal are most commonly

carried out using specially designed test coupons loaded in tension on universal materials testing machine [87, 89, 94, 96, 97]. Two of the shear test coupon designs without the need of removing any surface layer of the sheet metal were considered in this study: Type A as shown in Figure 5.4 per [76, 94] and Type-B as shown in Figure 5.4 per [88, 98]. The actual dimensions of each test coupon geometry used in this study are given in mm in each figure. Each shear test coupon was cut from an aluminum alloy sheet metal AA6111-T4 of 1.2mm in thickness on a CNC machine (Computer Numerical Control) using an end mill of 0.062 inches in diameter. A digital image of a close-up view of the shearing zone of each as-machined AA6111-T4 sheet test coupon is shown as an insert in each figure. The representative tensile properties of the aluminum sheet metal have been reported elsewhere [99]. The yield stresses and plastic strain ratios from three standard uniaxial tension tests on AA6111-T4 sheet used in this study are (σ_0, σ_{45}, σ_{90}) = (174.1, 173.4, 166.7) MPa and (R_0, R_{45}, R_{90}) = (0.93, 0.41, 0.66).

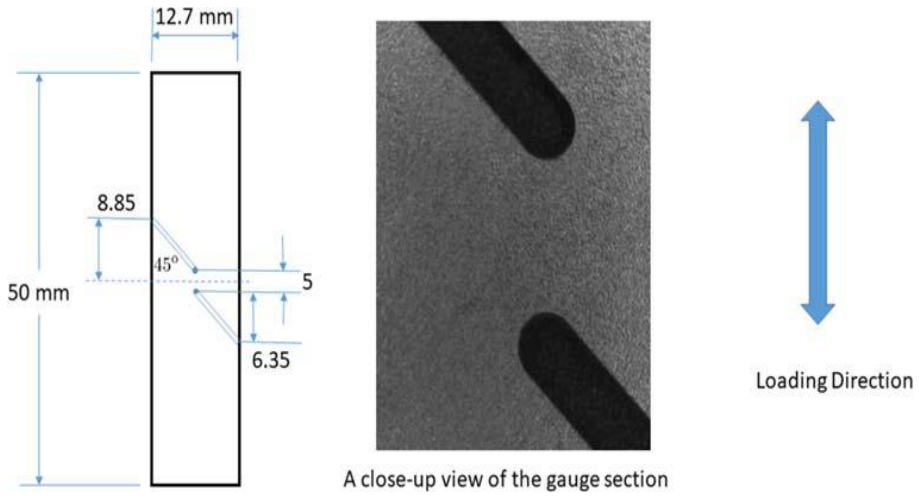

Figure 5.5: Dimensions of Type-B shearing test coupon and a close-up view image of an as-machined AA6111-T4 sheet sample with a thickness of 1.2mm.

The shearing experiments using Type-A and Type-B test coupons were carried out in the displacement control mode on an Instron 5967 universal materials test machine with a 30 kN static load cell. A constant crosshead speed of 1.8 mm/min was used in all experiments. A pair of RD and DD samples of Type-A and Type-B coupons were tested. They consist of samples subjected to the tensile loading along the RD and along with the DD or 45-

degree from the RD of the sheet metal, respectively. Each test coupon was held at both ends by a pair of wedge grips with flat but serrated faces and was tensile loaded to final fracture while the upper crosshead displacement and load cell readings were recorded continuously at 100 Hz data acquisition rate. During each shearing test, a monochrome digital CCD camera from Point Grey Research Inc. (www.ptgrey.com) with a zoom lens was used to image one surface of the shearing zone of the test sample at 1 frame per second. A total of about 100 images were acquired for each test. Each image has a size of 3376-by-2704 pixels with a typical pixel resolution of around 2.7 microns/pixel. Whole-field strain maps of the sheared samples at various deformation stages up to the maximum load level were obtained by digital image correlation (DIC) of in-situ acquired sample images based on the Lucas-Kanade inverse compositional algorithm [100-102]. At this particular magnification of the experiments, the natural contrast pattern on the surface of as-received aluminum sheet metals was used for the image-based deformation analysis (i.e., no sprayed paint droplets or ink marks were ever applied to the sample surfaces). A typical local DIC analysis used a subset of 61-by-61 pixels over 5-by-5-pixel grid spacing. The average displacement gradients were computed over each subset to obtain its local logarithmic strains commonly used in metal plasticity. For a few images at the very initial stage of each test, a large subset up to twice as big was used to reduce the noise levels in the local strain mapping data.

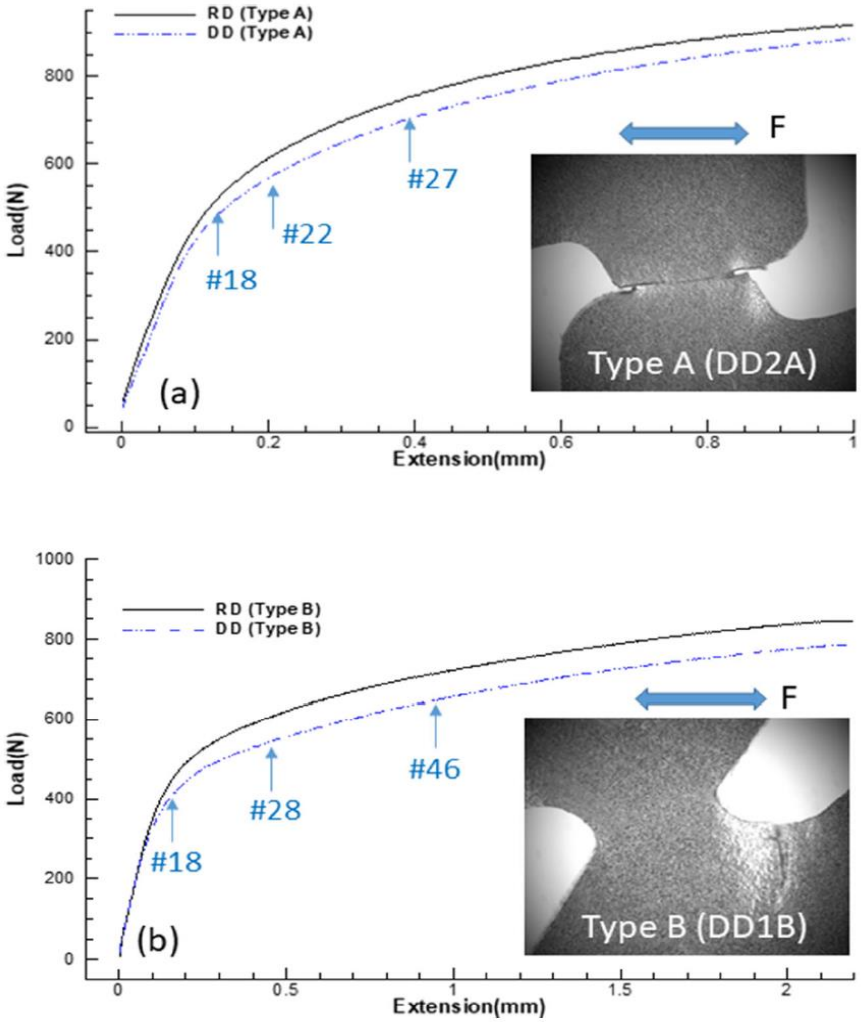

Figure 5.6: The load versus displacement data from four shearing tests on AA6111-T4 sheet: a two Type-A samples RD2A and DD2A; b two Type-B samples RD1B and DD1B. Frame numbers of three representative images recorded for DD2A and DD1B samples are also marked at their corresponding load and displacement levels. Images of shear test samples DD2A and DD1B after fracture are also inserted here.

5.2 Experimental Results

The measured tensile load versus the crosshead displacement data for shearing tests of the two Type-A samples (RD2A and DD2A) are shown in Figure 5.4(a). There is a significant difference between the RD2A and DD2A samples, reflecting the plastic anisotropy of the material. As shown in Figure 5.4(b), a similar difference between the RD1B and DD1B samples of Type-B was also observed in the measured tensile load versus the crosshead displacement data. That is, the load levels of the DD samples of both Type-

A and Type-B at a given displacement were found to be lower than those of the RD samples. Also shown in Figure 5.4(a) and (b) are the images of the fractured shear test samples DD2A and DD1B. Unlike the Type-A samples that failed in shear right at the gauging zone, all Type-B samples failed due to the tensile fracture at the location far away from the initial shearing zone (noting the applied loading direction for both samples in Figure 34(a) and (b) is horizontal).

Following the usual practice [76, 88, 94], one may obtain the nominal shear stress-strain curves ($\tau\eta\zeta$ vs $\gamma\eta\zeta$) for these four shear tests. The initial portion of their shear stress-strain curves up to shear strain $\gamma\eta\zeta$ = 0.24 is shown in Figure 5.4 Here the shear stress is the average shear stress over the cross-section across the narrowest width (along the horizontal tensile direction or η-axis) of the shearing zone in each sample. That is, $\tau\eta\zeta = F\eta / A_0 = F\eta / (w_0\, t_0)$, where $F\eta$ is the applied tensile force at the two ends of each shear sample and w_0 and t_0 is the initial width and thickness of the *out-of-plane* shearing zone cross-section. In our study here, w_0=3.568mm and 3.425mm respectively for Type-A and Type-B samples and t_0 = 1.2mm (so the aspect ratio of the shearing zone cross-section is about 3). The shear strain $\gamma\eta\zeta$ is the average of the local (logarithmic) shear strains obtained by the digital image correlation over the *in-plane* narrow rectangular region of the shearing zone in each sample. The region for computing the average shear strain is shown as a white horizontal rectangle on the image inserts of Figure 5.5 for a Type-A sample DD2A and a Type-B sample DD1B. The vertical height of the region h_0 is chosen to be about 0.350-0.375 mm (so the aspect ratio of the in-plane local rectangular gauge section is about 10). If one assumes that the shearing zone of each sample is under predominantly pure shear stressing loading initially (i.e., neglecting any in-plane normal stresses $\sigma\eta$ and $\sigma\zeta$), then the loading angle θ is thus approximately to be 45° for RD samples and 0° for DD samples (see section Two types of pure shear loading conditions on sheet metal for details). The initial yield stresses were obtained by a large offset method as $\sigma s45$ = 116.8 MPa and 113.1 MPa for the two RD samples (RD2A and RD1B) and as $\sigma s0$ = 104.8 MPa and 105.4 MPa for the two DD samples (DD2A and DD1B).

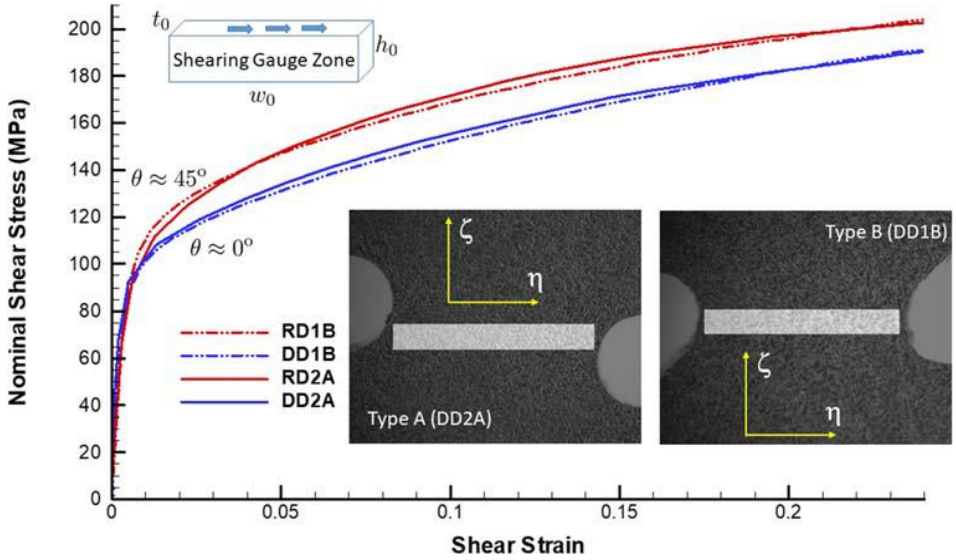

Figure 5.7: The nominal shear stress τηζ versus shear strain γηζ curves from the four shearing tests on AA6111-T4 sheet. The laboratory loading and measurement coordinates ηζ are shown in the image inserts of two selected samples DD2A and DD1B. A 3D schematic of the nominal shearing gauge zone with its width w_0, height h_0, and thickness t_0 is also given.

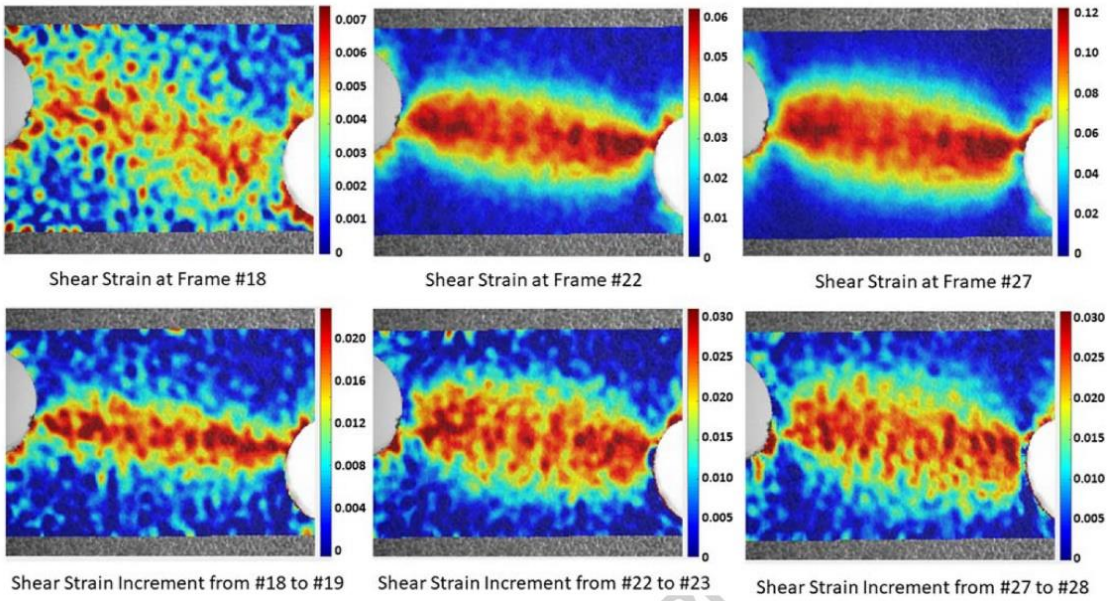

Figure 5.8: The total shear strain γηζ maps obtained from a digital image correlation analysis of image frame numbers 18, 22, and 27 for the shearing test sample DD2A. The corresponding incremental shear strain Δγηζ maps obtained from a digital image correlation analysis of image pairs 18-19, 22-23, and 27-28 are also shown in the lower half of the figure.

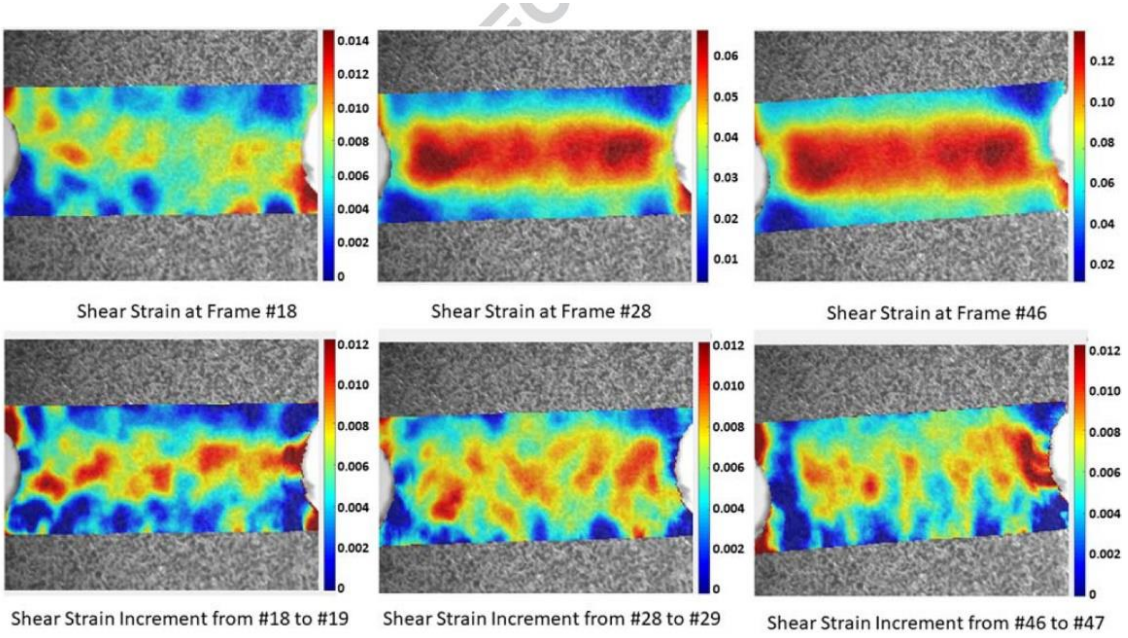

Figure 5.9: The total shear strain γηζ maps obtained from a digital image correlation analysis of image frame numbers 18, 28, and 46 for the shearing test sample DD1B. The corresponding incremental shear strain Δγηζ maps obtained from a digital image correlation analysis of image pairs 18-19, 28-29, and 46-47 are also shown in the lower half of the figure.

The actual state of the in-plane surface deformation inside the shearing gauge zone (w_0-by-h_0) and its surrounding regions of the two shearing test samples DD2A and DD1B in terms of total and incremental shear strain maps are shown in Figures 5.6 and 5.7 respectively for three selective load and deformation levels. Frame numbers of the images at those load and displacement levels during the tests of DD2A and DD1B samples are indicated in Figure 5.6(a) and (b). Those images approximately correspond to the average shear strains $\gamma\eta\zeta$ = 0.01, 0.05, and 0.1 of Figure 5.5. Also shown in both Figures 5.6 and 5.7 are the incremental shear strain maps for these two shearing test samples around those three load levels. Because the images were recorded at a frame rate of 1 frame per second in the tests, these incremental shear strain maps may be regarded approximately as the local shear strain rates of the test samples. A straight line cutting through the narrow shearing zone (i.e., the high shear strain strip) in each test sample is not parallel to the horizontal tensile loading direction at all. The angles between the active shearing zone in terms of the incremental shear strain maps in Figures 5.6 and 5.7 and the horizontal direction are about $6-8^{\circ}$ for the DD2A sample and $5-7^{\circ}$ for the DD1B sample.

The nature of the in-plane deformation of the shearing zone and its surrounding regions can

be further illustrated by additional maps for DD2A and DD1B samples. Maps of the sum of the two principal strains $\varepsilon_1 + \varepsilon_2$, the angle of the current principal shearing plane φ_s, and the angle of in-plane rigid-body rotation ω due to shearing are shown in Figure 5.8 for DD2A sample at load steps corresponding to image frames No.22 and No.27. Even at the interior center region of the shearing zone excluding the two regions near free edges, the average local $\varepsilon_1 + \varepsilon_2$ is found to be as high as -0.009 and -0.014 (noting $\varepsilon_1 - \varepsilon_2$ is about 0.05 and 0.1). The angle of the current principal shearing plane and the horizontal direction is about 4.5° and 7° at these two load steps. On the other hand, the rigid-body rotation due to shearing is only about 2.1° and 4.5° (counterclockwise).

Similarly, maps of the sum of the two principal strains $\varepsilon_1 + \varepsilon_2$, the angle of the current principal shearing plane φ_s, and the angle of in-plane rigid-body rotation ω due to shearing are shown in Figure 5.9 for DD1B sample at load steps corresponding to image frames No.28 and No.46. At the interior center region of the shearing zone, the average local $\varepsilon_1 + \varepsilon_2$ is found to be smaller values of -0.005 and -0.003 (noting $\varepsilon_1 - \varepsilon_2$ is again about 0.05 and 0.1). The angle of the current principal shearing plane and the horizontal direction is 4° and 1° at these two load steps. On the other hand, the rigid-body rotation due to shearing is only about 3.5° and 8° (counterclockwise).

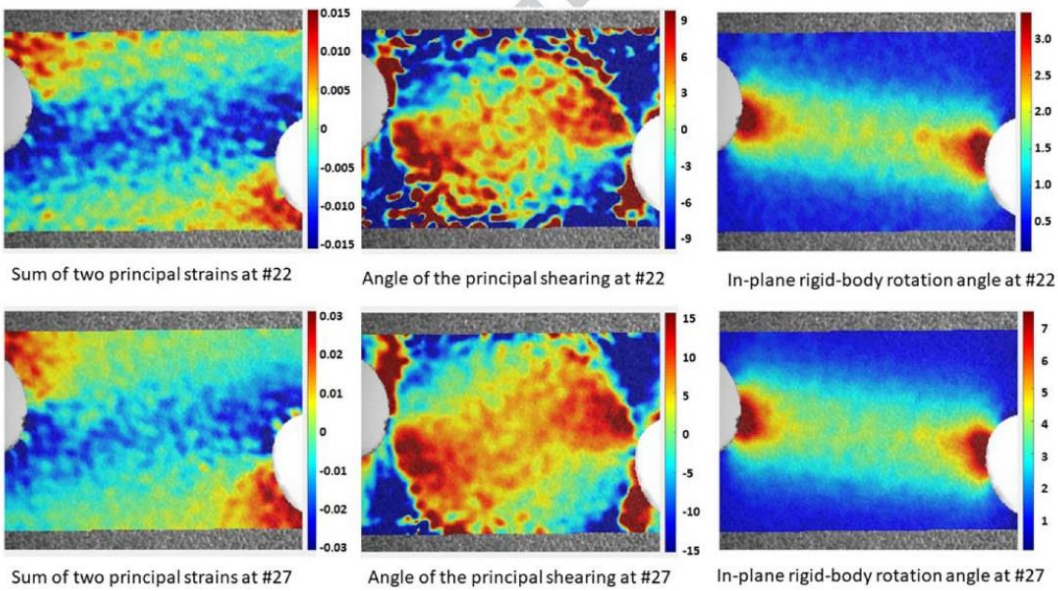

Figure 5.10: Three additional maps from the whole-field strain measurements for DD2A sample from image frame No.22 and No.27: (a) the sum of two in-plane principal strains (left); (b) the angle in degree of the principal shearing plane deviating from the horizontal direction (middle); (c) the angle in degree of the in-plane rigid-body rotation due to shearing (right).

5.3 Discussion and Conclusions

5.3.1 Calibrated Hill's and Gotoh's Yield Function for AA6111-T4 Sheet

When a total of seven experimental inputs (σ_0, σ_{45}, σ_{90}, σ_b , R_0, R_{45}, R_{90}) are provided, the material constants in Hill's quadratic yield function/flow potential Φ_{2Y}, Φ_{2P} and Gotoh's quartic yield function Φ_4 with reduced anisotropy are readily computed from simple algebraic relations [103]. For parameter identification on the AA6111-T4 sheet in this study, the yield stress under equal biaxial tension σ_b will be replaced by the shear yield stress under pure shear σ_{s0} = 105.1 MPa estimated approximately from simple shear experiments using DD2A and DD1B samples. As the uniaxial tensile yield stresses and plastic strain ratios of AA6111-T4 sheet used in this study are (σ_0, σ_{45}, σ_{90}) = (174.1, 173.4, 166.7) MPa and (R_0, R_{45}, R_{90}) = (0.93, 0.41, 0.66), the material constants for Hill's yield function/flow potential and Gotoh's yield function from these seven experimental inputs are subsequently obtained as

$$\begin{aligned} Y_1 = 1, Y_2 = -1.0513 + Y_3 = 1.0908, Y_4 = \ 2.9929 \\ P_1 = 1, P_2 = -0.9637, P_3 = 1.2120, P_4 = \ 2.2718 \end{aligned} \tag{96}$$

$$\begin{aligned} Y_1 A_1 = 1, A_2 = -1.9275 + A_3 = 2.7102, A_4 = -1.8921, A_5 \\ = 1.1897 + A_6 = \ 5.8027, A_7 = -2.5785, A_8 \\ = \ 6.1468, A_9 = \ 5.8085. \end{aligned} \tag{97}$$

The positivity and convexity of these calibrated yield functions are readily established (see [103]). If the AA6111-T4 sheet material is subjected to an on-axis pure shear in stress ($\sigma_1 = -\sigma_2$, $\theta = 0^\circ$), then the ratio of corresponding principal plastic strains $\varepsilon'_2/\varepsilon'_1$ via Eqs. $(88)_1$ and $(90)_1$ in Section 5.1.4 Principal plastic strain increment ratio in pure shear stressing would be -1.059, -1.143, and -1.040 as predicted by the calibrated Hill's yield function Φ_{2Y}, Hill's flow potential Φ_P, and Gotoh's yield function Φ_4. On the other hand, if the AA6111-T4 sheet material is subjected to an on-axis pure shear straining ($\varepsilon'_1 = -\varepsilon'_2$, $\theta = 0^\circ$), then the ratio of corresponding principal Cauchy stresses σ_2/σ_1 via Eq. $(92)_1$ and Eq. $(94)_1$ in Section 5.1.5 Principal stress ratio in pure shear straining would be -0.84, -0.71 and -0.914 as predicted by the calibrated Hill's yield function Φ_{2Y}, Hill's flow potential Φ_{2P} and

Gotoh's yield function Φ_4. The shearing test experiments described in the previous section were carried out under a fixed tensile loading direction and would be more closely approximated as a pure shear in stress especially at the initial stage of the shearing tests. The full-field strain mapping measurements of two shear samples DD2A and DD1B as presented in the previous section show that the resulting deformation in their shearing zones are close to but different from $\varepsilon'_2/\varepsilon'_1 = -1$ or $\varepsilon'_1 + \varepsilon'_2 = 0$, more consistent with the model predictions here assuming approximately on-axis pure shear in stress (neglecting the elastic strains as usual).

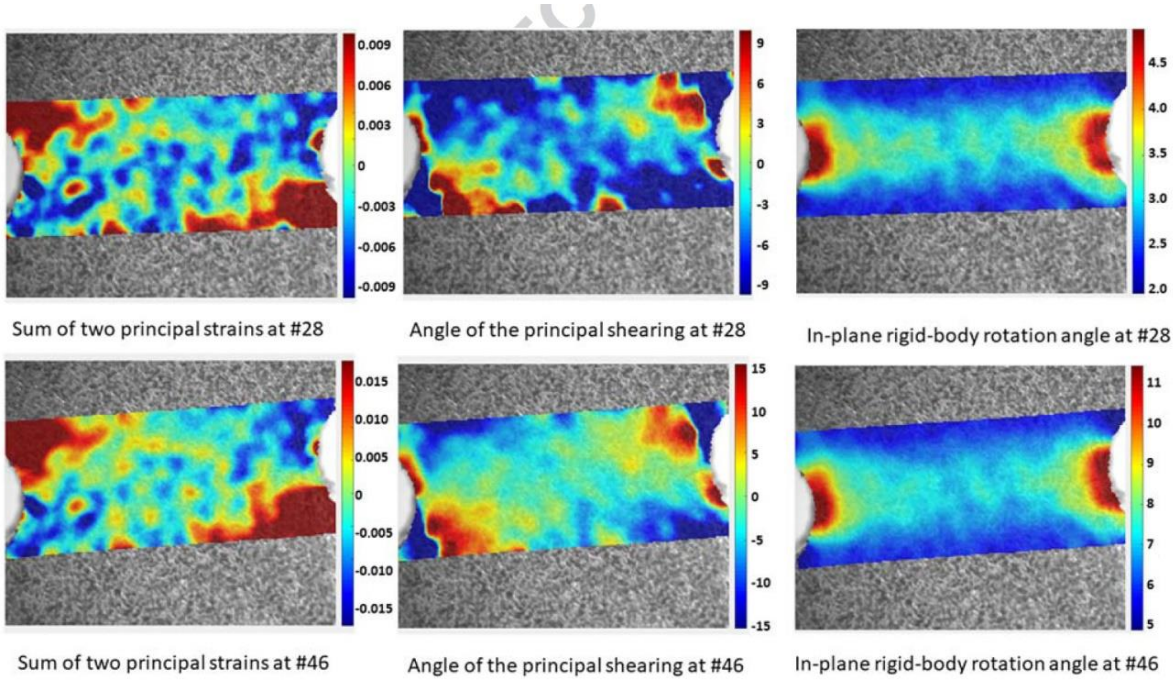

Figure 5.11: Three additional maps from the whole-field strain measurements for DD2A sample from image frame No.28 and No.46: (a) the sum of two in-plane principal strains (left); (b) the angle in the degree of the principal shearing plane deviating from the horizontal direction (middle); (c) the angle in the degree of the in-plane rigid-body rotation due to shearing (right).

5.3.2 Implications of the Newly Proposed Shear Constraint

As shown by the results of both Hill's quadratic and Gotoh's quartic models in Section 5.1.3 modeling pure shear by Hill's quadratic and Gotoh's quartic anisotropic plastic models, pure shear stressing and straining are found to be indeed identical when the shearing direction is parallel either to the rolling or to the transverse direction of a sheet metal (i.e., the loading angle $\theta = \pm 45^{\circ}$). This is, true for any orthotropic plasticity model

when the applied Cauchy stress $\sigma = (\sigma_x, \sigma_y, \tau_{xy}) = (0, 0, \pm\tau)$ or the applied plastic strain increments $\acute{\boldsymbol{\varepsilon}} = (\varepsilon'_x, \varepsilon'_y, \varepsilon'_{xy} = (0, 0, \pm\dot{\gamma}/2)$.

However, a general pure shear stressing condition in terms of the intrinsic variables (σ_1, σ_2) = ($\tau, -\tau$) and $\theta = \pm 45^\circ$ does not lead to a pure shear straining state, see Eqs. $(88)_1$, $(88)_3$, $(90)_1$ $(90)_3$. Similarly, a general pure shear straining condition in terms of the intrinsic variables $(\varepsilon'_1, \varepsilon'_2) = (\dot{\gamma}/2, -\dot{\gamma}/2)$ and $\theta = \pm 45^\circ$ does not always generate a pure shear stressing state, see Eqs. $(92)_1$, $(92)_3$, $(94)_1$ $(94)_3$. For the 45-degree and 135-degree pure shear stressing conditions considered in sections two types of pure shear loading conditions on sheet metal and "modeling pure shear by Hill's quadratic and Gotoh's quartic anisotropic plastic models" ($\theta = \theta' = 0^\circ$ or 90°), one has to set following conditions on material constants (Y_1, Y_3) for the associated Hill's model, (P_1, P_3) for the non-associated Hill's model, and (A_1, A_2, A_4, A_5) for the associated Gotoh's model respectively to generate a pure shear straining state ($\dot{\varepsilon}^{ps}_1 + \dot{\varepsilon}^{ps}_2 = 0$) per Eqs $(88)_1$, $(88)_3$, $(90)_1$ and $(90)_3$

$$Y_1 = Y_3, P_1 = P_3, 2A_1 - A_2 = 2A_5 - A_4 \tag{98}$$

Similarly, for the 45-degree and 135-degree pure shear straining conditions considered in Sections 5.1.1 and 5.2 two types of pure shear loading conditions on a sheet metal and modeling pure shear by Hill's quadratic and Gotoh's quartic anisotropic plastic models, one has to set the same conditions above on material constants for Hill's and Gotoh's models to generate a pure shear stressing state ($\sigma^{ss}_1 + \sigma^{ss}_2 = 0$) per Eqs. $(92)_1$, $(92)_3$, $(94)_1$ $(94)_3$. This effectively reduces the total number of independent on-axis polynomial coefficients in Hill's 1948 quadratic and Gotoh's 1977 stress functions from 3 to 2 and from 5 to 4 respectively. When the proposed shear constraint was applied to the non-quadratic yield function YLD2000-2D under the pure shear loading cases #1 and #3 by Abedini et al. [76], it also reduced its total number of independent material constants from 8 to 7.

Recall that the plastic strain ratio $R_b = \varepsilon'_2/\varepsilon'_1$ under equal biaxial tension $\sigma_2 = \sigma_1$is given these two yield functions as [104,105]

$$R_b \frac{P_2 + 2P_3}{2P_1 + P_2}, R_b \frac{A_2 + 2A_3 + 3A_4 + 4A_5}{4A_1 + 3A_2 + 2A_3 + A_4} \tag{99}$$

the imposed condition of Eq. $(98)_2$ by the new shear constraint would imply R_b = 1 for Hill's quadratic yield function as well. Abedini et al. [76] suggested that under pure shear stressing $\sigma_1 = -\sigma_2$, a sheet metal should undergo only pure shear straining $\varepsilon'_1 = -\varepsilon'_2$ as well and vice versa for all loading angles (i.e., not limited only to 0°, 45°, and 90° as considered above so far). By transforming Hill's quadratic flow potential function into a form in terms of intrinsic variables, one can show that the ratio of axial plastic strain increments $\acute{\varepsilon}_2/\acute{\varepsilon}_1$ is given as (under the off-axis pure shear stressing condition of $\sigma_1 = -\sigma_2$ and $0^\circ < \theta < 45^\circ$ or $45^\circ < \theta < 90^\circ$)

$$\frac{\varepsilon'_2}{\varepsilon'_1} = -\frac{P_1 - P_2 + P_3 + P_4 - 2(P_1 - P_3)\cos 2\theta + (P_1 - P_2 + P_3 - P_4)\cos 4\theta}{P_1 - P_2 + P_3 + P_4 + 2(P_1 - P_3)\cos 2\theta + (P_1 - P_2 + P_3 - P_4)\cos 4\theta} \quad (100)$$

That is, either $2\theta = 90^\circ$ or the shear constraint condition of Eq. $(98)_2$ will be sufficient to make it to be -1 (pure shear straining). Here the shearing strain ε'_{12} due to the off-axis loading is assumed to be negligible implicitly. Similarly, one obtains the following condition for Gotoh's yield function if $\varepsilon'_1 + \varepsilon'_2 = 0$ when $\sigma_1 = -\sigma_2$

$$cos\ 2\theta\ =\ 0, or\ 2A_1 - A_2 + A_4 - 2A_5 = 0, A_6 - A_8 = 0 \quad (101)$$

So, one additional condition on the two off-axis polynomial coefficients A_6 and A_8 is needed to meet the shear constraint $\varepsilon'_2/\varepsilon'_1 = -1$ for the loading angles other than 0°, 45°, and 90°. It is interesting to note that such a condition had indeed previously been assumed for a version of Gotoh's yield function with reduced anisotropy [106,107].

A non-zero hydrostatic stress $\sigma_1 + \sigma_2 \neq 0$ due to in-plane pure shear straining and a non-zero thickness strain increment $\varepsilon' \frac{p}{1} + \varepsilon' \frac{p}{2} \neq 0$ due to in-plane pure shear stressing can exist in-plane stress (with $\sigma_3 = 0$) for an orthotropic sheet metal per both Hill's quadratic and Gotoh's quartic models. That is, even when the principal stress axes $\sigma_1\sigma_2$ and principal plastic strain increment axes $\varepsilon'_1\varepsilon'_2$ in on-axis pure shear are coincided with each other (if the shearing directions are the same in both loading conditions), the induced principal plastic strain increment ratio $(\varepsilon'_2/\varepsilon'_1)_{ps}$ and the induced principal stress ratio in pure shear $(\sigma_2/\sigma_1)_{ss}$ are in general not equal to -1. They are not some non-physical artifacts as claimed

by Abedini et al. [76] but are instead some unique and intrinsic features due to the anisotropic nature of sheet metal. Per simple logic, the equivalence of pure shear stressing and straining claimed by Abedini et al. [76] for a non-quadratic isotropic plasticity model such as Hosford's model cannot be used to justify its validity for either quadratic or non-quadratic anisotropic plasticity models at all. As isotropic plasticity models are only a subset of anisotropic plasticity models, their insistence on the equivalence of pure shear stressing and straining conditions is not warranted for anisotropic sheet metals in general. In other words, the proposed shear constraint is neither a first level constraint (positivity and convexity) nor a second level constraint (pressure-independent plastic incompressibility, an associated or a non-associated plastic flow) as discussed in the Introduction that one shall commonly impose on anisotropic plasticity modeling of sheet metals. It is instead a third-level provisional constraint of reduced anisotropy between no anisotropy (isotropy) and full anisotropy for a given orthotropic yield function.

Chapter 6

6.1 Conclusions

In this study, a comprehensive testing method was developed for the analysis of the anisotropic plasticity of sheet metals. The plasticity tests do not only include traditional single-axis tractable testing in different material directions, but also specific joined-pressure/ and shear biaxial tests so that a practical 3d yield surface can be included. The research results indicate that the expulsion of AA6111-T4 is very anisotropic and has R-values varying from 0.19 and 1.08. The AA6111-T4 currently shows only traverse anisotropy with an almost unintended range of R-values.

A hole expansion experimental finite element investigation on a double phases sheet of steel was conducted by Kuwabara et al. [60] by utilizing ABAQUS user material subroutines UMAT and VUMAT. Convex 4^{th} and 6^{th} order homogenous polynomial yields were achieved by the application of uniaxial and biaxial yield strengths and the plastic strain proportions for finite element analysis of the experiment on dual-phase sheet steel. The polynomial performance feature of the sixth order has become more content factors and degrees of freedom for experimental data. The findings showed a similar pattern to the thickness pressure found experimentally at the bore end and along rolling and transverse directions of sheet metal. Using a specific finite element code, multiple CPUs can be used for lessening the time of computation. Here, 30 CPUs were utilized for the explicit calculations of the results.

Whole different content constants in their performance and flow stress functions must be an identical and a similar collection of test inputs must be utilized to regulate the matrix constants in each process for a more accurate and practical contrast between a non-associated model and the related model. This research has found a non-associated quadratic model and a similar quartic model that satisfies these criteria. For the adjustment of their material constants, both versions will require up to four yield strains and three uniaxial as well as equivalent biaxial pressure plastic strain ratios. In contrast to Hill's [56]. quadratic-associated model, each model, therefore, has superior anisotropic yielding and flow output of a sheet metal limited only to four content constants over a

total of four.

Nevertheless, there are certainly other important differences and variations in the mathematical features between the two models tested. For illustration, a plastically stable material must be positive and convex in its yield feature and input potential. Both versions use homogenous polynomial stress functions, which are positive and convex and must never be checked for each sheet of metal after they have been calibrated. The appropriate and sufficient conditions for the quadratic function of Hill with clear algebraic inequalities are often much simpler to define. The fact is for using even the simplest non-quadratic polynomial suggested by Gotoh et al. [58], there will be no simple algebraic inequalities. Although Gotoh's [58] fourth-order polynomial yield stress was documented and used for sheet metal modeling by several researchers over the years, the positivity and convexity of nearly all measured yield stress functions of Gotoh et al. [58] were not ever preciseness. Though, there was no explicit evidence or methods in the recorded works to confirm that it is positive and convex. In other terms, it was expected that Gotoh [58] has a standardized yield stress feature. Also, in his original work, [60] did not mention this particular mathematical problem. A rigorous proof of firm positivity and convexity of Gotoh [58] was just lately presented in examples of Gotoh's [58] yield stress function calibrated in the 1977 paper for two sheet metal. Only recently, a manageable method for numerical minimization has been implemented that could test for the purely positive and convex state of a tuned polynomial yield function of the Gotoh [58].

In further studies, a typical set of seven experimental inputs (σ_0, σ_{45}, σ_{90}, σ_b, R_0, R_{45}, R_{90}) were made available to the polynomial coefficients for both Hill's [56] quadratic and Gotoh's [58] quartic yield functions. As a result, they were readily determined directly from a set of algebraic equations without the unnecessary shear constraint imposed [103]. In this study, it was shown that the shear yield stress under on-axis pure shear σ_{s0} estimated approximately from a shearing experiment using either Type-A or Type-B sample geometry may substitute the yield stress under equal biaxial tension σ_b in parameter identification of both yield functions. The shearing experiments on the AA6111-T4 sheet presented in this study showed that the actual loading conditions and deformation states of

the shearing zone in sheet metal samples were rather complex. They may be approximated to a certain degree as pure shear in stress ($\sigma_2/\sigma_1 \approx -1$) but deviate from pure shear in straining (i.e., $\varepsilon_2/\varepsilon_1 \neq -1$). That is, limited by the experimental uncertainties of full-field strain measurements, one cannot unequivocally confirm that the ideal pure shear condition of $\varepsilon_2/\varepsilon_1 = -1$ has been uniformly and strictly achieved inside the gauge Section 5.1.1 of those two types of simple shear test coupons at low and moderate shear strain levels.

In conclusion, while the so-called shear constraint proposed by Abedini et al. [76] or some other similar third level constraints may be imposed for a subset of orthotropic materials or for some heuristic reasons such as when there are insufficient experimental inputs for fully calibrating an anisotropic yield function [103], such a constraint is not physically necessary due to lack of supporting experimental evidence in general and is overly restrictive in the context of modeling sheet metals with seven experimental inputs using either Hill's quadratic or Gotoh's yield quartic functions.

6.2 Suggestions for Future Studies

While this postulation on anisotropic plasticity and the split of sheet metals is a significant amount of research, there are still several unknown issues of strain: minimal disfiguring of kinematics: the criteria for this postulation, such as the phenomenological plasticity model shown in chapter two and the polycrystalline plasticity models included in Chapter 4 and 5; The corotational kinematics enables the fusion and minimal pivot analysis of small part versions. It thus constitutes a good proving ground for new and complex system models provided that, as compared to the related minimal stress conditions, the broad pressure constitutive conditions are usually simple to implement. Nevertheless, the picture of the commodity transition and the pressure of the co-rotational mechanism is distorted throughout. In line with this it is important to review the enormous strain of current models' constitutive structure, such as the Lagrangian cinematics and Kroner, within the thorough mechanical continuum modem structure Gurtin et al. [62], the book of Gurtin et al. [62] offers detailed dialogs on the concept of constitutive conditions following critical changes, thermodynamic regulation and the principle of edge loss. In particular, the use of corotational filmmaking in a polycrystalline model displayed in Chapter 4 ruins

crystallographic surface progress (computer time builds significantly inside the grid structure, see (Rousselier et al. [62]), which is an important factor for enormous mis-happening, while usually attracted to the Lagrangian system (Rousselier et al. [62]). The use of the RTM in this plan for the polycrystalline Taylor models embedded in the modem continuum dynamics method would be a positive and sufficient further review.

Cracks inside the polycrystalline system: although in this proposal the anisotropic plasticity was based on a polycrystalline construct, it is still phenomenological. Polycrystalline models can offer a ton of knowledge about the arrangement of a shear band, internal vacuum development, etc. Started thinking here, previously initiated with the integration of Mohr-Coulomb's grain-level slip framework work size impacts: While certain work has been done in this theory on the effect of work size, for example, the progress of regular work for relaxation after disappointment, the work impact analysis to achieve the results, the effect of work size is still inevitable. Methodologies and slope hypotheses for the non-neighborhood could provide answers. Furthermore, it is essential to understand the distinction in length between the reenactments of the crack alignment in the laboratory and enormous industrial reproductions. The effect of the thickness heterogeneity on the break: sheets rolling or expelled generally show the variability of the thickness in the size or position of grain. In this plan, its effects on plasticity were studied, but its influence on foldable breaks remains unclear.

This may also involve interesting issues such as the effect on delicate breaks of grain size or morphology. Blade or surface break: this idea mainly focuses on the creation of breaks within a separate body. Nevertheless, multiple splits exist at the end of the content in the realistic environment. In terms of physical structure and simulation, it is important to see better the difference between these two kinds of cracking modes.

Appendix A

The equation of coefficient C_0, C_1, C_2, D_0, D_1, D_2 in the associated quadratic model for 3 uniaxial tensile tests are given below

$$C_0 = R_0 + R_0R_{45} + R_0R_{90} + R_0R_{45}R_{90} + 2(R_{45} + R_0R_{45} + R_{45}R_{90} + R_0R_{45}R_{90})\ (\sigma_0^4/\sigma^4_{45}) + (R_{90} + R_0R_{90} + R_{45}R_{90} + R_0R_{45}R_{90})\ (\sigma_0^4/\sigma^4_{90}),$$

$$C_1 = 2(R_0 + R_0R_{45} + R_0R_{90} + R_0R_{45}R_{90}) - (R_{90} + R_0R_{90} + R_{45}R_{90} + R_0R_{45}R_{90})\ (\sigma_0^4/\sigma^4_{90}),$$

$$C_2 = R_0 + R_0R_{45} + R_0R_{90} + R_0R_{45}R_{90} - 2(R_{45} + R_0R_{45} + R_{45}R_{90} + R_0R_{45}R_{90})\ (\sigma_0^4/\sigma^4_{45}) + (R_{90} + R_0R_{90} + R_{45}R_{90} + R_0R_{45}R_{90})\ (\sigma_0^4/\sigma^4_{90}),$$

$$D_0 = 1 + R_{45} + R_{90} + R_{45}R_{90} + 2(1 + R_0 + R_{90} + R_0R_{90})\ (\sigma_0^4/\sigma^4_{45}) + (1 + R_0 + R_{45} + R_0R_{45})\ (\sigma_0^4/\sigma^4_{90}),$$

$$D_1 = 2(1 + R_{45} + R_{90} + R_{45}R_{90}) - 2(1 + R_0 + R_{45} + R_0R_{45})\ (\sigma_0^4/\sigma^4_{90}),$$

$$D_2 = 1 + R_{45} + R_{90} + R_{45}R_{90} - 2(1 + R_0 + R_{90} + R_0R_{90})\ (\sigma_0^4/\sigma^4_{45}) + (1 + R_0 + R_{45} + R_0R_{45})\ (\sigma_0^4/\sigma^4_{90}),$$

Appendix B

The algebraic relationship for material constants of non-associated model age given below

$S_1\sigma_x^2 + S_2\sigma_x\sigma_y + S_3\sigma_y^2 + S_4\tau_{xy}^2 > 0,$

Where

$S_1 = \lambda\,(4P_1Y_1 + 2P_2Y_1 + 2P_1Y_2 + P_2Y_2) + 2\mu\,(4P_1Y_1 + P_2Y_2),$

$S_2 = 2\lambda\,(P_2Y_1 + 2P_3Y_1 + P_1Y_2 + P_2Y_2 + P_3Y_2 + 2P_1Y_3 + P_2Y_3) + 4\mu\,(P_2Y_1 + P_1Y_2 + P_3Y_2 + P_2Y_3),$

$S_3 = \lambda\,(P_2Y_2 + 2P_3Y_2 + 2P_2Y_3 + 4P_3Y_3) + 2\mu\,(P_2Y_2 + 4P_3Y_3),$

$S_4 = 4\mu P_4Y_4.$

$(S_4 > 0$ *is* automatically satisfied as $Y_4 > 0, P_4 > 0$ *and* $\mu > 0)$ $S_1 > 0, S_3 > 0, 4S_1S_3 > S_2^2.$

In the case of planar isotropy and utilizing quadratic yield and flow stress functions

$S_1\sigma_1^2 + S_2\sigma_1\sigma_2 + S_3\sigma_2^2 > 0,$

Where

$S_1 = 4(\lambda + 2\mu) + 2\lambda\,(\sigma_0^2/\sigma_b^2) + 2[2\lambda - (\lambda + 2\mu)\,(\sigma_0^2/\sigma_b^2)]\,(R_0/1 + R_0),\ S_2 = 8\lambda + 4(\lambda + 2\mu)\,(\sigma_0^2/\sigma_b^2) + 4\,[2\lambda - (\lambda + 2\mu)\,(\sigma_0^2/\sigma_b^2)]\,(R_0/1 + R_0),$

$S_3 = 4(\lambda + 2\mu) + 2\lambda\,(\sigma_0^2/\sigma_b^2) - 2[2\lambda + (\lambda + 2\mu)\,(\sigma_0^2/\sigma_b^2)]\,(R_0/1 + R_0).$

One can show

$4S_1S_3 - S_2^2 = 64\mu\,(\lambda + \mu)\,(4 - (\sigma_0^2/\sigma_b^2))\,(1 + 2R_0)/(1 + R_0)^2 > 0.$

Appendix C

Some algebraic inequalities for making sure convexity of yield function of Gotoh are summarized here. Admissible values of material constants A_1, ..., A_9. Under-five simple plane-stress loading conditions (σ_x, 0, 0), (0, σ_y, 0), (0, 0, τ_{xy}), (σ_x, σ_y, 0) and (σ_x, -σ_y, 0),

$A_1 > 0, A_5 > 0, A_9 > 0, A_1 \pm A_2 + A_3 \pm A_4 + A_5 > 0,$

$A_6 > 0, A_8 > 0, 6A_1 \pm 3A_2 + A_3 > 0, A_6 \pm A_7 + A_8 > 0,$

$A_3 > 0, 8A_1A_3 > 3A_2^2, 8A_3A_5 > 3A_4^2, 4A_6A_8 > A_7^2, 4(6A_1 \pm 3A_2 + A_3)(A_3 - 3A_4 + 6A_5) > (3A_2 \pm 4A_3 + 3A_4)^2$

A_1, A_5, A_6, A_8 and A_9 $36A_1A_9 > A_6^2, 36A_5A_9 > A_8^2.$

Appendix D

SMU
SOUTHERN METHODIST UNIVERSITY

Department of Mechanical Engineering

January 30, 2021

To Whom It May Concern,

Per the request by Mr. Mohammed Alharbi, this letter is to provide the declaration of his co-authorship and co-contribution of the three published papers listed below. In general, all authors of each paper have contributed equally to the work carried out under my supervision and should be considered as co-first author. Some major contributions by Mr. Alharbi for each paper are detailed here:

1. *W. Tong and M. Albarbi. Comparative evaluation of non-associated quadratic and associated quartic plasticity models for orthotropic sheet metals. Int. J. Solids & Structures 128:133–148 (2017).*
   50% by M. Alharbi: Literature Review, Theoretical Analysis, Validation, Visualization, Writing – help with original draft.

2. *S. Yang, W. Tong, and M. Alharbi. Finite element calculations of hole expansion in a thin steel sheet with polynomial yield functions of four and six degrees. IOP Conf. Series: Journal of Physics: Conf. Series 1063:012095 (2018).*
   33% by M. Alharbi: Constitutive Modeling of Steel Sheet, Parameter Estimation, Verification.

3. *W. Tong, M. Alharbi, J. Sheng. On the new shear constraint for plane-stress orthotropic plasticity modeling of sheet metals. Exp. Mech. 60(7):889–905 (2020).*
   33% by M. Alharbi: Tensile and Shear Testing of Aluminum Sheet, Image Correlation Strain Analysis, Modeling Validation.

Please let me know if you have any additional questions.

Sincerely,

Wei Tong, Professor

School of Engineering
PO Box 750337 Dallas TX 75275-0337
214-768-3128 Fax 214-768-1473

References

[1] J. T. Ł. T. R. A. K. M. Bendarma A, "Experimental and numerical analysis of the aluminum alloy AW5005 behavior subjected to tension and perforation under dynamic loading.," Journal of Theoretical and Applied Mechanics, vol. 55, no. 4, pp. 1219-1233, 2017.

[2] L. M. K. D. K. C. W. M. B. F. Chung K, "Spring-back evaluation of automotive sheets based on isotropic-kinematic hardening laws and non-quadratic anisotropic yield functions: Part I: theory and formulation," *International Journal of Plasticity,* vol. 21, no. 5, pp. 861-82, 2005.

[3] A. K. H. J. J. L. M. B. F. Varma, "Advanced constitutive model for repeated stress relaxation accounting for transient mobile dislocation density and internal stress," Mechanics of Materials, vol. 133, pp. 138-153, 2019.

[4] B. A.-M. F. B. T. Haddag, "Strain localization analysis using a large deformation anisotropic elastic–plastic model coupled with damage," International Journal of Plasticity, vol. 25, no. 10, pp. 1970-1996, 2009.

[5] A. G. D. Y. J. Taherizadeh, "Evaluation of advanced anisotropic models with mixed hardening for general associated and non-associated flow metal plasticity," International Journal of Plasticity., vol. 27, no. 11, pp. 1781-1802, 2011.

[6] W. C. R. Coombs, "Non-associated Reuleaux plasticity: analytical stress integration and consistent tangent for finite deformation mechanics," Computer methods in applied mechanics and engineering, vol. 200, no. 9-12, pp. 1021-1037, 2011.

[7] Y. J. Stoughton TB, "A pressure-sensitive yield criterion under a non-associated flow rule for sheet metal forming," International Journal of Plasticity, vol. 20, no. 4-5, pp. 705-731, 2004.

[8] K. G., "A review of the tensile, compressive, flexural and shear properties of hybrid fibrereinforced," Composites., vol. 18, no. 1, pp. 13-23, 1987.

[9] M. M. D. Dunand, "hybrid experimental–numerical analysis of basic ductile

fracture experiments for sheet metals," International journal of solids and structures, vol. 47, no. 9, pp. 1130-1143, 2010.

[10] J. H. R. Bishop, "A theory of the plastic distortion of a polycrystalline aggregate under combined stresses," The London, Edinburgh, and Dublin Philosophical Magazine and Journal of Science, vol. 42, no. 327, pp. 414-427, 1951.

[11] A. G. D. G. A. Y. J. Taherizadeh, "A non-associated constitutive model with mixed iso-kinematic hardening for finite element simulation of sheet metal forming," International Journal of plasticity, vol. 26, no. 2, pp. 288-309, 2010.

[12] M. Geiger, "Manufacturing science–Driving force for innovation," Advanced Technology of Plasticity, vol. 1, pp. 17-30, 2002.

[13] V. KD, "Metal forming-A key technology for automobile production," Adv. Techn, vol. 1, no. 30, p. 16, 1999.

[14] T. W., The plastic anisotropy in single crystals and polycrystalline metals, Dordrecht, the Netherlands:: Kluwer Academic Publishers, 2001.

[15] T. N. U. H. S. T. H. R. Saito Y, "Scripta Materialia," vol. 39, pp. 1221-1227, 1998.

[16] M. M, "An inverse method for the mechanical characterization of Metals," 1995.

[17] B. S. J. J. J. B. H. O. C. S. W. Beausir, "Plastic anisotropy of ultrafine grained aluminium alloys produced by accumulative roll b," Materials Science and Engineering, vol. 527, no. 13-14, pp. 3271-3278, 2010.

[18] M. R., "Mechanic defrosted K6rper Plastics- deformable Outstand," pp. 582-592, 1913.

[19] B. JL, "Yield characterization of metals with transversely isotropic plastic properties.," International Journal of Mechanical Sciences, vol. 19, no. 11, pp. 651-660, 1977.

[20] R. Hill, "Constitutive modeling of orthotropic plasticity in sheet metals," Journal of the Mechanics and Physics of Solids, vol. 38, no. 3, pp. 405-417, 1990.

[21] H. R., "user-friendly theory of orthotropic plasticity in sheet metals," International Journal of Mechanical Sciences., vol. 35, no. 1, pp. 19-25, 1993.

[22] H. W. Logan RW, "Upper-bound anisotropic yield locus calculations assuming< 111>-pencil glide," International Journal of Mechanical Sciences, vol. 22, no. 7, pp. 419-430, 1980.

[23] O. Hoffman, "The brittle strength of orthotropic materials," Journal of Composite Materials, vol. 1, no. 2, pp. 200-206, 1967.

[24] F. L. D. B. J. Barlat, "A six-component yield function for anisotropic materials.," International Journal of plasticity, vol. 7, no. 7, pp. 693-712, 1991.

[25] F. Barlat and J. Y. J. C. K. D. R. L. D. P. F. C. S. C. E. Brem, "Plane stress yield function for aluminum alloy sheets—part 1: theory.," International Journal of Plasticity, vol. 19, no. 9, pp. 1297-1319, 2003.

[26] D. Banabic, H. Bunge, K. Pohlandt and A. Tekkaya, Formability of Metallic Materials, Berlin/Heidelberg: Springer,, 2000.

[27] T. C. W. H. Kocks UF, Texture and anisotropy: preferred orientations in polycrystals and their effect on materials properties, Cambridge university press, 1998.

[28] W. M. Z. X. Wu XD, "Biaxial tensile testing of cruciform specimen under complex loading.," Journal of Materials Processing Technology, vol. 168, no. 1, pp. 181-183, 2005.

[29] Y. K. J. C. H. C. P. S. D. L. J. H. H. Cho, "Analysis of transformation plasticity in steel using a finite element method coupled with a phase field model," PloS one, vol. 7, no. 4, 2012.

[30] T. L. N. K. Makinde A, "Development of an apparatus for biaxial testing using," Experimental mechanics, vol. 32, no. 2, pp. 138-144, 1992.

[31] K. T. K. M. Yoshida K, "Path-dependence of the forming limit stresses in a sheet metal.," International Journal of Plasticity, vol. 23, no. 3, pp. 361-384, 2007.

[32] A. T. P. Hannon, "review of planar biaxial tensile test systems for sheet metal," Journal of materials processing technology, vol. 198, no. 103, pp. 1-3, 2008.

[33] D. J. Lin SB, "Experimental study of the plastic yielding of rolled sheet metals with

the cruciform plate specimen," International Journal of plasticity, vol. 11, no. 5, pp. 583-604, 1995.

[34] W. N. Wagoner RH, "An experimental and analytical investigation of in-plane deformation of 2036-T4 aluminum sheet.," International Journal of Mechanical Sciences, vol. 21, no. 5, pp. 255-264, 1979.

[35] I. S. K. K. Kuwabara T, "Measurement and analysis of differential work hardening in cold-rolled steel sheet under biaxial tension," Journal of Materials Processing Technology, vol. 80, pp. 517-523, 1998.

[36] W. Hosford, The mechanics of crystals and textured polycrystals, USa: Oxford University Press, 1993.

[37] N. M. a. K. H. Kawabata S, "3—the finite-deformation theory of plain-weave fabrics part I: the biaxial-deformation theory," Journal of the textile institute, vol. 64, no. 1, pp. 21-46, 1973.

[38] R. KS, "simple technique to generate in-plane forming limit curves and selected applications.," Metallurgical and materials transactions, vol. 26, no. 8, pp. 2075-2084, 1995.

[39] Y. J. Kim KH, "Evolution of anisotropy under plane stress," Journal of the Mechanics and Physics of Solids., vol. 45, no. 5, pp. 841-851, 1997.

[40] K. Y. Z. J. K. I. Kuwabara T, "compression asymmetry of phosphor bronze for electronic parts and its effect on bending behavior," International Journal of Plasticity, vol. 25, no. 9, pp. 1759-1776, 2009.

[41] Z. Q. Losilla G. Boehler JP, "Mechanical Properties of Coated Plain Weave Fabrics under Biaxial Loads," vol. 144, pp. 169-218, 2000.

[42] Y. Dafalias, "Orientational evolution of plastic orthotropy in sheet metals," Journal of the Mechanics and Physics of Solids, vol. 48, no. 11, pp. 2231-2255, 2000.

[43] R. Bradt, "Ceramic Crystals and Polycrystals," Hardness of in Encyclopedia of Materials, 2001.

[44] R. EF., "Plastic anisotropy of sheet metals determined by simple shear tests,"

Materials Science and Engineering, vol. 241, no. 1-2, pp. 179-183, 1998.

[45] N. K. Tuğcu P, "On the implementation of anisotropic yield functions into finite strain problems of sheet metal forming," International Journal of Plasticity, vol. 15, no. 10, pp. 1021-1040, 199.

[46] S. B. F. B. J. Y. J. C. K. D. R. L. D. P. F. C. E. Choi, "Plane stress yield function for aluminum alloy sheets—part 1: theory.," International Journal of Plasticity, vol. 19, no. 9, pp. 1297-1319, 2003.

[47] W. C. D. J. V. J. Simons G, "Size effects in tensile testing of thin cold rolled and annealed Cu foils," Materials Science and Engineering, vol. 416, no. 1-2, pp. 290-299, 2006.

[48] P. O., "Über das Stauchen von Hohlzylindern und seine Eignung zur Bestimmung der Formänderungsfestigkeit dünner Bleche," Archiv für das Eisenhüttenwesen, vol. 38, no. 6, pp. 437-42, 1967.

[49] K. A. G. M. Merklein M, "Time dependent determination of forming limit diagrams," CIRP annals, vol. 59, no. 1, pp. 295-208, 2010.

[50] T. K. Y. Z. J. K. I. Kuwabara, "Tension–compression asymmetry of phosphor bronze for electronic parts and its effect on bending behavior," International Journal of Plasticity, vol. 25, no. 9, pp. 1759-1776, 2009.

[51] T. C. Lämmer H, "Discussion of coupled elasto-plasticity and damage constitutive equations for small and finite deformations.," International Journal of Plasticity, vol. 16, no. 5, pp. 495-523, 2000.

[52] D. Banabic, M. Vulcan and K. Siegert, "Bulge testing under constant and variable strain rates of superplastic aluminium alloys.," CIRP Annals, vol. 54, no. 1, pp. 205-208, 2005.

[53] P. K. D. E. Tekkaya A, "Methoden zur Bestimmung der Fließkurven von Blechwerkstoffen.–Ein Überblick," Teil II. Blech Rohre Profile, vol. 29, no. 10, pp. 414-417, 1982.

[54] M. K., "tress--Strain Relationship in Simple Shear of In-Plane Deformation for

Various Steel Sheets. InEfficiency in Sheet Metal Forming," DDRG 13 th Biennial Congress 1984, pp. 360-371.

[55] M. Z., "Assessment of material formability," Advanced Technology of Plasticity, vol. 1, pp. 685-94, 1984.

[56] K. H. H. A. D. R. H. A. Jawaid M, "Effect of jute fibre loading on tensile and dynamic mechanical properties of oil palm epoxy composites," Composites Part B: Engineering, vol. 45, no. 1, pp. 619-624, 2013.

[57] B. P. G. G. G. Beckers, "Modeling of Inelastic Deformation and Phase Transformations," in In Proceedings of Conference on Constitutive and Damage, Neat Press, Fulton, Maryland, USA, 1998.

[58] A. H. W. Graf, "Effect of changing strain paths on. Metallurgical transactions," A, vol. 24, no. 11, 1993.

[59] A. B.-S. H. E. A. Bastawros, "Experimental analysis of deformation mechanisms in a closed-cell aluminum alloy foam.," Journal of the Mechanics and Physics of Solids, vol. 48, no. 2, pp. 301-22, 2000.

[60] D. J. Marciniak Z, "Bending, Mechanics of Sheet Metal Forming. Arnold, Great Britain," Arnold, Great Britain, pp. 68-99, 1992.

[61] R. Hill, "theory of the yielding and plastic flow of anisotropic metals," Series A. Mathematical and Physical Sciences, vol. 193, no. 1033, pp. 281-297, 1948.

[62] R. Pearce, Some aspects of anisotropic plasticity in sheet metals, Int. J. Mech. Sci. 10 (1968) 995{1004.

[63] M. K. M. Y. M. Gotoh, "Studies of stretch-drawing process of sheet metals.," Journal of materials processing technology., vol. 63, no. 1-3, pp. 123-128, 1997.

[64] Belytschko T, Liu W K, Moran B *Nonlinear Finite Elements for Continua and Structures* (Chichester: John Wiley Sons)

[65] I. S. K. K. Kuwabara T, "Measurement and analysis of differential work hardening in cold-rolled steel sheet under biaxial tension," Journal of Materials Processing Technology, vol. 80, pp. 517-523, 1998.

[66] Dodds R 1987 Numerical techniques for plasticity computations in finite element analysis *Comp. Struct.* 26767

[67] R. Hill, "The mathematical theory of plasticity, Clarendon," *Oxford*, vol. 613, p. 614, 1950.

[68] J. Lubliner, *Plasticity theory*: Courier Corporation, 2008.

[69] G. A. Maugin, *The thermomechanics of plasticity and fracture* vol. 7: Cambridge University Press, 1992.

[70] F. Barlat and D.-J. Kim, "Advanced constitutive modeling and application to industrial forming processes," in *MATEC Web of Conferences*, 2016, p. 15013.

[71] D. C. Drucker, "A definition of stable inelastic material," BROWN UNIV PROVIDENCE RI1957.

[72] R. Hill, "A general theory of uniqueness and stability in elastic-plastic solids," *Journal of the Mechanics and Physics of Solids*, vol. 6, pp. 236-249, 1958.

[73] R. Hill, "Constitutive dual potentials in classical plasticity," *Journal of the Mechanics and Physics of Solids*, vol. 35, pp. 23-33, 1987.

[74] W. Tong, "Algebraic Convexity Conditions for Gotoh's Nonquadratic Yield Function," *Journal of Applied Mechanics*, vol. 85, 2018.

[75] R. Hill, "A theory of the yielding and plastic flow of anisotropic metals," *Proceedings of the Royal Society of London. Series A. Mathematical and Physical Sciences*, vol. 193, pp. 281-297, 1948.

[76] A. Abedini, C. Butcher, T. Rahmaan, and M. J. Worswick, "Evaluation and calibration of anisotropic yield criteria in shear Loading: Constraints to eliminate numerical artefacts," *International Journal of Solids and Structures*, vol. 151, pp. 118-134, 2018.

[77] M. Gotoh, "A theory of plastic anisotropy based on a yield function of fourth order (plane stress state)—I," *International Journal of Mechanical Sciences*, vol. 19, pp. 505-512, 1977.

[78] W. Hußnätter and M. Merklein, "Characterization of material behavior under pure shear condition," *International Journal of Material Forming*, vol. 1, pp. 233-236, 2008.

[79] R. W. Ogden, *Non-linear elastic deformations*: Courier Corporation, 1997.

[80] O. Yeoh, "Analysis of deformation and fracture of ‘pure shear’rubber testpiece," *Plastics, rubber and composites,* vol. 30, pp. 389-397, 2001.

[81] R. Hibbeler, "Mechanics of Materials Ninth Editldn," ed: Pearson Education, Inc, 2014.

[82] F. Barlat, Y. Maeda, K. Chung, M. Yanagawa, J. Brem, Y. Hayashida, *et al.*, "Yield function development for aluminum alloy sheets," *Journal of the Mechanics and Physics of Solids,* vol. 45, pp. 1727-1763, 1997.

[83] H. Vegter and A. H. van den Boogaard, "A plane stress yield function for anisotropic sheet material by interpolation of biaxial stress states," *International journal of plasticity,* vol. 22, pp. 557-580, 2006.

[84] Y. Tozawa, "Plastic deformation behavior under conditions of combined stress," in *Mechanics of Sheet Metal Forming*, ed: Springer, 1978, pp. 81-110.

[85] H.-C. Wu, Z. Xu, and P. T. Wang, "Torsion test of aluminum in the large strain range," *International journal of plasticity,* vol. 13, pp. 873-892, 1997.

[86] T. Balawender, "A comparison of a tensile test with a planar simple shear test in sheet metals," *Scientific Bulletin Series C: Fascicle Mechanics, Tribology, Machine Manufacturing Technology,* vol. 19, p. 1, 2005.

[87] S. Bouvier, H. Haddadi, P. Levée, and C. Teodosiu, "Simple shear tests: Experimental techniques and characterization of the plastic anisotropy of rolled sheets at large strains," *Journal of Materials Processing Technology,* vol. 172, pp. 96-103, 2006.

[88] K. A. Gardner, J. D. Seidt, M. Isakov, and A. Gilat, "Characterization of sheet metals in shear over a wide range of strain rates," in *Dynamic Behavior of Materials, Volume 1*, ed: Springer, 2014, pp. 313-317.

[89] K. Miyauchi, "Stress--Strain Relationship in Simple Shear of In-Plane Deformation for Various Steel Sheets," in *Efficiency in Sheet Metal Forming, IDDRG 13 th Biennial Congress,* 1984, pp. 360-371.

[90] E. Rauch, "Plastic anisotropy of sheet metals determined by simple shear tests," *Materials Science and Engineering: A,* vol. 241, pp. 179-183, 1998.

[91] D. Bae and A. Ghosh, "A planar simple shear test and flow behavior in a superplastic Al-Mg alloy," *Metallurgical and Materials Transactions A*, vol. 34, pp. 2465-2471, 2003.

[92] A. Pacheco and R. Batra, "Instabilities in shear and simple shear deformations of gold crystals," *Journal of the Mechanics and Physics of Solids*, vol. 56, pp. 3116-3143, 2008.

[93] D. C. Drucker, "A definition of stable inelastic material," BROWN UNIV PROVIDENCE RI1959.

[94] J. Peirs, P. Verleysen, and J. Degrieck, "Novel technique for static and dynamic shear testing of Ti6Al4V sheet," *Experimental mechanics*, vol. 52, pp. 729-741, 2012.

[95] R. Hill, "Theoretical plasticity of textured aggregates," in *Mathematical Proceedings of the Cambridge Philosophical Society*, 1979, pp. 179-191.

[96] A. Güner, B. Zillmann, T. Lampke, and A. Tekkaya, "In-situ measurement of loading stresses with X-ray diffraction for yield locus determination," *International Journal of Automotive Technology*, vol. 15, pp. 303-316, 2014.

[97] J. Kang, D. S. Wilkinson, P. Wu, M. Bruhis, M. Jain, J. D. Embury, *et al.*, "Constitutive behavior of AA5754 sheet materials at large strains," *Journal of engineering materials and technology*, vol. 130, 2008.

[98] A. B831-19. (2019). *Standard Test Method for Shear Testing 789 of Thin Aluminum Alloy Products*. Available: www.astm.org

[99] G. Yang, J. Sheng, W. Tong, B. E. Carlson, H.-P. Wang, and R. Kovacevic, "Tensile behavior of fusion-brazed aluminum alloy coach-peel joints fabricated by a dual-beam laser," *Journal of Materials Processing Technology*, vol. 261, pp. 184-192, 2018.

[100] J. Blaber, B. Adair, and A. Antoniou, "Ncorr: open-source 2D digital image correlation matlab software," *Experimental Mechanics*, vol. 55, pp. 1105-1122, 2015.

[101] B. Pan, K. Li, and W. Tong, "Fast, robust and accurate digital image correlation calculation without redundant computations," *Experimental Mechanics*, vol. 53, pp.

1277-1289, 2013.

[102] W. Tong, "Formulation of Lucas–Kanade digital image correlation algorithms for non-contact deformation measurements: a review," *Strain,* vol. 49, pp. 313-334, 2013.

[103] W. Tong and M. Alharbi, "Comparative evaluation of non-associated quadratic and associated quartic plasticity models for orthotropic sheet metals," *International Journal of Solids and Structures,* vol. 128, pp. 133-148, 2017.

[104] W. Tong, "Application of Gotoh's Orthotropic Yield Function for Modeling Advanced High-Strength Steel Sheets," *Journal of Manufacturing Science and Engineering,* vol. 138, 2016.

[105] W. Tong, "Generalized fourth-order Hill's 1979 yield function for modeling sheet metals in plane stress," *Acta Mechanica,* vol. 227, pp. 2719-2733, 2016.

[106] W. Hu, "Characterized behaviors and corresponding yield criterion of anisotropic sheet metals," *Materials Science and Engineering: A*, vol. 345, pp. 139-144, 2003.

[107] W. Tong, "An improved method of determining gotoh's nine material constants for a sheet metal with only seven or less experimental inputs," *International Journal of Mechanical Sciences,* vol. 140, pp. 394-406, 2018.

[108] A. L. Gurtin ME, "Thermodynamics applied to gradient theories involving the accumulated," Journal of the Mechanics and Physics of Solids, vol. 57, no. 3, pp. 405-421, 2009.

[109] Rousselier G, Barlat F, Yoon JW. A novel approach for anisotropic hardening modeling. Part I: Theory and its application to finite element analysis of deep drawing. International Journal of Plasticity. 2009 Dec 1; 25(12):2383-409.

[110] C. Vial-Edwards, Yield loci of FCC and BCC sheet metals, International Journal of Plasticity 13 (5) (1997) 521{531.

[111] S. Tamura, S. Sumikawa, H. Hamasaki, T. Uemori, F. Yoshida, Elasto- plasticity behavior of type 5000 and 6000 aluminum alloy sheets ad its constitutive modeling, NUMIFORM 2010 Proc. of the 10th Intl. Conf. (edited by F. Barlat, Y.H. Moon and M.G. Lee) (2010) 630{637.

[112] F. Yoshida, H. Hamasaki, T. Uemori, A user-friendly 3D yield function to describe anisotropy of steel sheets, International Journal of Plasticity 45 (2013) 119{139.